NOTE TO USERS

This reproduction is the best copy available.

UNIVERSITÉ DE SHERBROOKE

SIMULATION MONTE-CARLO DE LA RADIOLYSE DU DOSIMÈTRE DE FRICKE PAR DES NEUTRONS RAPIDES

MONTE-CARLO SIMULATION OF FAST NEUTRON RADIOLYSIS IN THE FRICKE DOSIMETER

par

Thititip TIPPAYAMONTRI

Département de médecine nucléaire et de radiobiologie

Mémoire présenté à la Faculté de médecine et des sciences de la santé
en vue de l'obtention du grade de maître ès sciences (M.Sc.) en radiobiologie

Juillet 2009

Jury

P[r] Pierre Lavigne	*Examinateur*, Département de pharmacologie, Faculté de médecine et des sciences de la santé
P[r] Michael A. Huels	*Examinateur*, Département de médecine nucléaire et de radiobiologie, Faculté de médecine et des sciences de la santé
P[r] Jean-Paul Jay-Gerin	*Directeur de recherche*, Département de médecine nucléaire et de radiobiologie, Faculté de médecine et des sciences de la santé

Your file Votre référence
ISBN: 978-0-494-64341-9
Our file Notre référence
ISBN: 978-0-494-64341-9

TABLE OF CONTENTS

LIST OF TABLES

LIST OF FIGURES

WATT (1996) and in the compilation of ICRU REPORT 49 (1993) for liquid water (density 1 g/cm^3) are also shown for the sake of comparison.

Figure IV.1: Time evolution of $G(Fe^{3+})$ (in molec./100 eV) in the radiolysis of air-saturated solution of 5 m*M* $FeSO_4$ in aqueous 0.4 *M* H_2SO_4 as obtained from our simulations for 300-MeV incident protons (LET ~ 0.3 keV/μm) at 25 °C. The concentration of dissolved oxygen used in the calculations is ~2.5×10^{-4} *M*. The solid line corresponds to our simulated kinetics of Fe^{3+} ion formation. The arrow on the right of the figure shows the yield of the Fricke dosimeter recommended for ^{60}Co γ-rays and fast electrons (15.6 molec./100 eV).

Figure IV.2: Time evolution of $G(Fe^{3+})$ (in molec./100 eV) for 0.8-MeV irradiating neutrons in aerated solutions of 5 m*M* $FeSO_4$ in aqueous 0.4 *M* H_2SO_4 at different temperatures in the range 25-300 °C. Yields of Fe^{3+} were obtained from Eqs. (52) and (53) taking into account recoil protons only (see text). The different lines correspond to our theoretical simulations at 25 (——), 50 (- - - -), 100 (·····), 200 (— — —), and 300 (— · — ·) °C.

Figure IV.3: Time evolution of $G(Fe^{3+})$ (in molec./100 eV) for 300-MeV incident protons in aerated solutions of 5 m*M* $FeSO_4$ in aqueous 0.4 *M* H_2SO_4 at different temperatures in the range 25-300 °C. The different lines correspond to our theoretical simulations at 25 (——), 50 (- - - -), 100 (·····), 200 (— — —), and 300 (— · — ·) °C.

Figure IV.4: Plot of the ferric ion yield $G(Fe^{3+})$ (in molec./100 eV) for the aerated Fricke solution at 25 °C against LET in the range ~0.3-70 keV/μm. The solid curve represents the values of $G(Fe^{3+})$ calculated from our Monte-Carlo simulations using incident protons of various initial energies between ~300 and 0.15 MeV. The dashed line corresponds to the Fricke *G*-values calculated by AUTSAVAPROMPORN et al. (2007) for LET varying from ~0.3 to 15 keV/μm. Experimental data: (▽) HARDWICK, 1952 - see also ALLEN, 1954; (⊠) DONALDSON and MILLER, 1955; (◇) HART et al., 1956; (⊗) HAYBITTLE et al., 1956; (△) BACK and MILLER, 1957; (■) LEFORT, 1957, 1958 - see also COTTIN and LEFORT, 1956; (☆) BARR and SCHULER, 1959; (◁) PEISACH and STEYN, 1960; (◀) ANDERSON

and HART, 1961; (×) SHALEK et al., 1962; (○) KOCHANNY et al., 1963; (▷) DAVIES et al., 1963; (▲) FREGENE, 1967; (○) SAUER et al., 1978; (★) ICRU REPORT 34, 1982; (□) LAVERNE and SCHULER, 1987; (●) ELLIOT et al., 1996*b*; and (◭) KLASSEN et al., 1999. Dose-average LET values used here for the various radiation types considered are taken from WATT (1996). Note that, for X-rays, there are in certain cases insufficient experimental details for an estimate of the average energy of electrons resulting from photon absorption in the solution to be made. This results in some uncertainty in assigning an average LET value to the corresponding reported $G(Fe^{3+})$ results.

Figure IV.5: Yield of ferric ions $G(Fe^{3+})$ (in molec./100 eV) for fast neutrons in the aerated Fricke solution at 25 °C as a function of incident neutron energy in the range ~0.5-10 MeV. The solid line shows our $G(Fe^{3+})$ values for neutrons calculated from Eq. (54) taking into account 4 neutron collisions in the medium and using the elastic scattering cross sections σ_H and σ_O shown in Fig. II.2. The dash-dot line represents our neutron $G(Fe^{3+})$ values calculated from Eq. (55) also considering 4 neutron collisions in the solution but assuming that σ_H and σ_O are all equal over all the neutron energy range considered. The dot line represents the $G(Fe^{3+})$ values obtained from our Monte-Carlo simulations taking into account recoil protons only. The dash-dot-dot line represents the $G(Fe^{3+})$ values assuming that the neutrons are stopped only by oxygen nuclei (see text). The dash line shows the neutron *G*-values for the Fricke dosimeter predicted by LAWSON and PORTER (1975) using a semi-empirical method based on published charged particle *G*-values along with neutron-induced particle spectra calculated for monoenergetic neutron interactions with the dosimeter medium. Experiment (at 25 °C): (■) GREENE et al., 1973*a*; (⬢) LAW et al., 1974; (▼) LAWSON and PORTER, 1975; (▲) GREENE et al., 1975; (▶) PEJUAN and KÜHN, 1981; and (◀) KATSUMURA et al., 1989.

Figure IV.6: Yield of Fe^{3+} in aerated Fricke solution as a function of temperature, for 300-MeV irradiating protons (LET ~ 0.3 keV/μm). The solid line shows the values of $G(Fe^{3+})$ obtained (at ~50 s) from our Monte-Carlo simulations. The dot

line shows the G-values for the Fricke dosimeter predicted by BĚGUSOVÁ and PIMBLOTT (2002) using the stochastic IRT simulation method, incorporating simulated electron track structures. Experiment: (☆) HOCHANADEL and GHORMLEY, 1962; (○) BALAKRISHNAN and REDDY, 1972; (●) KABAKCHI and LEBEDEVA, 1984; (▽) ISHIGURE et al., 1987; and (▲) KATSUMURA et al., 1988.

Figure IV.7: Yield of Fe^{3+} in the aerated Fricke solution as a function of temperature for 0.8-MeV incident neutrons. The solid line shows our simulated results for $G(Fe^{3+})$, calculated from Eq. (55) taking into account four neutron collisions and assuming all the neutron energy is absorbed by protons only (i.e., ignoring the contribution due to recoil oxygen ions). The symbol (○) refers to the experimental data of KATSUMURA et al. (1989, 1992).

Figure IV.8: Yields of Fe^{3+} in aerated Fricke solution as a function of temperature, for 300-MeV (LET ~ 0.3 keV/μm) irradiating protons. The thick solid curve shows the values of $G(Fe^{3+})$ obtained directly from our Monte-Carlo simulations. All the other curves show our $G(Fe^{3+})$ values calculated at different times between 10^{-6} and 10^{-8} s from Eq. (22) using the radical and molecular product yields obtained at those times from our Monte-Carlo simulations of the radiolysis of acidic (0.4 *M* H_2SO_4) aqueous solutions. Each curve is associated to a given symbol representing a given time (indicated on the right of the figure).

Figure IV.9: Time of spur expansion as a function of temperature for 300-MeV (LET ~ 0.3 keV/μm) irradiating protons (see text). The line indicates the time required to observe, at a given temperature, the transition from nonhomogeneity to homogeneity in the distribution of the reactive species.

ABSTRACT

MONTE-CARLO SIMULATION OF FAST NEUTRON RADIOLYSIS IN THE FRICKE DOSIMETER

Thititip TIPPAYAMONTRI

Monte-Carlo calculations are used to simulate the stochastic effects of fast neutron-induced chemical changes in the radiolysis of the ferrous sulfate (Fricke) dosimeter. To study the dependence of the yield of ferric ions, $G(Fe^{3+})$, on fast neutron energy, we have simulated, at 25 °C, the oxidation of ferrous ions in aerated aqueous 0.4 *M* H_2SO_4 (pH 0.46) solutions when subjected to ~0.5-10 MeV incident neutrons, as a function of time up to ~50 s. The radiation effects due to fast neutrons are estimated on the basis of track segment (or "escape") yields calculated for the first four recoil protons with appropriate weighting according to the energy deposited by each of these protons. For example, a 0.8-MeV neutron generates recoil protons of 0.505, 0.186, 0.069, and 0.025 MeV, with linear energy transfer (LET) values of ~41, 69, 82, and 62 keV/μm, respectively. In doing so, we consider that further recoils make only a negligible contribution to radiation processes. Our results show that the radiolysis of dilute aqueous solutions by fast neutrons produces smaller radical yields and larger molecular yields (relative to the corresponding yields for the radiolysis of water by ^{60}Co γ-rays or fast electrons) due to the high LET associated to fast neutrons. The effect of recoil ions of oxygen, which is also taken into account in the calculations, is shown to decrease $G(Fe^{3+})$ by about 10%. Our calculated values of $G(Fe^{3+})$ are found to increase slightly with increasing neutron energy over the energy range covered in this study, in good agreement with available experimental data.

We have also simulated the effect of temperature on the $G(Fe^{3+})$ values in the fast neutron radiolysis of the Fricke dosimeter from 25 to 300 °C. Our results show an

increase of $G(Fe^{3+})$ with increasing temperature, which is readily explained by an increase in the yields of free radicals and a decrease in those of molecular products. For 0.8-MeV incident neutrons (the only case for which experimental data are available in the literature), there is a ~23% increase in $G(Fe^{3+})$ on going from 25 to 300 °C. Although these results are in reasonable agreement with experiment, more experimental data, in particular for different incident neutron energies, would be needed to test more rigorously our Fe^{3+} ion yield results at elevated temperatures.

Keywords: liquid water, aerated sulfuric acid aqueous solutions, radiolysis, fast neutrons, recoil ions (protons and oxygen ions), linear energy transfer (LET), free-radical and molecular yields, Fricke (ferrous sulfate) dosimeter, kinetics of formation and yield of Fe^{3+} ions, time scale for spur expansion, temperature, Monte-Carlo simulations.

RÉSUMÉ

SIMULATION MONTE-CARLO DE LA RADIOLYSIS DU DOSIMÈTRE DE FRICKE PAR DES NEUTRONS RAPIDES

Thititip TIPPAYAMONTRI

À l'aide de calculs de simulation Monte-Carlo, nous avons étudié les effets stochastiques liés aux changements chimiques induits par l'action de neutrons rapides lors de la radiolyse de solutions acides de sulfate ferreux (dosimètre de Fricke). Nos simulations de l'oxydation radio induite des ions ferreux en milieu H_2SO_4 0,4 *M* (pH 0,46) aéré en fonction du temps jusqu'à ~50 s ont permis d'obtenir, à 25 °C, la dépendance du rendement en ions ferriques, $G(Fe^{3+})$, avec l'énergie des neutrons incidents lorsque celle-ci varie entre 0,5 et 10 MeV. Les effets radiolytiques dus aux neutrons rapides sont évalués en s'appuyant sur les rendements primaires de la radiolyse calculés sur des segments de trajectoires de protons de recul d'énergies variées, avec une pondération appropriée selon l'énergie déposée par ces derniers. Par exemple, un neutron de 0,8 MeV est considéré générer des protons de recul de ~0,505, 0,186, 0,069 et 0,025 MeV ayant des valeurs de transfert d'énergie linéique (TEL) respectivement de ~41, 69, 82 et 62 keV/μm. Par une telle procédure, nous considérons que la contribution dominante à la radiolyse provient des quatre premières collisions d'un neutron avec l'eau. Nos résultats montrent qu'une telle radiolyse par des neutrons rapides génèrent des rendements radicalaires plus faibles et des rendements moléculaires plus importants (par rapport aux valeurs correspondantes observées pour la radiolyse par les rayons γ de ^{60}Co ou des électrons rapides de même énergie) dû au TEL élevé associé à ces particules. L'influence des ions de recul d'oxygène, qui a aussi été prise en compte dans nos calculs, conduit à une diminution de $G(Fe^{3+})$ d'environ 10%. Un bon accord a été

obtenu entre nos valeurs de $G(Fe^{3+})$ calculées, qui augmentent légèrement avec l'énergie des neutrons rapides sur la gamme d'énergie considérée dans cette étude, et les données expérimentales disponibles dans la littérature.

Nous avons également simulé les effets de la température sur les valeurs de $G(Fe^{3+})$ dans la radiolyse du dosimètre de Fricke par des neutrons rapides entre 25 et 300 °C. Nos résultats indiquent une augmentation des rendements radicalaires et une diminution des rendements moléculaires. Pour des neutrons incidents de 0,8 MeV (seul cas pour lequel des données expérimentales sont disponibles actuellement), nous trouvons une augmentation de $G(Fe^{3+})$ d'environ 23% en passant de 25 à 300 °C. Bien qu'un bon accord soit obtenu avec l'expérience dans le cas étudié, des données expérimentales supplémentaires, en particulier pour différentes énergies de neutrons, seraient nécessaires afin de pouvoir comparer de façon plus critique nos résultats sur le rendement en ions Fe^{3+} à températures élevées.

Mots-clés : eau liquide, solutions aqueuses d'acide sulfurique, radiolyse, neutrons rapides, ions de recul (protons et ions de l'oxygène), transfert d'énergie linéique (TEL), rendements radicalaires et moléculaires, dosimètre de Fricke (sulfate ferreux), cinétique de formation et rendement des ions Fe^{3+}, temps de vie des grappes, température, simulations Monte-Carlo.

CHAPTER I

INTRODUCTION

Radiation chemistry of liquid water is of considerable importance, on the one hand, for the intrinsic scientific interest it generates, but as well, because of its relevance to a number of practical applications, particularly in radiation biology (where living cells are composed of about 70%-85% water by weight). It is also of importance in nuclear technology, such as in water-cooled nuclear power reactors (where water, used both as moderator and as a heat transport medium, is circulating around the reactor core at temperatures of 250-310 °C); as such, and in order to control water chemistry to mitigate the effects of water radiolysis and thus minimize corrosion (that occurs through the radiolytic production of oxidizing species, such as $^{\bullet}OH$, H_2O_2, O_2, etc.), the yields and activities of decomposition products of water must be well understood. In fact, the radiolysis of water and aqueous solutions has been the subject of numerous experimental and theoretical investigations for almost a century (more is known about the radiation chemistry of water than any other liquid). A good summary of aqueous radiation chemistry is given in the review articles of BUXTON (1987), FERRADINI and JAY-GERIN (1999), and LAVERNE (2004).

Stochastic simulation methods employing Monte-Carlo techniques have been used with success to model the complete evolution of physical and chemical events generated by the interaction of ionizing radiation with pure liquid water. These simulation methods have permitted detailed studies of the relationship between track structure and radiation-induced chemical change. On the theoretical side, the entire water radiolysis process can be efficiently modeled, using Monte-Carlo computer codes, to simulate the primary interactions and to describe the fast kinetics of reactive radicals and ions as a function of the linear energy transfer (LET) of the ionizing radiation, pH, and temperature. Such a modeling can also be done in a

nuclear reactor, where the cooling water undergoes radiolytic decomposition induced by gamma, fast electron, and neutron radiation in the core. As experiments at high temperatures and pressures and in mixed radiation fields are difficult to perform, computer simulations in this latter case are a particularly important route of investigation.

In the present study, Monte-Carlo calculations are used to predict the yields for the action of "fast" (~0.5-10 MeV) neutrons in the Fricke (ferrous sulfate) dosimeter (FRICKE and HART, 1966) as a function of the incident neutron energy, and to examine their temperature dependences for the range 25-300 °C.

I.1 Radiolysis of liquid water and aqueous solutions

I.1.1 The radiolysis of water

A thorough understanding of the radiolysis of water involves knowledge of the early deposition of the energy of the incident ionizing radiation (mainly through ionization, electronic excitation, and dissociation of the water molecules), and the subsequent physicochemical and nonhomogeneous chemical evolution of the system (PLATZMAN, 1958; KUPPERMANN, 1959) to times, at room temperature, on the order of the microsecond, after which the remaining radiolytic products are usually regarded as homogeneously distributed in the bulk of the solution. Briefly, the radiolysis of pure deaerated liquid water by low-LET radiation (such as ^{60}Co γ-rays, hard X-rays, fast electrons, or high-energy protons) principally leads to the formation of the radicals and molecular products e^-_{aq} (hydrated electron), $H^\bullet$ (hydrogen atom), H_2 (molecular hydrogen), $^\bullet OH$ (hydroxyl radical), H_2O_2 (hydrogen peroxide), $HO_2^\bullet/O_2^{\bullet-}$ (hydroperoxyl/superoxide anion radicals, pK_a = 4.8), H^+, OH^-, etc. (for a review, see: SPINKS and WOODS, 1990). Under ordinary irradiation conditions, these species are generated nonhomogeneously on subpicosecond time scales in small, spatially isolated regions of dense ionization and excitation events, commonly referred to as "spurs" (MAGEE, 1953), along the track of the radiation. Owing to diffusion from their initial positions, the radiolytic products then either react within the spurs as they

expand or escape into the bulk solution. At ambient temperature, this spur expansion is essentially complete by about 1 μs after the initial energy deposition. The so-called "primary" radical and molecular yields ("long-time" or "escape" yields) $G_{e^-_{aq}}$, $G_{H\cdot}$, G_{H_2}, $G_{\cdot OH}$, $G_{H_2O_2}$, etc., represent the numbers of species of each kind formed or destroyed per 100 eV of absorbed energy that remain after spur expansion and become available to react with added solutes (treated as spatially homogeneous) at moderate concentrations.

For low-LET radiation, the radiolysis of pure deaerated (air-free) liquid water can be described by the following *global* equation, written for an absorbed energy of 100 eV (FERRADINI and JAY-GERIN, 1999) (the symbol ~~> is used to distinguish reactions brought about by the absorption of ionizing radiation):

$$G_{-H_2O}\ H_2O \ \sim\sim>\ G_{e^-_{aq}}\ e^-_{aq} + G_{H\cdot}\ H^\bullet + G_{H_2}\ H_2 + G_{H^+}\ H^+ + G_{OH^-}\ OH^-$$
$$+ G_{\cdot OH}\ {}^\bullet OH + G_{H_2O_2}\ H_2O_2 + G_{HO_2^\bullet/O_2^{\bullet-}}\ HO_2^\bullet/O_2^{\bullet-} + \ldots, \qquad (1)$$

where the coefficients G_X are the primary radical and molecular yields of the various radiolytic species X, and G_{-H_2O} denotes the corresponding yield for net water decomposition. For ^{60}Co γ-rays (photon energies of 1.17 and 1.33 MeV), hard X-rays or fast electrons of the same energies, at neutral pH and 25 °C (average LET ~ 0.3 keV/μm), the most recently reported values of the primary yields are (LAVERNE, 2004) (in units of molecules per 100 eV):[1]

$$G_{e^-_{aq}} = 2.50 \qquad G_{H\cdot} = 0.56 \qquad G_{H_2} = 0.45$$
$$G_{\cdot OH} = 2.50 \qquad G_{H_2O_2} = 0.70. \qquad (2)$$

These primary yield values, including the contribution of $HO_2^\bullet/O_2^{\bullet-}$ [note that, for low-LET radiolysis, $HO_2^\bullet/O_2^{\bullet-}$ is a minor radiolytic product because its very small yield of

[1] These units (abbreviated as "molec./100 eV") for *G*-values are used throughout in this work. For conversion into SI units (mol J^{-1}): 1 molec./100 eV ≈ 1.0364×10^{-7} mol J^{-1}.

~0.02 molec./100 eV (HART, 1955; BJERGBAKKE and HART, 1971) accounts for less than 1% of the other primary radiolytic species], are linked by the following relationships:

$$G_{e^-_{aq}} + G_{OH^-} = G_{H^+}$$

$$G_{e^-_{aq}} + G_{H\cdot} + 2\,G_{H_2} = G_{\cdot OH} + 2\,G_{H_2O_2} + 3\,G_{HO_2\cdot/O_2\cdot^-}, \qquad (3)$$

expressing the charge conservation and material balance of Eq. (1).

Within the lifetime of a spur, the yields of the radical and molecular species produced by the irradiation vary with time, and also depend on the radiation type (or LET) and the added solute (scavenger) concentration. One of the main goals in the study of the radiation chemistry of water is the determination of those yields and their time dependences, under different irradiation conditions.

I.1.2 Time scale of events and formation of primary radical and molecular products in neutral water radiolysis

The overall process of producing chemical changes by ionizing radiation can be conveniently divided into three, more or less clearly delineated, consecutive, temporal stages (PLATZMAN, 1958; KUPPERMANN, 1959) (the time scale of events that occur in the radiolysis of water and aqueous solutions is shown in Fig. I.1) that are briefly described below.

(i) The "*physical stage*" consists of the phenomena by which energy is transferred from the incident high-energy radiation (energetic photons, for example, γ-rays from ^{60}Co or X-ray photons, or charged particles, such as fast electrons, protons or heavy ions generated by a particle accelerator, or neutron radiation, or high-energy α-particles from suitable radioactive nuclides) to the water. It lasts not more than ~10^{-16} s. The result of this energy absorption is the production, along the path of the radiation, of a large number of ionized and electronically excited water molecules (denoted $H_2O^{\bullet+}$ and $H_2O^*_{elec}$, respectively; note that $H_2O^*_{elec}$ represents here the many excited states, including the so-called superexcitation states

(PLATZMAN, 1962*a*) and the collective electronic oscillations of the "plasmon" type (HELLER et al., 1974; KAPLAN and MITEREV, 1987; WILSON et al., 2001). The earliest processes in the radiolysis of water are:

$$H_2O \sim\sim> H_2O^{\bullet+} + e^- \quad (4)$$

$$H_2O \sim\sim> H_2O^*_{elec} \quad (5)$$

Generally, the electron ejected in the ionization event has sufficient energy to ionize or excite one or more other water molecules in the vicinity, and this leads, as mentioned above, to the formation of track entities, or "spurs", that contain the products of the events. For low-LET radiation, the spurs are separated by large distances relative to their diameter and the track can be viewed, at this stage, as a random succession of isolated spherical spurs.

(ii) The "*physicochemical stage*" consists of the processes that lead to the establishment of thermal equilibrium in the system. The duration of this stage is of the order of 10^{-12} s for aqueous solutions. During this stage, the ions and excited-state water molecules dissipate their excess energy by bond rupture, luminescence, energy transfer to neighboring molecules, etc.

The ionized water molecules are unstable. They are allowed to undergo a random walk during their very short lifetime (~10^{-14} s) (MOZUMDER and MAGEE, 1975) via a sequence of electron transfers (about 20, one the average, over a few molecular diameters; COBUT et al., 1998) from neighboring water molecules to the $H_2O^{\bullet+}$ hole (i.e., electron-loss center) (OGURA and HAMILL, 1973). These short-lived $H_2O^{\bullet+}$ radical cations subsequently decompose to form $^{\bullet}OH$ radicals by transferring a proton to an adjacent H_2O molecule:

$$H_2O^{\bullet+} + H_2O \rightarrow H_3O^+ + {}^{\bullet}OH\,, \quad (6)$$

where H_3O^+ (or equivalently, H^+_{aq}) represents the hydrated hydrogen ion.

The energetic secondary electrons lose kinetic energy by a sequence of interactions with the medium until they attain thermal energies (~0.025 eV at 25 °C)

after about 4×10^{-14} s (MEESUNGNOEN et al., 2002*a*). In the course of their thermalization, the slowing-down (or "dry") electrons can be recaptured by their parent ions due to the Coulomb attraction of the latter which tends to draw them back together to undergo electron-cation "geminate" recombination:

$$e^- + H_2O^{\bullet+} \rightarrow H_2O^*_{vib} \qquad (7)$$

As the electron is recaptured, the parent ion is transformed into a (vibrationally) excited neutral molecule.

The electron released in the ionization event can cause further ionization and excitation to occur if it has sufficient kinetic energy. Eventually, its energy falls below the first electronic excitation threshold of water (~7.3 eV; see: MICHAUD et al., 1991), forming the so-called "subexcitation electron" (PLATZMAN, 1955). This latter loses the rest of its energy relatively slowly by exciting vibrational and rotational modes of water molecules. Once it is thermalized (e^-_{th}), it can be localized or "trapped" (then forming the so-called "wet" electron whose exact physical nature is still the subject of investigation) (e^-_{tr}) in a pre-existing potential energy well of appropriate depth in the liquid before it reaches a fully relaxed, hydrated state (e^-_{aq}) as the dipoles of the surrounding molecules orient under the influence of the negative charge of the electron. In liquid water at 25 °C, thermalization, trapping, and hydration can then follow in quick succession in less than $\sim 10^{-12}$ s (for example, see: JAY-GERIN et al., 2008, and references therein):

$$e^- \rightarrow e^-_{th} \rightarrow e^-_{tr} \rightarrow e^-_{aq} \qquad (8)$$

In the course of its thermalization, the ejected electron can also temporarily be captured by a water molecule to form a transient anion

$$e^- + H_2O \rightarrow H_2O^- \qquad (9)$$

This anion then undergoes dissociation mainly into H^- and $^\bullet OH$ according to

$$H_2O^- \rightarrow H^- + {}^\bullet OH\,, \qquad (10)$$

followed by the reaction of the hydride anion with another water molecule through a fast proton transfer reaction:

$$H^- + H_2O \rightarrow H_2 + OH^- . \qquad (11)$$

Reactions (9) and (10) correspond to the so-called "dissociative electron attachment" (or DEA) process, which has been observed in amorphous solid water at ~20 K for electron energies between about 5 and 12 eV (ROWNTREE et al., 1991). DEA to water was suggested to be responsible, at least in part, for the yield of "nonscavengeable" molecular hydrogen in the radiolysis of liquid water at early times (PLATZMAN, 1962*b*; FARAGGI and DÉSALOS, 1969; GOULET and JAY-GERIN, 1989; KIMMEL et al., 1994; COBUT et al., 1996). This proposed mechanism for the production of H_2 has received strong support from recent experiments that have shown that the previously accepted nonscavengeable yield of H_2 is due to precursors of e^-_{aq} and it can be lowered with appropriate (dry electron) scavengers at high concentration (PASTINA et al., 1999).

Excited molecules may be produced directly in an initial act [reaction (5)] or by neutralization of an ion [reaction (7)]. We have little knowledge about the channels through which the excited water molecules in the liquid phase decay and the branching ratios associated with each of them. Fortunately, the contribution of the water excited states to the primary radical and molecular products in the water radiolysis is of relatively minor importance in comparison with that of the ionization processes, so that the lack of information about their decomposition has only limited consequences. Consequently, the competing deexcitation mechanisms of H_2O^* are generally assumed to be essentially the same as those reported for an isolated water molecule (it should be noted here that the same decay processes have been reported to occur for the electronically and vibrationally excited H_2O molecules in the gas phase), namely (see, for example: SWIATLA-WOJCIK and BUXTON, 1995; COBUT et al., 1998; MEESUNGNOEN and JAY-GERIN, 2005*a*):

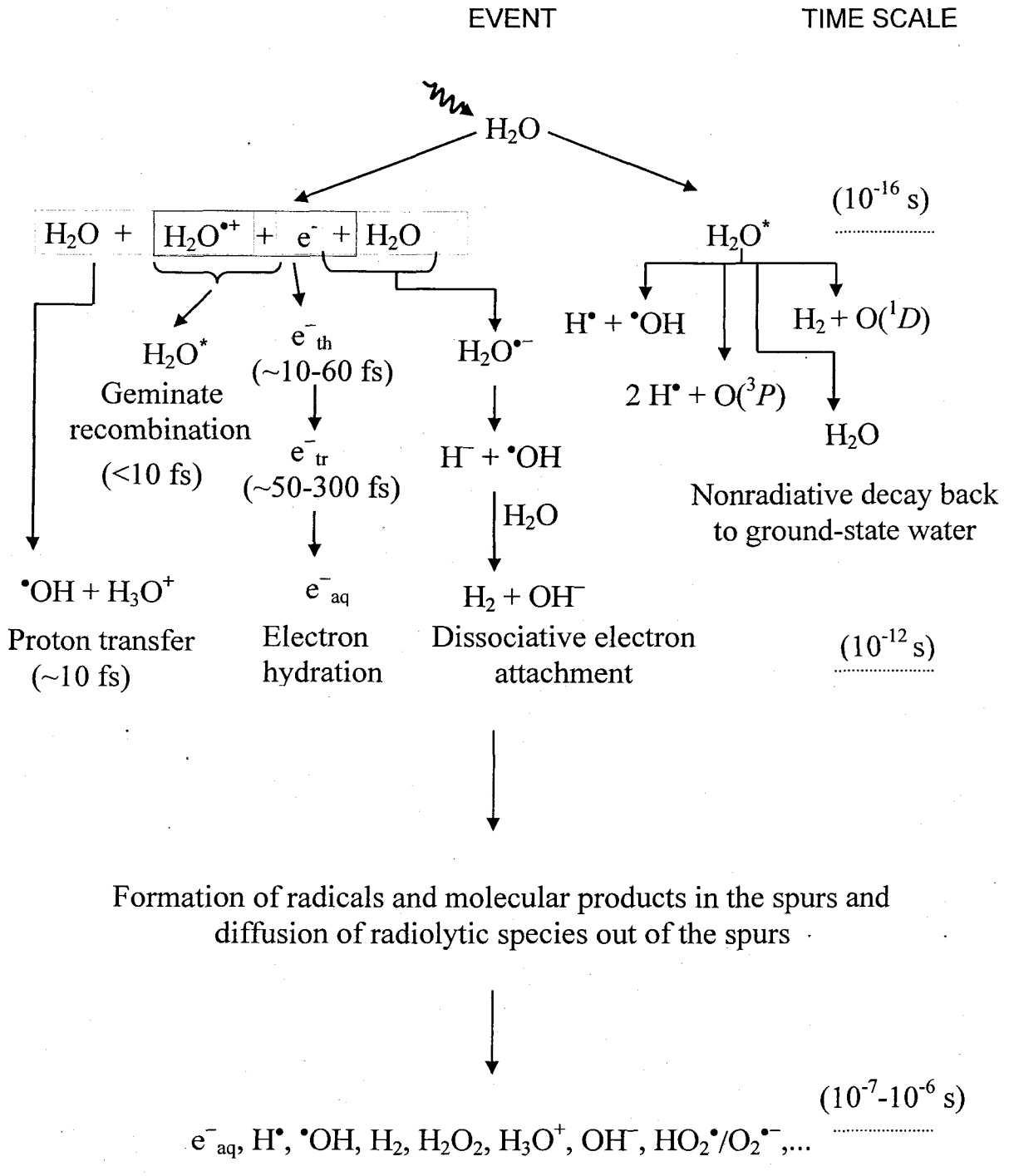

Figure I.1: Time scale of events that occur in the low-LET radiolysis of neutral water (from MEESUNGNOEN, 2007).

$$H_2O^* \rightarrow H^\bullet + {}^\bullet OH \quad (12a)$$

$$H_2O^* \rightarrow H_2 + O(^1D) \quad (12b)$$

$$H_2O^* \rightarrow 2\,H^\bullet + O(^3P) \quad (12c)$$

$$H_2O^* \rightarrow H_2O + \text{release of thermal energy} \quad (12d)$$

where $O(^1D)$ and $O(^3P)$ represent oxygen atoms produced in their singlet ^1D excited state and triplet ^3P ground state, respectively (see Fig. I.1). Note that the dissociation of H_2O^* via reaction (12*a*) is the main source of the "initial" (at ~10^{-12} s, i.e., at the end of the physicochemical stage, prior to spur or track expansion) yield of hydrogen atoms. As for the different branching ratios (or decay probabilities) associated with reactions (12*a-d*), they are chosen in order to consistently match the observed picosecond *G*-values of the various spur species (MUROYA et al., 2002; MEESUNGNOEN and JAY-GERIN, 2005*a*). It should also be noted here that the $O(^1D)$ atoms produced in reaction (12*b*) react very efficiently with water to form H_2O_2 or possibly also $2\,{}^\bullet OH$ (TAUBE, 1957; BIEDENKAPP et al., 1970). By contrast, ground-state oxygen atoms $O(^3P)$ in aqueous solution are rather inert to water but react with most additives (AMICHAI and TEININ, 1969).

(iii) The "*nonhomogeneous chemical stage*" consists of the period after ~10^{-12} s, during which the radiolytic species generated previously in a nonhomogeneous track structure (e^-_{aq}, ${}^\bullet OH$, $H^\bullet$, H_3O^+, H_2, OH^-, ${}^\bullet O^\bullet$,...) undergo chemical reactions as they diffuse away from the site where they were originally produced. These species react together to form molecular or secondary radical products, or with dissolved solutes (if any) present at the time of irradiation, until all spur/track reactions are complete. Table 1 gives the principal reactions that are likely to occur while the spurs expand. The time for completion of spur processes is generally taken to be ~10^{-7}-10^{-6} s. By this time, the spatially nonhomogeneous distribution of reactive species has relaxed. Beyond a few microseconds, the reactions which occur in the bulk solution can usually be described with conventional homogeneous chemistry methods (for example, see: PASTINA and LAVERNE, 2001).

Table 1: Main spur/track reactions and rate constants (k) for the radiolysis of pure liquid water at 25 °C (from MEESUNGNOEN, 2007).

Reaction	k (M^{-1} s^{-1})	Reaction	k (M^{-1} s^{-1})
$H^{\bullet} + H^{\bullet} \rightarrow H_2$	5.03×10^9	$e^-_{aq} + e^-_{aq} \rightarrow H_2 + 2\ OH^-$	5.0×10^9
$H^{\bullet} + {}^{\bullet}OH \rightarrow H_2O$	1.55×10^{10}	$e^-_{aq} + H^+ \rightarrow H^{\bullet}$	2.11×10^{10}
$H^{\bullet} + H_2O_2 \rightarrow H_2O + {}^{\bullet}OH$	3.5×10^7	$e^-_{aq} + O_2^{\bullet -} \rightarrow H_2O_2 + 2\ OH^-$	1.3×10^{10}
$H^{\bullet} + e^-_{aq} \rightarrow H_2 + OH^-$	2.5×10^{10}	$e^-_{aq} + HO_2^- \rightarrow O^{\bullet -} + OH^-$	3.51×10^9
$H^{\bullet} + OH^- \rightarrow H_2O + e^-_{aq}$	2.51×10^7	$e^-_{aq} + O^{\bullet -} \rightarrow 2\ OH^-$	2.31×10^{10}
$H^{\bullet} + O_2 \rightarrow HO_2^{\bullet}$	2.1×10^{10}	$e^-_{aq} + H_2O \rightarrow H^{\bullet} + OH^-$	15.8
$H^{\bullet} + HO_2^{\bullet} \rightarrow H_2O_2$	1.0×10^{10}	$e^-_{aq} + O_2 \rightarrow O_2^{\bullet -}$	1.74×10^{10}
$H^{\bullet} + O_2^{\bullet -} \rightarrow HO_2^-$	1.0×10^{10}	$e^-_{aq} + HO_2^{\bullet} \rightarrow HO_2^-$	1.28×10^{10}
$H^{\bullet} + HO_2^- \rightarrow {}^{\bullet}OH + OH^-$	1.46×10^9	$e^-_{aq} + O(^3P) \rightarrow O^{\bullet -}$	2.0×10^{10}
$H^{\bullet} + O(^3P) \rightarrow {}^{\bullet}OH$	2.02×10^{10}	$e^-_{aq} + O_3 \rightarrow O_3^{\bullet -}$	3.6×10^{10}
$H^{\bullet} + O^{\bullet -} \rightarrow OH^-$	2.0×10^{10}	$H^+ + O^{\bullet -} \rightarrow {}^{\bullet}OH$	4.78×10^{10}
$H^{\bullet} + O_3 \rightarrow O_2 + {}^{\bullet}OH$	3.7×10^{10}	$H^+ + O_2^{\bullet -} \rightarrow HO_2^{\bullet}$	4.78×10^{10}
$H^{\bullet} + O_3^{\bullet -} \rightarrow OH^- + O_2$	1.0×10^{10}	$H^+ + OH^- \rightarrow H_2O$	11.3×10^{10}
${}^{\bullet}OH + {}^{\bullet}OH \rightarrow H_2O_2$	5.5×10^9	$H^+ + O_3^{\bullet -} \rightarrow {}^{\bullet}OH + O_2$	9.0×10^{10}
${}^{\bullet}OH + H_2O_2 \rightarrow HO_2^{\bullet} + H_2O$	2.87×10^7	$H^+ + HO_2^- \rightarrow H_2O_2$	5.0×10^{10}
${}^{\bullet}OH + H_2 \rightarrow H^{\bullet} + H_2O$	3.28×10^7	$OH^- + O(^3P) \rightarrow HO_2^-$	4.2×10^8
${}^{\bullet}OH + e^-_{aq} \rightarrow OH^-$	2.95×10^{10}	$OH^- + HO_2^{\bullet} \rightarrow O_2^{\bullet -} + H_2O$	6.3×10^9
${}^{\bullet}OH + OH^- \rightarrow O^{\bullet -} + H_2O$	6.3×10^9	$O_2 + O^{\bullet -} \rightarrow O_3^{\bullet -}$	3.7×10^9
${}^{\bullet}OH + HO_2^{\bullet} \rightarrow O_2 + H_2O$	7.9×10^9	$O_2 + O(^3P) \rightarrow O_3$	4.0×10^9
${}^{\bullet}OH + O_2^{\bullet -} \rightarrow O_2 + OH^-$	1.07×10^{10}	$HO_2^{\bullet} + O_2^{\bullet -} \rightarrow HO_2^- + O_2$	9.7×10^7
${}^{\bullet}OH + HO_2^- \rightarrow HO_2^{\bullet} + OH^-$	8.32×10^9	$HO_2^{\bullet} + HO_2^{\bullet} \rightarrow H_2O_2 + O_2$	8.3×10^5
${}^{\bullet}OH + O(^3P) \rightarrow HO_2^{\bullet}$	2.02×10^{10}	$HO_2^{\bullet} + O(^3P) \rightarrow O_2 + {}^{\bullet}OH$	2.02×10^{10}
${}^{\bullet}OH + O^{\bullet -} \rightarrow HO_2^-$	1.0×10^9	$HO_2^{\bullet} + H_2O \rightarrow H^+ + O_2^{\bullet -}$	1.29×10^4
${}^{\bullet}OH + O_3^{\bullet -} \rightarrow O_2^{\bullet -} + HO_2^{\bullet}$	8.5×10^9	$O_2^{\bullet -} + O^{\bullet -} \rightarrow O_2 + 2\ OH^-$	6.0×10^8
${}^{\bullet}OH + O_3 \rightarrow O_2 + HO_2^{\bullet}$	1.11×10^8	$O_2^{\bullet -} + H_2O \rightarrow HO_2^{\bullet} + OH^-$	0.075
$H_2O_2 + e^-_{aq} \rightarrow OH^- + {}^{\bullet}OH$	1.1×10^{10}	$O_2^{\bullet -} + O_3 \rightarrow O_3^{\bullet -} + O_2$	1.5×10^9
$H_2O_2 + OH^- \rightarrow HO_2^- + H_2O$	4.75×10^8	$HO_2^- + H_2O \rightarrow H_2O_2 + OH^-$	3.83×10^4
$H_2O_2 + O(^3P) \rightarrow HO_2^{\bullet} + {}^{\bullet}OH$	1.6×10^9	$HO_2^- + O^{\bullet -} \rightarrow O_2^{\bullet -} + OH^-$	3.5×10^8
$H_2O_2 + O^{\bullet -} \rightarrow HO_2^{\bullet} + OH^-$	5.55×10^8	$HO_2^- + O(^3P) \rightarrow O_2^{\bullet -} + {}^{\bullet}OH$	5.3×10^9
$H_2 + O(^3P) \rightarrow H^{\bullet} + {}^{\bullet}OH$	4.77×10^3	$O^{\bullet -} + O^{\bullet -} \rightarrow H_2O_2 + 2\ OH^-$	1.0×10^8
$H_2 + O^{\bullet -} \rightarrow H^{\bullet} + OH^-$	1.21×10^8	$O^{\bullet -} + O_3^{\bullet -} \rightarrow 2\ O_2^{\bullet -}$	7.0×10^8
$O(^3P) + O(^3P) \rightarrow O_2$	2.2×10^{10}	$O^{\bullet -} + H_2O \rightarrow {}^{\bullet}OH + OH^-$	1.02×10^6
$O(^3P) + H_2O \rightarrow 2\ {}^{\bullet}OH$	1.9×10^3	$O_3^{\bullet -} + H_2O \rightarrow O^{\bullet -} + O_2$	48.0

I.1.3 The effect of pH

Although the standard Fricke dosimeter (dilute aqueous solution of ferrous ions in 0.4 *M* sulfuric acid) was developed as early as 1927 (see below), the great majority of radiolysis experiments concerning acidic aqueous solutions were conducted only from the 1950's. The acid most often utilized was H_2SO_4 in 0.4 *M* aqueous solutions (pH ~ 0.46). One of the reasons having originally dictated this choice came from the fact that the dominant anion HSO_4^- was then considered as not intervening, under these conditions, in the course of the radiolysis (FRICKE and HART, 1966; FERRADINI and JAY-GERIN, 1999). As for the radical and molecular yields, the values obtained from the study of a large number of systems, both inorganic (such as Fe^{2+}, Ce^{IV}, Tl^+, and V^V) and organic (e.g., formic acid, oxalic acid, and other organic compounds), in sulfuric acid medium present a remarkable agreement (FERRADINI and JAY-GERIN, 2000). For all chosen solutes within certain limits of concentrations, the generally adopted primary yields (expressed in units of molec./100 eV) of radicals and molecular products obtained in the ^{60}Co γ-irradiation of 0.4 *M* H_2SO_4 aqueous solutions at 25 °C are (HOCHANADEL and LIND, 1956; FERRADINI and PUCHEAULT, 1983):

$$G_{e^-_{aq}} + G_{H\cdot} = 3.70 \qquad G_{H_2} = 0.40 \qquad G_{\cdot OH} = 2.90 \qquad G_{H_2O_2} = 0.80. \tag{13}$$

It is interesting to note that a few other acids like HCl, $HClO_4$ (perchloric acid), and $(COOH)_2$ (oxalic acid) were also employed in radical and molecular yield determinations at low pH. A comparison of the results obtained shows that the primary yield values given in Eq. (13) are generally similar for solutions of the *same* pH.

Figure I.2 shows the variation of the primary yields of radicals and molecular products in the γ-radiolysis of (air-free) water as a function of pH in the range 1.3-13 (DRAGANIĆ et al., 1969; DRAGANIĆ and DRAGANIĆ, 1971). As we can see, above pH 4 up to strongly alkaline solutions, the radical and molecular yields are essentially constant and independent of pH. In acid solutions with pH < 4, the yield of the

"reducing" free radicals e^-_{aq} and $H^\bullet$, represented by the sum $G_{e^-_{aq}+H^\bullet} = G_{e^-_{aq}} + G_{H^\bullet}$, increases as the proportion of $H^\bullet$ increases through the reaction:

$$e^-_{aq} + H^+ \rightarrow H^\bullet \qquad (14)$$

($k_{14} \approx 1.12 \times 10^{10}\ M^{-1}\ s^{-1}$, taking into account ionic strength effects; see below)

competing with other reactions of e^-_{aq} in the spurs. At the acid concentration of 0.4 *M* H_2SO_4, the H^+ ions very rapidly scavenge most, if not all, of the e^-_{aq} radicals in spurs to form $H^\bullet$ atoms (HAYON, 1968; BUXTON, 1967, 1968; DRAGANIĆ and DRAGANIĆ, 1971). An increase in acidity below pH 4 also leads to slight increases in the primary yields of "oxidizing" products $G_{\cdot OH}$ and $G_{H_2O_2}$, while there is a slight decrease in G_{H_2} (for example, see: FERRADINI and JAY-GERIN, 2000).

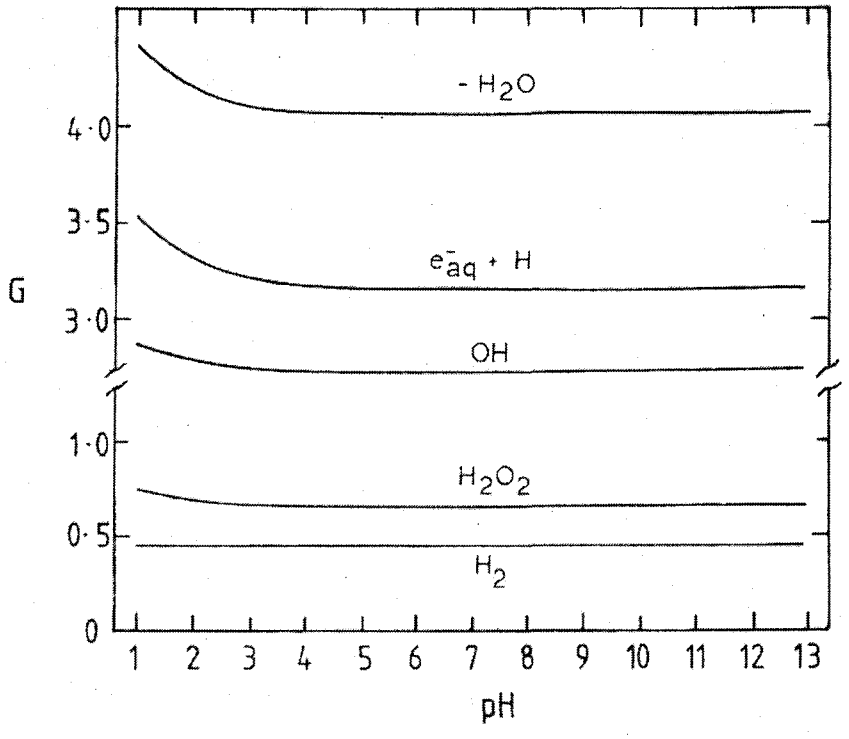

Figure I.2: The effect of pH on the primary radical and molecular yields in γ-radiolysis of water. There is a relatively small increase (~7%) in water decomposition (G_{-H_2O}) when the pH is varied from 3 to 1.3 (from DRAGANIĆ et al., 1969).

At high acidities (pH < 1), a certain proportion of the $^{\bullet}OH$ radicals react with hydrogen sulfate anions HSO_4^- to form the sulfate radical $SO_4^{\bullet-}$ according to

$$^{\bullet}OH + HSO_4^- \rightarrow H_2O + SO_4^{\bullet-} \qquad (15)$$

with a rate constant taken to be $k_{15} = 1.5 \times 10^5\ M^{-1}\ s^{-1}$ (MEESUNGNOEN et al., 2001*a*; AUTSAVAPROMPORN et al., 2007). As a result of reaction (15), $G_{\bullet OH}$ reaches a weakly pronounced maximum around pH 1 and then diminishes steeply as the pH is reduced below 1. This has been well reproduced by AUTSAVAPROMPORN et al. (2007) who used Monte-Carlo simulations to investigate the influence of acidity on the primary yields of chemical species produced in the radiolysis of deaerated aqueous sulfuric acid solutions over the range from neutral solution to 0.4 *M* H_2SO_4.

The values of the radical and molecular yields given here for the radiolysis of aqueous solutions at low pH mainly concern low-LET radiation (γ-rays or fast electrons, LET ~ 0.3 keV/μm). In contrast, fast neutrons, particles of interest to us in this study, constitute high-LET radiation (see below). Neutrons fall into this high-LET category because they are stopped by collisions with atomic nuclei, which become recoil protons and oxygen ions, losing their energy in dense tracks (see, for example: McCRACKEN et al., 1998). In acid water, very little work has been done with fast-neutron radiation. In fact, the only experimental data available in the literature are those of KATSUMURA and coworkers (1989, 1992), who determined the primary yields of water decomposition products in 0.4 *M* H_2SO_4 aqueous solutions irradiated with 0.8-MeV neutrons at elevated temperatures up to 275 °C. At room temperature, these *G*-values are (KATSUMURA et al., 1989):

$$G_{e^-_{aq}} + G_{H^{\bullet}} = 1.25 \qquad G_{H_2} = 0.99 \qquad G_{\bullet OH} = 0.68 \qquad G_{H_2O_2} = 1.27. \qquad (16)$$

As we can see, the yields of free radicals are decreased and the molecular product yields increased compared with those for γ-radiolysis [given in Eq. (13); see also Fig. I.2], reflecting the high-LET character of fast neutrons.

I.1.4 The influence of LET

A great many experimental and theoretical studies have shown that the yields in the radiolysis of water and aqueous solutions are strong functions of the quality of the incident radiation, a measure of which is its LET (for example, see: ALLEN, 1948, 1961; BARR and SCHULER, 1959; ANDERSON and HART, 1961; PUCHEAULT, 1961; BURNS and SIMS, 1981; MAGEE and CHATTERJEE, 1987; APPLEBY, 1989; McCRACKEN et al., 1998; MOZUMDER, 1999; LAVERNE, 2000, 2004; MEESUNGNOEN and JAY-GERIN, 2005*a*). Let us briefly consider the changing phenomena in tracks as LET increases.

At the lowest LET (for example, for sparsely ionizing radiation such as fast electrons), tracks are clearly separated initially into spurs that develop independently in time (see above). If the spurs are taken as spherical beads, then the low-LET track would look like a "string of beads" (SAMUEL and MAGEE, 1953; GANGULY and MAGEE, 1956). Even the adjacent spurs are so far apart that there is practically no overlapping among reactants. In this case, the predominant effect is radical production. As LET increases, the mean separation distance between the spurs decreases, and the isolated "spur" structure changes to a situation in which the spurs are not initially overlapping but they will overlap shortly thereafter (due to diffusion of the reactive species) before the expansion of the track is complete. As LET continues to increase, the spurs are merged initially to form a dense continuous cylindrical track. This permits more radicals to be formed in close proximity with correspondingly greater probability of reacting with one another to produce molecular products or to recombine to water. Densely ionizing radiations therefore tend to produce high yields of molecular products, at the expense of free-radical yields. Various examples of the primary radical and molecular yields in 0.4 *M* H_2SO_4 aqueous solutions, obtained with radiations of increasing LET up to ~4000 keV/μm (radiolysis with fission fragments from dissolved ^{252}Cf) are given in Table 2.

Table 2: Dependence of the primary yields (in molec./100 eV) of free radical and molecular products from irradiated 0.4 *M* H_2SO_4 aqueous solutions on LET, at room temperature.

Radiation	LET [(a)] (keV/μm)	$G_{e^-_{aq}}+G_{H^\bullet}$	$G_{^\bullet OH}$	G_{H_2}	$G_{H_2O_2}$	References
^{60}Co γ-rays	~0.2	3.7	2.9	0.4	0.8	Hochanadel & Lind (1956); Ferradini & Pucheault (1983)
8-kV X-rays (Cu)	3.1	2.55	1.9	0.7	1.05	Lefort (1957, 1958)
$^3H^+$ β-particles (mean energy: ~5.7 keV) [(b)]	3.5	2.91	2	0.53	0.97	Collinson et al. (1962)
18-MeV deuterons	5	2.39	1.75	0.71	1.03	Barr & Schuler (1957)
8-MeV deuterons	9.5	1.71	1.45	1.05	1.17	Barr & Schuler (1957)
32-MeV $^4He^{++}$ ions	22	1.28	1.06	1.14	1.25	Barr & Schuler (1957)
0.8-MeV neutrons	~60	1.25	0.68	0.99	1.27	Katsumura et al. (1989, 1992)
5.3-MeV α-particles (^{210}Po)	88	0.6	0.3	1.4	1.25	Vladimirova (1999)
		0.6	0.5	1.57	1.45	Lefort & Tarrago (1959)
		0.49	0.5	1.57	1.25	Mariano & Santos (1967)
		0.77	0.67	1.51	1.56	Burch (1959)
$^{10}B(n, \alpha)^7Li$ recoils	~250	0.23	0.41	1.66	1.57	Barr & Schuler (1957)
		0.69	0.37	1.08	1.24	Pucheault & Sigli (1976)
20-MeV $^{12}C^{6+}$ ions	535	0.29	0.19	1.48	1.18	LaVerne (1989)
Fission fragments from dissolved ^{252}Cf	~4000	0	0	2.1	0.96	Bibler (1975) [(c)]

[(a)] "Incident" LET values, taken from WATT (1996).

[(b)] In 0.05 *M* H_2SO_4 solutions (pH ~ 1.3).

[(c)] The author also includes a yield of $HO_2^\bullet$ radicals of 0.5 molec./100 eV.

There are two exceptions to this rule: (i) the primary yield of $HO_2^\bullet$ (or its basic form $O_2^{\bullet-}$ at neutral pH) radicals, which are the most abundant radicals produced at high LET, increases with increasing LET, a behavior that is akin to the molecular yields, and (ii) the primary yield of H_2O_2 rises with increasing LET to a maximum,

after which it falls. The origin of these two exceptions has received much attention recently. It has been hypothesized (FERRADINI and JAY-GERIN, 1998) and then demonstrated using Monte-Carlo track structure simulations that multiple ionization of water molecules (and especially the mechanism of double ionization) is responsible for the formation of $HO_2^{\bullet}$ at high LET (MEESUNGNOEN et al., 2003; MEESUNGNOEN and JAY-GERIN, 2005*a*; GERVAIS et al., 2006) and for the maximum in $G_{H_2O_2}$ as a function of LET (MEESUNGNOEN and JAY-GERIN, 2005*a*, *b*). Moreover, MEESUNGNOEN and JAY-GERIN (2009) have shown that this mechanism of multiple ionization could also be at the origin of the substantial production in situ of molecular oxygen observed in heavy-ion tracks (for radiation of low LET, O_2 is *not* a radiolytic product), a result of particular significance in radiobiology and of practical relevance in radiotherapy.

The exact structure of a particle track is determined by a number of particle characteristics including its charge, energy, LET, and other parameters. These characteristics are responsible not only for the detailed geometry of the track (commonly referred to as the "track structure"), but also for the subsequent chemistry that occurs in it. At high LET, tracks can be visualized as a cylinder; this cylinder has a "core" of high ionization density, due to the passage of the incident particle, and is surrounded by a region (called the "penumbra") of less dense ionizations arising from comparatively low-LET secondary electrons (or "δ-rays") that are ejected at various angles (depending upon their energies) to the track axis (MOZUMDER et al., 1968). Based on the quantum mechanical theory of stopping power ($-dE/dx$, usually assumed to be equivalent to LET) of BETHE (1930), one can readily observe that LET does not uniquely characterize product yields in the heavy ion radiolysis of water (for a review, see: LAVERNE, 2004). This irradiating-ion dependence of the yields at a given LET is explained by the differences in the microscopic track structure due to the spatial distributions of the ejected secondary electrons (for example, see: MUROYA et al., 2006). Nevertheless, the LET still remains nowadays the most commonly used parameter to describe the observed yields because it gives a

general, although not an exact, representation of the concentration of reactive species in the particle track.

I.1.5 The influence of temperature

An obvious reason for understanding the radiation chemistry of liquid water at high temperatures is the technologically important application of such knowledge to the design and chemistry control of water-cooled nuclear power reactors, which currently operate with temperatures in the range ~250-330 °C and ~70-150 atm pressure. The aqueous radiolysis products generated in these reactors must be assessed since they can induce deleterious corrosion, hydriding, and cracking processes both in the core and in the associated piping components (there are many papers on this subject, the following are just examples: BURNS and MOORE, 1976; COHEN, 1980; HICKEL, 1991; ELLIOT, 1994; ELLIOT et al., 1996*a*; McCRACKEN et al., 1998; BUXTON, 2001; STUART et al., 2002; KATSUMURA, 2004; CHRISTENSEN, 2006; EDWARDS et al., 2007). However, direct measurement of the chemistry in reactor cores is extremely difficult. The extreme conditions of high temperature, pressure, and mixed neutron/gamma radiation fields are, of course, not compatible with normal chemical instrumentation. For these reasons, theoretical calculations and chemical models have been used, with some simplifying assumptions, to simulate and predict the detailed radiation chemistry of the water in the core and the consequences for materials.

Of basic interest is knowledge of the effect of temperature on the primary yields of the radiolysis products e^-_{aq}, $H^\bullet$, $^\bullet OH$, H_2, and H_2O_2, as well as on the rate constants of their reactions. Experimental determinations using low-LET (gamma or fast electron) radiation at temperatures from ambient up to ~300 °C (KENT and SIMS, 1992*a*, *b*; ELLIOT et al., 1993, 1996*a*, *b*; ELLIOT, 1994; SUNARYO et al., 1995*a*, *b*; ISHIGURE et al., 1995; KATSUMURA et al., 1998; ŠTEFANIĆ and LAVERNE, 2002;

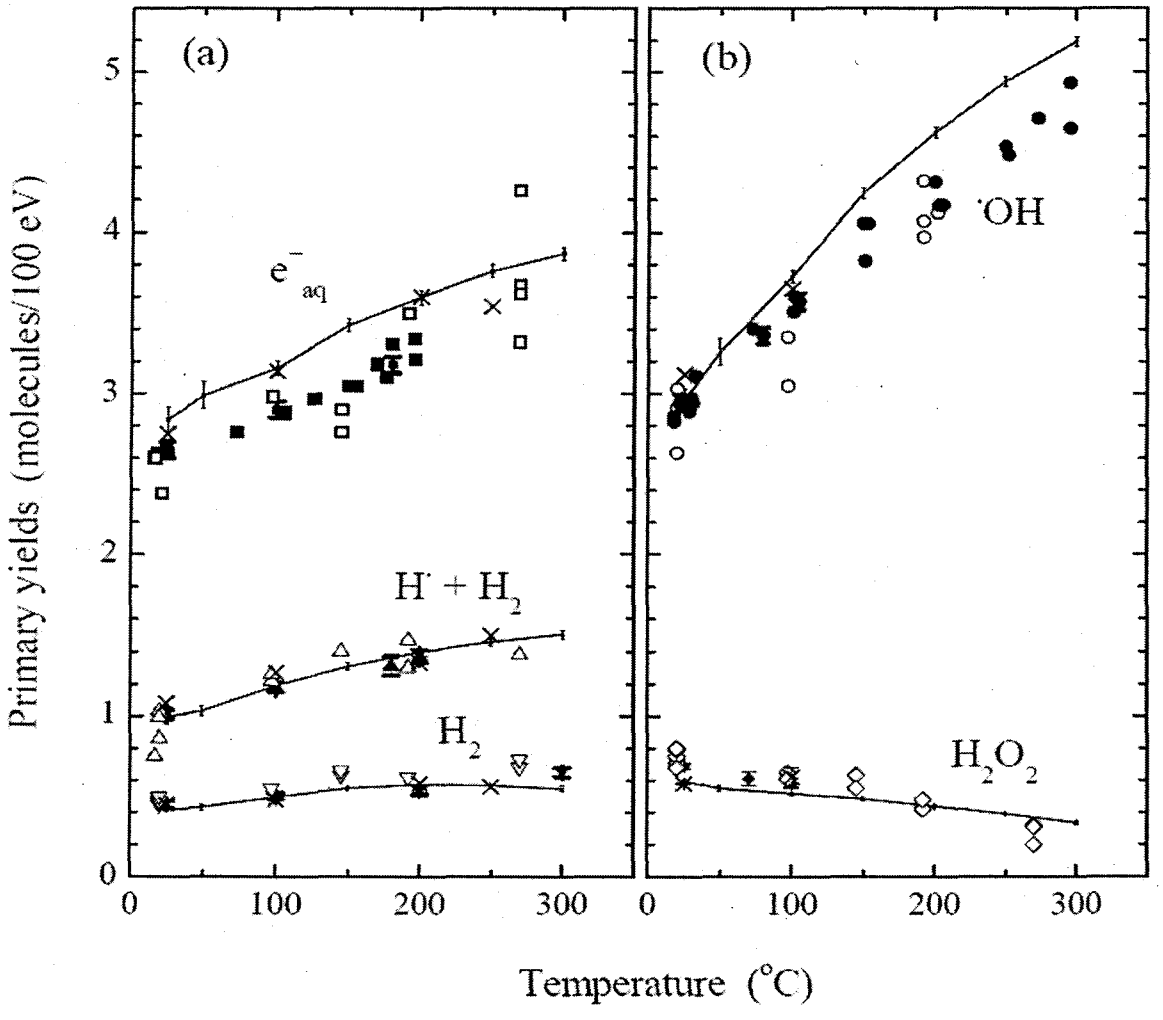

Figure I.3: Variation of *G*-values (in molec./100 eV) for the radiolysis of liquid water as a function of temperature: (a) "reducing" species $G_{e^-_{aq}}$, $G_{H^{\cdot}} + G_{H_2}$, and G_{H_2} and (b) "oxidizing" species $G_{^{\cdot}OH}$ and $G_{H_2O_2}$. The solid lines represent the Monte-Carlo simulated results of HERVÉ DU PENHOAT et al. (2000), obtained at 10^{-7} s from averages over 150 track segments of 300-MeV protons (average LET ~ 0.3 keV/μm). The various symbols are experimental data (from HERVÉ DU PENHOAT et al., 2000).

see also: MEESUNGNOEN et al., 2002*a* and references therein) have shown that $G_{e^-_{aq}}$, $G_{e^-_{aq}}$, $G_{H^{\cdot}}$, $G_{^{\cdot}OH}$, and G_{H_2} continuously increase, while $G_{H_2O_2}$ decreases, with increasing temperature. Measured *G*-values are shown in Fig. I.3. ELLIOT and coworkers (1993, 1994) proposed the following equations (obtained from least-

square fits to the experimental data) for the temperature dependences of the radical and molecular radiolysis yields (expressed in molec./100 eV):

$$G_{e^-_{aq}} = 2.56 + 3.40 \times 10^{-3}\, t$$

$$G_{\cdot OH} = 2.64 + 7.17 \times 10^{-3}\, t$$

$$G_{H_2} + G_{H\cdot} = 0.97 + 1.98 \times 10^{-3}\, t \qquad G_{H_2} = 0.43 + 0.69 \times 10^{-3}\, t$$

$$G_{H\cdot} = 0.54 + 1.28 \times 10^{-3}\, t \text{ (calculated by difference)}$$

$$G_{H_2O_2} = 0.72 - 1.49 \times 10^{-3}\, t\,,^{2}$$

where t is the temperature in °C.[3]

---

[2] In a recent work, ŠTEFANIĆ and LAVERNE (2002) measured the temperature dependence of the H_2O_2 production in the γ-radiolysis of neutral water over the range 25-150 °C, using methanol, ethanol, and bromide as •OH radical scavengers. They also reported a correlation between the temperature and the G-value, given by $G_{H_2O_2} = 0.78 - 2.43 \times 10^{-3}\, t$ for methanol and $0.74 - 2.40 \times 10^{-3}\, t$ for bromide. For both of the scavengers examined, these correlations give larger negative slopes than those of ELLIOT and coworkers (1993, 1994) and KENT and SIMS (1992*a*, *b*), suggesting that the yield of H_2O_2 decreases faster with increasing temperature.

[3] In the past few years, measurements of the yields for e^-_{aq}, H• atom, H_2, and •OH radical production in low-LET radiolysis of water have been extended up to ~400 °C, i.e., beyond the thermodynamic critical point of water (t_c = 373.95 °C, P_c = 217.7 atm). Very peculiar, and even sometimes contradictory, behaviors have been observed thus far in going from the subcritical to the supercritical regime (BURNS and MARSH, 1981; SIMS, 2006; LIN et al., 2004, 2005, 2008; JANIK et al., 2007). Note here that supercritical water is of particular interest nowadays because of its possible use as the heat transport medium in the next-generation ("Generation IV") technologies of nuclear reactors aimed at supplying future worldwide needs for electricity, hydrogen, and other products (OKA and KOSHIZUKA, 1998; GUZONAS

These observed temperature dependences of the G-values have been reproduced satisfactorily by deterministic diffusion-kinetic modeling of spur processes (KABAKCHI and BUGAENKO, 1992; LAVERNE and PIMBLOTT, 1993; SWIATLA-WOJCIK and BUXTON, 1995, 1998, 2000) and Monte-Carlo simulations (HERVÉ DU PENHOAT et al., 2000, 2001). That the yields of free radicals increase with temperature is a matter that can readily be explained from the fact that many important reactions are not diffusion controlled and therefore have rate constants that increase *less* steeply with temperature than do the diffusion coefficients of the individual species (for example, see: ELLIOT et al., 1996*b*; HERVÉ DU PENHOAT et al., 2000).[4] In other words, as the temperature is raised, diffusion of free radical species out of spurs/tracks increases more rapidly than recombination, and one should have less molecular recombination products (namely, water, H_2, and H_2O_2) (ELLIOT et al., 1993; JANIK et al., 2007). One difficulty, however, appears in explaining the experimentally observed monotonic increase of G_{H_2}. In fact, although the above calculations have explained an increase of G_{H_2} up to about 200 °C as resulting from the bimolecular reaction of e^-_{aq} (SWIATLA-WOJCIK and BUXTON, 1995; HERVÉ DU PENHOAT et al., 2000), above 200 °C the computed G_{H_2} tends to decrease with increasing temperature (see Fig. I.3). The fact that G_{H_2} continues to increase with temperature (even though the yield of the other molecular recombination product, H_2O_2, decreases) raises interesting questions about the physicochemical stage of the radiolysis of water such as, for example, the need to postulate an additional channel for H_2 formation (SWIATLA-WOJCIK and BUXTON, 2005; BARTELS, 2009).

---

et al., 2009 and references therein). However, this range of elevated temperatures (and pressures) is beyond the scope of the present study.

[4] Just recall here that, most generally, the yield of a species that escapes the spur/track depends on the competition between reactions in the spur/track and escape by diffusion out of the spur/track.

Rate constants are sensitive functions of temperature and for this reason are important parameters in predictive modeling of high temperature water chemistry. What is generally known is the temperature dependence of the observed reaction rate constant (k_{obs}), from which it is possible to extract information on the temperature dependences of the "activation" and "diffusion" processes that are involved in the reaction. For reactions whose rates are nearly diffusion-controlled at room temperature, k_{obs} is best described by the Noyes equation:

$$\frac{1}{k_{obs}} = \frac{1}{k_{diff}} + \frac{1}{k_{act}} , \tag{17}$$

where k_{diff} is the rate constant for a truly diffusion-controlled reaction and k_{act} is the rate constant that would be measured if diffusion had no influence on the reaction rate (NOYES, 1961). A number of reactions pertinent to the radiation chemistry of water have been found to be best described by Eq. (17) (see, for example: ELLIOT, 1994). The Arrhenius equation is used to evaluate k_{act} empirically:

$$k_{act} = A \exp(-E_{act}/RT) , \tag{18}$$

where E_{act} is the activation energy of the process, A is referred to as the pre-exponential factor, R is the gas constant and T is the absolute temperature (in Kelvin). k_{diff} is given by the Smoluchowski equation (see, for example: ELLIOT et al., 1990; ELLIOT, 1994; SWIATLA-WOJCIK and BUXTON, 1995; HERVÉ DU PENHOAT et al., 2000):

$$k_{diff} = 4\pi \beta N_{Av} (D_A + D_B) a_{A,B} \tag{19}$$

where N_{Av} is Avogadro's number, $(D_A + D_B)$ is the sum of diffusion coefficients for both reacting species, β is a spin statistical factor for radical-radical reactions, and $a_{A,B}$ is the encounter (or reaction) distance. When the reactants are ions, Eq. (19) is multiplied by the Debye factor (DEBYE, 1942):

$$f_D = \frac{\delta}{e^{\delta} - 1} \tag{20}$$

where δ is given by

$$\delta = \frac{Z_A Z_B e^2}{4\pi\varepsilon_0\, \varepsilon(T)\, a_{A,B}\, k_B T}\ , \tag{21}$$

where Z_A and Z_B are the charge on the ions, e is the electron charge, ε_0 is the permittivity of free space, $\varepsilon(T)$ is the dielectric constant of the medium, and k_B is Boltzmann's constant.[5]

A few reactions, all involving the hydrated electron (BUXTON, 1991, 2001), have been found to exhibit *negative* Arrhenius activation energies at elevated temperatures. In other words, the rate of reaction falls with increasing temperature. We can cite here, for example, the bimolecular recombination of two e^-_{aq} ($e^-_{aq} + e^-_{aq} \rightarrow H_2 + 2\ OH^-$) (CHRISTENSEN and SEHESTED, 1986; STUART et al., 2002; MARIN et al., 2007), an important contributor to G_{H_2} in water radiolysis and a fascinating reaction from the point of view of fundamental chemical physics. This is

---

[5] Note that, in the case of a reaction between identical species, the term 4π in Eq. (19) is replaced by 2π in order to avoid counting twice every pair of reactants. For reactions between ions, both k_{diff} and k_{act} must be corrected for the effect of ionic strength (see Sect.III.2). In evaluating the reaction between two radicals, the electron spin of the radical has to be taken into account; the statistical spin factor β introduced in Eq. (19) accounts for the fact that only those random encounters that produce a *singlet* electronic state will contribute to the reaction rate. For free radicals, such a singlet state is reactive whereas the complementary triplet state is not. The value of β is actually set by the spin relaxation time of the radicals involved. For most radicals, the spin-lattice relaxation time is much longer than the encounter time (i.e., there are no triplet-singlet transitions during the encounter), so that a β of 0.25 is appropriate (FISCHER and PAUL, 1987; ELLIOT et al., 1990; ELLIOT, 1994; FRONGILLO et al., 1998).

illustrated in Fig. I.4. As we can see, k_{obs} shows basically Arrhenius behavior up to 150 °C with an activation energy of 20 kJ/mol, reaches a maximum value of 4.5 × 10^{10} M^{-1} s^{-1} at 150 °C, and then rapidly declines above this temperature. The mechanistic details of the apparent peculiarity of this reaction have been discussed by several authors (CHRISTENSEN and SEHESTED, 1986; FERRADINI and JAY-GERIN, 1993; HAN and BARTELS, 1992; STUART et al., 2002; MARIN et al., 2007).

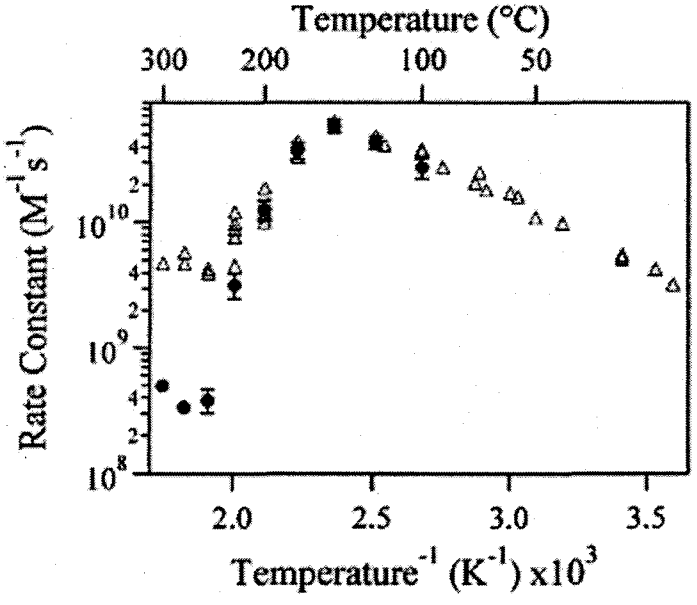

Figure I.4: Arrhenius plot of the rate constant for the self-reaction of the hydrated electron in water. Data are from MARIN et al. (2007) (solid circles) and CHRISTENSEN and SEHESTED (1986) (open triangles) (from MARIN et al., 2007).

Very little information is available for the temperature dependence of fast neutron *G*-values. At the University of Tokyo, experiments on 0.4 *M* H_2SO_4 solutions at temperatures up to 250 °C were carried out in the "YAYOI" source reactor where 95% of the radiation energy came from fast neutrons (KATSUMURA et al., 1985, 1989). In these experiments, the average energy and LET of the fast neutrons were calculated to be ~0.8 MeV and ~60 keV/μm, respectively (KATSUMURA et al., 1989, 1992). The *G*-values of water decomposition products were determined by using a combination of the aerated and deaerated Fricke dosimeter and the ceric sulfate

dosimeter. The data reported by these authors (KATSUMURA et al., 1989, 1992) indicated that the *G*-value for free-radical species increased significantly with temperature whereas the yield of the molecular species decreased. ELLIOT and coworkers (1996*a*, *b*) used another approach to estimate the temperature dependence of *G*-values for fast neutron radiolysis. In water, most of the fast-neutron energy is deposited through ionization of the water by recoil protons, which are formed from the elastic scattering of the neutrons (see Chapter II). The initial energy of these protons varies from the maximum energy of the fast neutrons down to zero; the actual distribution of the proton energies can easily be calculated (see Chapter II). For example, for an incident 2-MeV neutron,[6] it can be shown (see Chapter II) that the most significant contribution to the radiolysis comes from the first four collisions that generate recoil protons, having LET values of ~23, 43, 71, and 80 keV/μm, respectively. The radiation chemical yields corresponding to these four values of LET (assuming that LET can be used as a unifying parameter to connect yields) can be estimated experimentally (using different high-energy ion beam radiolysis results, as shown in Figs. 1 and 2 of ELLIOT et al., 1996*b*). The fast-neutron yields are then the sum of these yields after appropriate weighting has been made according to the fraction of total energy deposited by each of these protons.[7] Using this procedure, ELLIOT and coworkers (1996*a*, *b*) estimated the *G*-values of primary species for an incident 2-MeV neutron at 25, 250, and 300 °C (see Table 3). Finally, let us mention

---

[6] The 2-MeV neutron was chosen by these authors because the in-reactor fission-neutron flux peaks at this energy (COHEN, 1980).

[7] This modeling approach to estimating the water radiolysis yields for the action of neutron radiation has been employed in the present work. As it will be seen in Chapters III and IV, Monte-Carlo simulations are used to calculate the yields corresponding to each of the recoil ions considered. Note that this procedure has also been employed by other authors (for example, see: LAWSON and PORTER, 1975; GORDON et al., 1983; SWIATLA-WOJCIK and BUXTON, 1998).

the work of SUNARYO et al. (1994, 1995*a*, *b*) who reported experimental *G*-values for the decomposition products of neutral water up to 250 °C for ~0.8-MeV fast neutrons from the YAYOI reactor (see also: ISHIGURE et al., 1995; KATSUMURA et al., 1998).[8] Their data, also shown in Table 3, are qualitatively similar to those of ELLIOT et al. (1996*b*) except for $G_{H_2O_2}$, which they report as being much larger and always increasing with temperature. Possible physical and chemical reasons for these differences have been discussed by McCRACKEN et al. (1998).

Table 3: Dependence of the primary yields (in molec./100 eV) of radical and molecular products for neutral water irradiated with fast neutrons on temperature.

Temperature (°C)	$G_{e^-_{aq}}$	$G_{H\cdot}$	G_{H_2}	$G_{\cdot OH}$	$G_{H_2O_2}$	References
25	0.52	0.34	0.97	0.72	0.92	Elliot et al. (1996*b*) [(a)]
	0.43	0.58	1.07	0.86-0.70	1.14-1.22	Katsumura et al. (1998)
100	0.49	0.78	1.2	0.89-1.68	1.39-1.0	Ishigure et al. (1995)
200	0.72	0.64	1.26	1.1	1.37	Ishigure et al. (1995)
250	0.60	0.34	1.16	2.39	0.33	Elliot et al. (1996*b*) [(a)]
	0.68	0.52	1.52	1.66	1.29	Sunaryo et al. (1995*b*)
300	0.61	0.34	1.21	2.76	0.19	Elliot et al. (1996*b*) [(a)]

[(a)] The authors also include a yield of $HO_2^{\cdot}$ radicals of 0.05 molec./100 eV.

[8] These are the only data that have been obtained using reactor radiation.

I.2 The Fricke, or ferrous sulfate, chemical dosimeter

In chemical dosimetry, radiation dose is determined from the chemical change produced in an appropriate medium. Any well-characterized quantitative chemical reaction may serve as the basis for a dosimeter. One of the most studied systems in radiation chemistry is the air-saturated (~2.5×10^{-4} *M* O_2) solution of 1-10 m*M* ferrous sulfate in aqueous 0.4 *M* H_2SO_4, which is referred to as the "*Fricke dosimeter*" after Hugo Fricke who first published accounts of its properties in 1927-1929 (FRICKE and MORSE, 1927, 1929). Of all aqueous systems studied, the Fricke, or ferrous sulfate, dosimeter is the best understood, and the most widely used, liquid chemical dosimeter. It is straightforward to prepare and it provides an easy quantification of the energy deposited by ionizing radiation. The chemistry of this system is based upon the oxidation of ferrous ions to ferric ions by the oxidizing species $^{\bullet}OH$, $HO_2^{\bullet}$ (the radiation-induced reducing radicals e^-_{aq} and $H^{\bullet}$ are rapidly transformed into $HO_2^{\bullet}$ at low pH and in the presence of oxygen; see Chapter III), and H_2O_2 that are produced in the radiolytic decomposition of water (ALLEN, 1961; FRICKE and HART, 1966; DAS, 1971; SPINKS and WOODS, 1990). From this mechanism, the yield of Fe^{3+} ions in an irradiated Fricke dosimeter can be expressed in terms of the escape yields of the radical and molecular products of the radiolysis of the solution by the following stoichiometric equation (SPINKS and WOODS, 1990):

$$G(Fe^{3+}) = 3\,(G_{e^-_{aq}+H^{\bullet}} + G_{HO_2^{\bullet}}) + G_{^{\bullet}OH} + 2\,G_{H_2O_2} \qquad (22)$$

This relationship, which has been confirmed by experiment, shows that the production of Fe^{3+} ions is highly sensitive to factors that alter the free-radical yields, especially the yield of $H^{\bullet}$ atoms. In particular $G(Fe^{3+})$ depends on the type of the radiation used. Data by a number of different authors have shown that $G(Fe^{3+})$ steadily decreases with increasing LET, this dependence reflecting the lower yields of radicals that escape the high-LET track as compared with low-LET radiolysis (for example, see: AUTSAVAPROMPORN et al., 2007, and references therein).

Representative values of $G(Fe^{3+})$ for several types of radiation, including fast neutrons, are collected in Table 4.

Table 4: Values of ferric-ion yields $G(Fe^{3+})$ (in molec./100 eV) for the Fricke dosimeter irradiated with different types of radiation, at room temperature.

Radiation	LET [(a)] (keV/μm)	$G(Fe^{3+})$	References
^{60}Co γ-rays	~0.3	15.6 ± 0.3	Hochanadel & Ghormley (1953)
2-MeV cathode rays (electrons)	~0.3	15.45 ± 0.11	Schuler & Allen (1956)
20-MeV X-rays	~0.3	15.55 ± 0.1	Klassen et al. (1999)
^{137}Cs γ-rays	~0.91 [(b)]	15.3 ± 0.3	ICRU Report 34 (1982)
250-kV X-rays	1.9	14.9 ± 0.8	Back & Miller (1957)
60-kV$_p$ X-rays [(c)]	2.6	14.1 ± 0.3	Fregene (1967)
8-kV X-rays (Cu)	6.5	13.4 ± 0.6	Lefort (1957, 1958)
$^3H^+$ β-particles (mean energy: ~5.7 keV)	9.5	12.7 ± 0.3	Hart (1954)
23-MeV deuterons	11.9	12.15 ± 0.45	Elliot et al. (1996)
2.466-keV monochromatic synchrotron X-rays	~14	9.36 ± 0.48	Watanabe et al. (1995)
12-MeV deuterons	17.7	9.81	Hart et al. (1956)
7.6-MeV neutrons	~21	9.4 ± 0.6	Greene et al. (1975)
3-MeV neutrons	~34.5	7.2 ± 0.6	Pejuan & Kühn (1981)
2.3-MeV neutrons (^{252}Cf)	~39.5	7.5 ± 1.1	Greene et al. (1973*a*)
1.5-MeV neutrons	~47	7.6 ± 0.9	Law et al. (1974)
0.8-MeV neutrons (reactor YAYOI)	~60	6.95	Katsumura et al. (1989, 1992)

[(a)] "Mean" LET values, taken from WATT (1996) and AUTSAVAPROMPORN et al. (2007).

[(b)] MEESUNGNOEN et al. (2001*a*).

[(c)] In 0.05 *M* H_2SO_4 solutions (pH ~ 1.3).

The part played by sulfuric acid and its anions is generally ignored when the ferrous sulfate system is described, although with the standard dosimeter solution (0.4 *M* H_2SO_4) a certain proportion of the hydroxyl radicals react with HSO_4^- ions to form the sulfate radical $SO_4^{\bullet-}$ [see reaction (15)]. However, this does not affect the overall ferric ion yield $G(Fe^{3+})$, which remains the same as given by Eq. (22), since $SO_4^{\bullet-}$ (or, equivalently, its protonated form $HSO_4^{\bullet}$, although no pK_a value has been determined) is stoichiometrically equivalent to $^{\bullet}OH$, oxidizing one ferrous ion to a ferric ion (NETA et al., 1988):

$$Fe^{2+} + SO_4^{\bullet-} \rightarrow Fe^{3+} + SO_4^{2-} \qquad (23)$$

($k_{23} \approx 2.79 \times 10^8\ M^{-1}\ s^{-1}$, taking into account ionic strength effects; see below)

(note that, contrary to HSO_4^-, the sulfate ion SO_4^{2-} has been reported to be unreactive toward $^{\bullet}OH$) or dimerizing to a product ($S_2O_8^{2-}$) that, like H_2O_2, oxidizes two ferrous ions (SPINKS and WOODS, 1990).

The usual range of the Fricke dosimeter is from ~30 to 400 Gy. The upper limit is set by oxygen depletion [when oxygen is consumed, $G(Fe^{3+})$ decreases to ~8.2 molec./100 eV for fast electron and ^{60}Co γ radiation; see, for example: FRICKE and HART, 1966] and the lower limit by the analytical method. By suitable modifications of the composition of the system or of its analysis, it is possible to extend the useful range beyond these limits. Higher doses can be measured by means of the "super" Fricke dosimeter, which consists of 10 m*M* Fe^{2+} in 0.4 *M* H_2SO_4 and is saturated with pure oxygen (~1.25×10^{-3} *M* O_2). This system can be used up to 2000 Gy.

The Fricke dosimeter is widely accepted in radiation-chemical work because of the accuracy, reproducibility, and linearity of its response as a function of dose (with care, Fricke dosimetry is capable of 0.1% precision for ^{60}Co γ-rays, high-energy X-rays or fast electrons) (KLASSEN et al., 1999). It has been accurately standardized by calorimetry, ionization measurements, and other physical methods, and is nowadays used not only for absolute dose measurements but also as a standard

against which most other systems are calibrated (for example, see: ICRU REPORT 34, 1982; SPINKS and WOODS, 1990).

I.3 Research objectives

This study addresses the effect of fast neutrons on the chemistry and the yield of Fe^{2+} oxidation of the Fricke dosimeter. Following a procedure already employed by other authors (for example, see: LAWSON and PORTER, 1975; GORDON et al., 1983; ELLIOT et al., 1996*a*; SWIATLA-WOJCIK and BUXTON, 1998), the neutron *G*-values reported here are calculated from the weighted *G*-values for the recoil charged particles (mainly protons, or deuterons for the case of heavy water, and to a smaller extent, oxygen nuclei) released by neutron interactions in the $FeSO_4$ medium. Monte-Carlo computer simulations are used (i) to model the physicochemical development, the nonhomogeneous chemical kinetics, and the diffusion of the reactive species induced by these recoil ions in radiolysis, and (ii) to determine the corresponding ferric-ion yields. As is well-known, the combined application of stochastic track structure simulation and track chemistry modeling has proven to offer an efficient approach (i) to understand the underlying reaction mechanisms and pathways by which radiolytic species are formed at the molecular level following irradiation and (ii) to place on a quantitative basis the effects of the various parameters that can influence the radiation chemical data (for a review, see: BALLARINI et al., 2000). This present work focuses, in particular, on the temperature dependence of the oxidation of Fe^{2+} to Fe^{3+} in the fast neutron radiolysis of the Fricke solution (see, for example: HERVÉ DU PENHOAT et al., 2000; BĚGUSOVÁ and PIMBLOTT, 2002).

More specifically, the main objectives of this work are:

(i) To study the oxidation of ferrous ions in the Fricke dosimeter subjected to fast (~0.5-10 MeV) neutron irradiation, and to calculate the time profiles of the chemical yield of ferric ions $G(Fe^{3+})$.

(ii) To investigate the dependence of $G(Fe^{3+})$ on the energy of incident neutrons over the range of temperature from ambient up to ~300 °C.

(iii) To compare the simulation results with experimental data currently available in the literature in order to validate the assumptions employed in the calculations.

CHAPTER II

INTERACTION OF NEUTRONS IN WATER

II.1 Review of some basic neutron physics

II.1.1 Elementary facts about the neutron

The neutron (*n*), a radioactive particle of charge zero and mass slightly greater (by ~1.293 MeV) than that of a proton (*p*), was discovered by James Chadwick in the Cavendish Laboratory, Cambridge, England (CHADWICK, 1932*a*, *b*). Like the proton, it is a spin one-half fermion. Together with the proton, the neutron is a constituent particle of all atomic nuclei (except, obviously, ^{1}H) (recall here that protons and neutrons attract each other with a short range but very strong force, called the *nuclear force*; in nuclei, they are referred to as *nucleons*). While neutrons can be stable when bound inside nuclei, free (or isolated) neutrons are unstable and undergo β-decay, disintegrating into a proton, an electron (with a maximum kinetic energy of 782 keV), and an antineutrino ($\bar{\nu}$) with a characteristic half-life of 10.61 ± 0.16 min (CHRISTENSEN et al., 1972):

$$n \rightarrow p + e^- + \bar{\nu} \ . \qquad (24)$$

Even though it is not a chemical element, the free neutron is often included in tables of nuclides. It is then considered to have an atomic number of zero and a mass number of one.

II.1.2 Neutron energy ranges

The interaction of the neutron depends very much on its kinetic energy. In this respect, it is customary to class the possible neutron kinetic energies into four ranges to facilitate discussion about the different possible interactions of neutrons with matter. Table 5 lists some commonly used energy ranges and the names applied

(ANDERSON, 1984). The categories are useful since dominant interactions can usually be identified in the regions given.

Table 5: Neutron energy ranges. The actual boundary energies do not imply a discontinuous change in properties and these demarcations should not be emphasized in themselves (from ANDERSON, 1984).

Type	Energy range
Slow neutrons [a]	$0 \leq E_n < 1$ keV
Intermediate neutrons	1 keV $\leq E_n <$ 500 keV
Fast neutrons	500 keV $\leq E_n <$ 10 MeV
High-energy neutrons	$E_n \geq$ 10 MeV

[a] The "slow" neutron category listed here includes several other well-known groups, such as "thermal" and "cold" neutrons. Thermal neutrons are in thermal equilibrium with the medium in which they are diffusing; they possess a Maxwell-Boltzmann velocity distribution determined by the absolute temperature of the medium. At 20 °C, thermal neutrons have a most probable energy of 0.025 eV. Cold neutrons have energies considerably less than 0.025 eV, often as low as 0.001 eV.

Beams of neutrons can be produced from a variety of nuclear reactions. We cannot accelerate neutrons as we can for charged particles, but we can start with high-energy neutrons and reduce their energy through collisions with atoms of various materials. This process of slowing is called "moderating" the neutrons (KRANE, 1988).

II.1.3 Types of interactions

Because neutrons carry no charge, their interaction with electrons is exceedingly small, and direct ionization by neutrons in passing through matter is a completely negligible effect. The interaction of neutrons with matter is confined to nuclear effects and may be one of two major types: "scattering" or "absorption".

These include *elastic* and *inelastic scattering*, *nuclear reactions*, and *capture processes*. Figure II.1 shows the most important types of interactions (for reviews of the characteristics of the different types of neutron interactions, see, for example: AUXIER et al., 1968; RINARD, 1991). Note that a simple notation for nuclear reactions is used to give a concise indication of an interaction of interest and to distinguish between scattering and absorption reactions. If a neutron *n* impinges on a target nucleus T, a resultant nucleus R is formed and an outgoing particle *g* is released; this interaction is shown as T(*n*,*g*)R. To denote a type of interaction without regard for the initial and final nuclei involved, only the portion written in parentheses is shown. The symbols *n*, *p*, *d*, α, e^-, and γ, are used in this notation to represent neutron, proton, deuteron, α-particle, electron, and gamma ray, respectively.

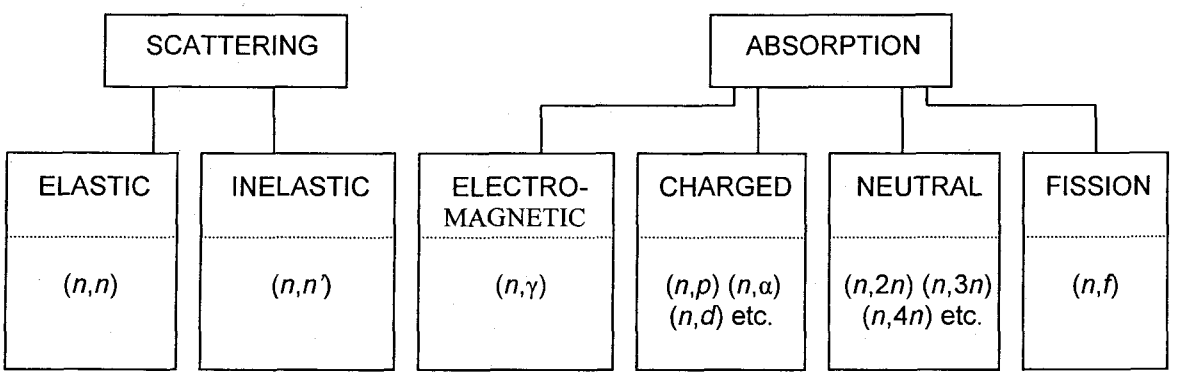

Figure II.1: Various categories of neutron interactions. The letters separated by commas in the parentheses show the incoming and outgoing particles (from RINARD, 1991).

When a neutron is scattered by a nucleus, its energy and direction change but the nucleus is left with the same number of protons and neutrons it had before the interaction. The nucleus will have some recoil velocity and it may be left in an excited state, which will lead to the eventual release of radiation. In "elastic" scattering, indicated by (*n*,*n*), the energy of the incident neutron is shared between the recoiling neutron and nucleus. "Inelastic" scattering, referred to (*n*,*n'*), is similar to elastic scattering except that the nucleus undergoes an internal rearrangement into an excited state from which it eventually releases radiation (most reactions are

accompanied by the emission of a nuclear deexcitation γ-ray); in this case, part of the original kinetic energy of the incoming neutron is used to place the nucleus into an excited state. Obviously, if all the excited states of the nucleus are too high in energy to be reached with the energy available from the incoming neutron, inelastic scattering is impossible. In particular, the hydrogen nucleus does not have internal excitation states, so only elastic scattering events can occur in that case. When a neutron is "absorbed" or "captured" by a nucleus, a wide range of radiation can be emitted or fission can be induced. The compound nucleus may rearrange its internal structure and release one or more γ-rays. Charged particles may also be emitted, the more common ones being protons, deuterons, and α-particles. The nucleus may also promptly reemit excess neutrons (note that the reemission of one neutron is indistinguishable from a scattering event). Finally, there may be a fission event in which, after the neutron is captured, the nucleus fragments into several parts with creation of fission products (nuclei of intermediate atomic weight) (*f*).

II.2 Slowing down of fast neutrons

II.2.1 Hydrogen-containing substances as the most effective media for neutron moderation

For "fast" neutrons (i.e., those with kinetic energies below about 10 MeV; see Table 5) which will concern us in this work, most slowing down is accomplished through a process of many successive "billiard-ball" elastic collisions with atomic nuclei, following the simple laws of conservation of energy and momentum of classical particle physics (note here that in this energy range, fast neutrons can be considered as non-relativistic particles, since their mass is much larger than their kinetic energy; the description of neutron elastic collision can thus be performed using non-relativistic mechanics). In elastic scattering, the total kinetic energy of the neutron and nucleus is unchanged by the interaction. During the interaction, a fraction of the neutron's kinetic energy is transferred to the nucleus. For a neutron of

kinetic energy E_n, encountering a nucleus of mass number A, the energy E_r transferred to the struck nucleus (assumed to be initially at rest) is given by (for example, see: AUXIER et al., 1968; FRIEDLANDER et al., 1981; ANDERSON, 1984; KRANE, 1988; RINARD, 1991):

$$E_r = E_n \frac{4A}{(1+A)^2} \cos^2 \theta_r , \tag{25}$$

where θ_r is the recoil-nucleus angle with respect to the original direction of travel of the neutron (in the laboratory system of coordinates). According to Eq. (25), E_r ranges from zero up to a *maximum*:

$$(E_r)_{\max} = E_n \frac{4A}{(1+A)^2}, \tag{26}$$

while the range for the kinetic energy retained by the scattered neutron (by energy conservation) is:

$$\left[1 - \frac{4A}{(1+A)^2}\right] E_n \le E'_n \le E_n , \tag{27}$$

If all energy transfers between zero and $(E_r)_{\max}$ are equally probable (i.e., if the elastic scattering angular distribution is spherically symmetric in the centre-of-mass system, which is certainly a good assumption at the energies considered here), the *average* recoil energy imparted to the struck nucleus after a collision is

$$\overline{E_r} = E_n \frac{2A}{(1+A)^2}, \tag{28}$$

which leads to

$$\overline{E'_n} = E_n \left[1 - \frac{2A}{(1+A)^2}\right] \tag{29}$$

for the average energy of the outgoing neutron (quantities with bars over them denote mean values). Clearly, Eqs. (28) and (29) show that the lighter the nucleus with which a neutron collides, the greater the fraction of the neutron's kinetic energy

that can be transferred in the elastic collision. In other words, in order to reduce the speed of neutrons (i.e., to *moderate* them) with the fewest number of elastic collisions, target nuclei with low atomic number should be used. Biological tissues and other materials containing a large proportion of hydrogen or deuterium (such as light or heavy water) are thus favored for slowing down of neutrons. In fact, for $A = 1$ (scattering from hydrogen), the average energy loss has its largest value of $E_n/2$.

II.2.2 Average logarithmic energy decrement per collision

Consider a series of moderating collisions $1 \rightarrow k$ for a single neutron. Suppose that the initial neutron kinetic energy is $(E_n)_0$ and the final value is $(E_n)_k$. Intermediate kinetic energies are $(E_n)_1$, $(E_n)_2$,..., $(E_n)_i$,..., and so forth, for k collisions. One can write (FRIEDLANDER et al., 1981):

$$(E_n)_k = (E_n)_0 \, f_1 \, f_2 \ldots f_i \ldots f_k \, , \tag{30}$$

where

$$f_i = \frac{(E_n)_i}{(E_n)_{i-1}} . \tag{31}$$

Average kinetic energy values are desired since one usually deals with a beam of many neutrons. Assuming again the scattering to be isotropic (in the centre-of-mass coordinates), the values of f_i are uniformly distributed between 1 and the minimum value $[1 - 4A/(1+A)^2]$ given by Eq. (27). It is clear that Eq. (30) has an infinite number of possible solutions for any value of k (above a certain minimum value determined by the mass of the scattering nucleus). At this stage, it would be tempting to put the average value of f from Eq. (29) into Eq. (30), but this would be wrong (for the same reason that the average square of a set of random numbers is, in general, not equal to the square of the average). To make the calculations quantitative, it is convenient to take the logarithm of both sides of Eq. (30) so that fractions can be separated before averaging:

$$\ln\left[\frac{(E_n)_k}{(E_n)_0}\right] = \ln\left(f_1 f_2 ... f_i ... f_k\right) = \sum_{i=1}^{k} \ln f_i \ . \tag{32}$$

The average value of $\ln[(E_n)_k/(E_n)_0]$ is then simply equal to the sum of the averages, that is,

$$\overline{\ln\left[\frac{(E_n)_k}{(E_n)_0}\right]} = k\,\overline{\ln f_i} \ . \tag{33}$$

This last equation represents the average result of k individual elastic scattering collisions. Defining the "*average change in the natural logarithm of the neutron energy after a single collision*" as $\xi = -\overline{\ln f_i}$ or, from Eq. (31), as

$$\xi = \overline{\ln\left[\frac{(E_n)_{i-1}}{(E_n)_i}\right]} \ , \tag{34}$$

it can be shown that (for a derivation, see, for example: FRIEDLANDER et al., 1981; ANDERSON, 1984; PERALTA, 2002)

$$\xi = 1 + \frac{(A-1)^2}{2A} \ln\left(\frac{A-1}{A+1}\right) . \tag{35}$$

The value of ξ is independent of the initial energy and it is this fact which makes it important. It follows that the average value of $\ln(E_n)$ is decreased after each collision by an amount ξ. After k collisions, the average decrease will be $k\xi$ and the average value of $\ln(E_n)_k$ is

$$\overline{\ln\left(E_n\right)_k} = \overline{\ln\left(E_n\right)_0} - k\xi \ , \tag{36}$$

which follows directly from Eq. (34).

For collisions with protons ξ becomes unity [note that Eq. (35) is not defined when $A = 1$, but the limit as A approaches unity is valid in this case]. When A is large ($A >> 1$), for heavy elements: $\xi \approx 2/A$. Equations (35) and (36) will be used copiously in the present study.

In studying neutron elastic scattering, we also resort frequently to the average number of collisions required to reduce a neutron's average energy from E_0 to a value which is characteristic of thermal motion (about 0.025 eV at ordinary room temperature). This number can be estimated by dividing $\ln(E_0/0.025)$ by ξ for the given medium. For several elements of interest, the number of collisions to "thermalize" a neutron of 2 MeV (energy typical for neutrons emitted in fission) is given in Table 6. It is worth noting that the whole slowing-down process requires less than 10^{-3} s (FRIEDLANDER et al., 1981).

Table 6: Scattering properties of moderating nuclei.

Element	Mass number (A)	ξ	Average number of collisions to thermalize
Hydrogen	1	1.000	18
Deuterium	2	0.725	25
Helium	4	0.425	43
Carbon	12	0.158	114
Oxygen	16	0.120	150
Uranium	238	0.0084	2166

II.2.3 Viewpoint of the radiation chemist, radiobiologist, and radiation therapist

The study of the action of fast neutrons is highly relevant to the various fields of radiation chemistry, radiobiology, and clinical radiation oncology. For radiation chemists, the scattering of neutrons by elastic collisions with atomic nuclei is a process of most interest since the recoil nuclei so generated will be charged and will deposit their ionizing energy into the stopping material in a similar manner to other (high-LET) heavy charged particles (see Sect. I.1.4) (Note that, in general, nuclear

reactions and capture, the latter giving an isotope of the target element, tend to be an embarrassment in radiation-chemical applications because of the possibility that the product nuclei will be radioactive, introducing handling and disposal problems; for example, see: SPINKS and WOODS, 1990). For the fast neutron radiolysis of water and aqueous systems and the incident neutron energies of interest to us here, the neutrons are stopped mainly by both protons and oxygen nuclei, producing a spectrum of recoil-ion energies from which the LET along the track of each densely ionizing heavy charged particle recoil released can be assigned and the chemical yields for the various species formed can be obtained (see Chapter III and IV).

From the viewpoint of the radiation biologist, because of the predominance of hydrogen in tissue, 85% of the energy of fast neutrons is transferred to hydrogen nuclei (protons) resulting in the emission of recoil protons. In other words, the *n-p* collision is by far the most important mechanism for energy transfer under these conditions. The remaining 15% of the absorbed dose is due to additional elastic scattering of neutrons with the light elements oxygen, carbon, and nitrogen (representing the major constituents of tissue), in that order of importance (BEWLEY, 1963, 1989; ICRU REPORT 26, 1977; ALPEN, 1998). As mentioned above (see Tables 2 and 4), fast neutrons are indirectly ionizing radiations, generating at a site of interaction charged particle recoils of high LET (>10 keV/μm). The biological properties of neutron beams are thus directly correlated to those of these high-LET recoiling nuclei produced. Compared to low-LET X- or γ-ray photons and fast electrons, the main radiobiological effects of fast neutron radiation are (for reviews, see, for example: BEWLEY, 1989; TUBIANA et al., 1990; WAMBERSIE et al. 1994; BRITTEN et al., 2001; HALL and GIACCIA, 2006):

(i) The cytotoxic effectiveness is less dependent on oxygen concentration or, in other words, the "oxygen effect" is less dominant. Recall here that a measure of the degree of cellular radiosensitization by O_2 is given by the "*oxygen enhancement ratio*" or OER, defined as the ratio of doses without and with oxygen needed to produce the *same* biological effect. For most cellular organisms, the value of OER

decreases with increasing LET (BARENDSEN, 1968; ALPER and BRYANT, 1974; MEESUNGNOEN and JAY-GERIN, 2009 and references therein). While the OER for cell killing is generally found between 2.5 and 3 for low-LET radiations with conventional dose rates, fast neutrons exhibit much lower OER values in the range from 1.5 to 1.8. Thus tumors containing hypoxic cells are, in principle, less protected against neutrons.

(ii) DNA damage is less repairable by tumor cells than that induced by photons or fast electrons and the efficiency of cell killing per unit dose is increased. In fact, low-LET γ or X rays will cause mostly single strand breaks of the DNA helix, as the ionization density is low and no target is likely to be hit more than once. Single strand breaks of DNA molecules can be readily repaired, and so the effect on the target cell is not necessarily lethal. By contrast, the high-LET charged particles produced from neutron irradiation cause many ionizations and excitations in close proximity as they traverse a cell, and so double-strand breaks (DSB) of the DNA molecule and other more complex clustered DNA lesions, in which DSB lesions are associated with different types of DNA damage (such as base and sugar modifications, base losses, and DNA-DNA and DNA-protein crosslinks), are possible (WARD, 1988; GOODHEAD, 1994; BOUDAÏFFA et al., 2000; VON SONNTAG, 2006). These "clustered" types of lesions, whose complexity increases with increasing LET, are much more difficult for a cell to repair, and more likely lead to cell death.

This increased efficiency of cell killing by high-LET neutron beams compared with photons per unit of absorbed dose can be quantified by the "*relative biological effectiveness*" or RBE, defined as the ratio of the dose of a "reference radiation" (normally 250-kV X-rays or ^{60}Co γ-rays) to the dose of the radiation under study that is necessary to produce the *same* level of biological effect. Because of the high LET, the RBE of fast neutrons is 2-6 times that of X-ray photons, with a mean value of about 4 (WAMBERSIE and MENZEL, 1997; SLABBERT et al., 2000; SÖDERBERG, 2007). This means that 1 Gy of fast neutrons is equal to 4 Gy of X-rays. These RBE values were found in many biological systems, including bacteria, plants,

transplanted animal cancers, and human tumor cell lines spanning a wide range of radiosensitivities. It should be noted here that the RBE of fast neutrons depends not only on the dose level or fractionation and the specific biological endpoint used, but also on the LET distribution of charged recoil particles and on neutron energy. Therefore, fast neutron beams produced with different energy spectra at different facilities generally have different RBE values (HALL et al., 1992; PIGNOL and SLABBERT, 2001). Actual evaluations must also account for the low-LET gamma-ray component always present in a neutron radiation field or generated by nuclear reactions in the system. As will be discussed in Chapter IV, these mixed-field situations usually lead to complications due to the difficulty in assessing the energy deposited by each of the qualitatively different radiation types, or in other words, in determining the separate absorbed doses of neutrons and of photons (ICRU REPORT 26, 1977; McCRACKEN et al., 1998; EDWARDS et al., 2007).

(iii) The variation in cell response with the phase of the mitotic cell cycle has a less pronounced influence on cell killing (for example, see: CHAPMAN, 1980).

Because of the basic radiobiological advantages of high-LET radiation, fast neutron therapy is, for the radiation therapist, an alternative to conventional photon (or electron) therapy in clinical radiation oncology (for a historical background, see: SVENSSON and LANDBERG, 1994). However, previous multicentric clinical trials comparing neutron and photon beams have failed to show clear indications of the suggested therapeutic advantages. While local/regional tumor control may be more efficiently achieved for some tumors, the degree of side effects and late complications seem to be more severe for neutron radiotherapy. One reason for these hitherto inconclusive findings may be the poorer physical dose distributions achievable with the neutron beams used in the randomized trials (SÖDERBERG and CARLSSON, 2000). With the recent development of more sophisticated beam delivery and collimation systems, the most promising reported results for the future use of fast-neutron beams as a therapeutic modality appear to be in the treatment of large, slowly-growing or photon-resistant tumors such as inoperable salivary gland

tumors, locally advanced prostatic adenocarcinomas, low-grade soft-tissue sarcomas and some sarcomas of bone (for example, see: SÖDERBERG, 2007; SABATTIER et al., 2007 and references therein).

II.3 Interaction of fast neutrons with water

II.3.1 Scattering cross sections

By definition, the "*cross section*" represents a measure of the probability of any particular event occurring between a neutron and a single nucleus. This quantity is usually given the symbol σ and is expressed in area units. The practical unit is a *barn*, where 1 barn = 10^{-24} cm^2. A neutron can have many types of (competing) interactions (scattering or absorption) with a nucleus (see Fig. II.1), each of them having its own probability and cross section. The probability of occurrence for each type of event is independent of the probability of the others, so the sum of all the possible individual interaction cross sections defines what we call the "total cross section".

All of the cross sections are critically dependent on the energy of the neutron involved and on the type of the target nucleus (for reviews, see, for example: ANDERSON, 1984; KRANE, 1988; RINARD, 1991; SHULTIS and FAW, 2002). Note that, as a general rule the cross section is a lot larger at low energies than at high energies. At energies usually less than 1 keV, the elastic cross section is nearly constant, whereas the inelastic scattering cross section and absorption (capture) cross sections exhibit a $1/\sqrt{E_n}$ behavior (this inverse proportionality is also called the $1/v$ law, where v is the neutron velocity; see, for example: CEMBER and JOHNSON, 2009). So at low energies the total cross section can be nearly constant or decreasing with increasing energy, depending on which type of event dominates. At higher energies the cross section may have large peaks superimposed on the $1/v$ background. These peaks are called "resonances" and occur at neutron kinetic energies where reactions with nuclei are enhanced. For example, a resonance will occur if the target nucleus and the captured neutron form a "compound nucleus", and

the excitation energy brought by the incident neutron corresponds to a quantum state of the resulting compound system. Scattering and absorption cross sections exhibit resonance peaks at neutron kinetic energies corresponding to those quantum nuclear states. In general, resonances occur at lower energies for heavy nuclei than for light nuclei. In heavy nuclei, large and narrow resonances appear in the slow neutron region. For intermediate energies the resonances can be too close together to evaluate. As we move to energies in the MeV range, the resonances are sparser and have very broad shapes. For light nuclear targets, resonances appear only in the MeV region and are broad and relatively small. Of all the nuclides, only hydrogen and its isotope deuterium exhibit no resonances at all. Exceptions to the general trends also exist in some nuclei with "magic" numbers of protons or neutrons (those nuclei have a completely filled shell of either protons or neutrons; they are said to be "magic" because they are relatively more stable than nuclei with either a larger or a smaller number of nucleons) where the behavior may be similar to that of light nuclei despite the actual atomic weight. In practice, it is necessary to rely on tables of cross sections for the nuclei of interest because there is no convenient way to calculate cross sections [for example, see: *Nucl. Data Sheets* **107**, 2931-3118 (2006), a special issue ("*Evaluated Nuclear Data File ENDF/B-VII.0*") on evaluations of neutron cross sections from the U.S. Cross Section Evaluation Working Group of the National Nuclear Data Center of Brookhaven National Laboratory (http://www.nndc.bnl.gov/csewg/); see also the T-2 Nuclear Information Service of the Los Alamos National Laboratory (http://t2.lanl.gov/data/data.html), which provides access to a variety of nuclear data, including the ENDF/B-VII.0 library of evaluated neutron data with links to PDF plots of the cross sections and angular distributions for most nuclides over the neutron energy range up to 200 MeV].

II.3.2 Elastic scattering interactions of fast neutrons in water

As already pointed out, fast neutrons at incident energies less than about 10 MeV cause radiation effects primarily through the generation of elastically scattered

charged nuclei of the absorbing medium. In the case of the fast-neutron radiolysis of water, the ionizing particles involved are thus proton and oxygen ion recoils. It is in fact important to note that, in this energy range, the contributions resulting from the $^{16}O(n,\alpha)^{13}C$ reaction (threshold at ~3.8 MeV), producing α-particles and recoiling carbon ions, and especially from the inelastic scattering with oxygen (first level at ~6.05 MeV), producing gamma radiation, can be neglected to a very good approximation. This is because the cross sections for these nuclear reactions are about an order of magnitude less than the cross sections for hydrogen and oxygen elastic scattering for most of the energies that interest us here (notice that they rise steeply, however, as neutron energy increases, but become significant only at neutron energies around or greater than 10 MeV) [data from the Brookhaven ENDF/B-VII.0 library (2006); see also AUXIER et al., 1968]. From the radiolysis point of view and as long as the energy is less than ~10 MeV, we therefore need only consider *elastic* neutron-proton (*n-p* collisions) and to a smaller extent (see below) neutron-oxygen scattering interactions.

Figure II.2 shows a comparison of the elastic cross sections for *n-p* scattering and for neutrons incident on oxygen nuclei in the energy range from 5 keV to 10 MeV (WATT, 1996). As can be seen, the cross-section curve for neutrons incident on ^{1}H is featureless (no resonances are present) and decreases continuously with increasing neutron energy. For neutrons incident on ^{16}O, the cross section is quite flat in the region below ~0.3 MeV but shows resonance peaks at higher energies. Moreover, below about 0.3 MeV, the scattering for proton recoils is very high and largely dominates the oxygen elastic scattering; however, in the energy range ~0.3-10 MeV, because of the occurrence of the various resonances in oxygen, the cross section for oxygen elastic scattering tends to become more or less the same as that for *n-p* collisions (see Fig. II.2).

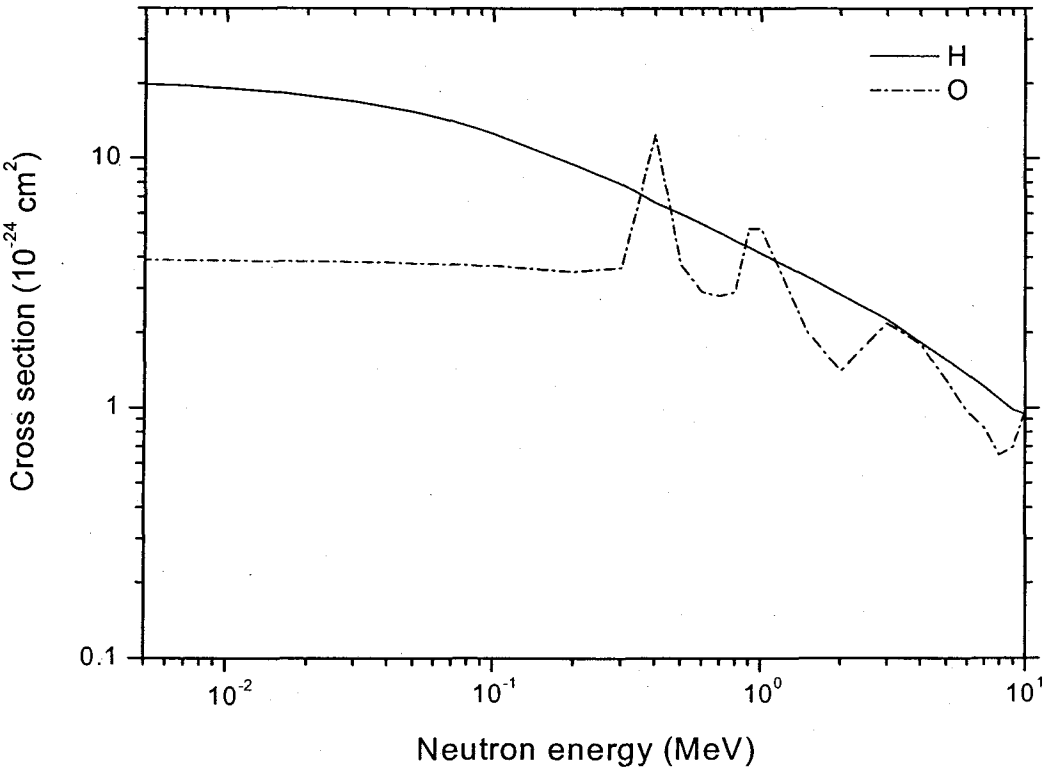

Figure II.2: Comparison of elastic scattering cross sections (in barn) for fast neutrons incident on hydrogen (solid line) and oxygen (dash-dot line) targets as a function of neutron energy (from WATT, 1996).

It is worth noting that the (elastic) scattering cross sections shown in Fig. II.2 describe the interactions of a neutron with a *single* nucleus, hydrogen or oxygen. These cross sections, referring to an individual element, are often called "microscopic" cross sections (RINARD, 1991). If the studied sample is now a compound containing several elements instead of a simple element, the cross section is simply the sum of the cross sections of the individual target nuclei. For example, for the case of the water molecule (H_2O), which contains two hydrogen atoms and one oxygen atom, the cross section describing the interaction of a neutron with the molecule is

$$\sigma_{H_2O} = 2\,\sigma_H + \sigma_O \,, \tag{37}$$

where σ_H and σ_O are the microscopic cross sections for hydrogen and oxygen, respectively. More generally, for bulk materials containing a mixture of elements *i* with density N_i and individual cross section σ_i, we can define the so-called "macroscopic" cross section (denoted here by the symbol μ and with dimensions of cm^{-1}), given by (RINARD, 1991)

$$\mu = \sum_i N_i \sigma_i . \tag{38}$$

As an illustration of Eq. (38), the macroscopic cross section for neutrons in water is

$$\mu_{water} = \frac{N_{Av}\rho}{M}\left(n_H \sigma_H + n_O \sigma_O\right), \tag{39}$$

where ρ = 1 g/cm^3 is the density of water, M = 18 is its molecular weight, N_{Av} is Avogadro's number (6.022×10^{23} mol^{-1}), and n_H = 2 and n_O = 1 are the numbers of atoms of hydrogen and oxygen in one molecule, respectively. Interestingly, the fact that there are twice as many hydrogen atoms as oxygen atoms per given volume of water also contributes to making oxygen ion recoils of minor importance in the fast-neutron radiolysis of water. In fact, EDWARDS et al. (2007) estimated that, in the energy range below 10 MeV, 88% of the neutron energy is absorbed by protons and 12% by oxygen recoils.

II.3.3 Neutron mean free path and ranges of recoil protons and oxygen ions in water: information on track structure

A very descriptive feature of the transmission of neutrons through bulk matter is the "*mean free path*" (λ), which is the average distance a neutron travels between two consecutive interactions. It is defined as the reciprocal of the macroscopic cross section μ given in Eq. (38):

$$\lambda = \frac{1}{\mu} . \tag{40}$$

λ is a key parameter in the study of neutron transport and interactions in matter and has many qualitative applications in assay instruments and shielding. For example, it

is found that, under the conditions of the transmission of a pencil beam of monoenergetic neutrons incident normally (along the direction z) on a thick sample of infinite lateral extent, the relative number of neutrons that travel a distance z in the sample (the origin being at the point where the neutrons enter the sample) without experiencing a collision falls off exponentially as $\exp(-z/\lambda)$ (RINARD, 1991; CEMBER and JOHNSON, 2009). Mathematically, this is a representation of the Poisson distribution and corresponds to the probability of no event when, on the average, z/λ events should occur (EVANS, 1955). Importantly, λ also determines the free flight distances of individual neutrons in Monte-Carlo procedures that are used to simulate how neutrons are transported through matter. In those computer calculations, individual free flight distances for a large number of simulated neutrons must be selected randomly so as to give the observed $\exp(-z/\lambda)$ distribution (TURNER et al., 1985).

The mean free path depends on both the type of material and the energy of the neutron. For the case of 100-keV incident neutrons in water, λ can easily be calculated from Eqs. (39) and (40) to be ~1.04 cm, using the microscopic cross section values $\sigma_H \approx 12.5$ and $\sigma_O \approx 3.65$ barns (WATT, 1996). The mean free path of neutrons in water as a function of neutron energy is shown in Fig. II.3. After each collision, the neutron's energy is decreased and the cross section changes, thereby affecting the mean free path accordingly. For the range of the energies that interest us here, λ decreases as the neutron's energy decreases (see Fig. II.3). It is worth mentioning that λ in water is equal to ~0.71 cm at 10 keV and ~0.67 cm at 1 keV according to the cross-section data taken from WATT (1996).

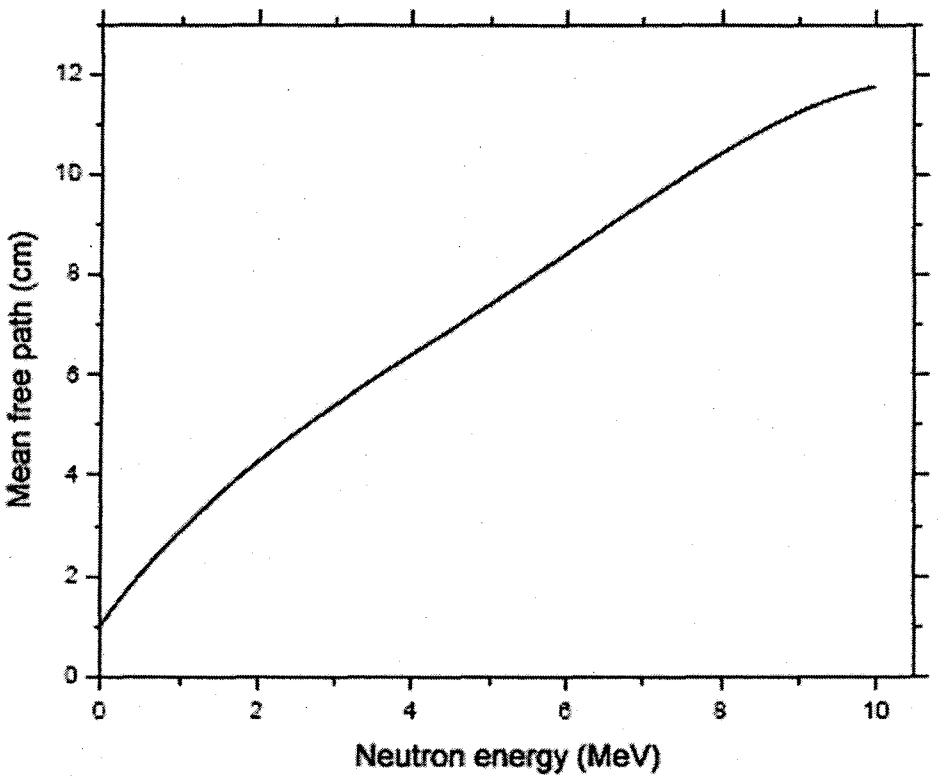

Figure II.3: Neutron mean free path for water as a function of neutron energy (from SCHRÖDER, 2009).

Table 7: Neutron mean free path and maximum ranges for elastically scattered protons and oxygen ions in water.

Neutron energy (MeV)	Neutron mean free path (λ) (cm)	Secondary-proton maximum range (cm)	Secondary-oxygen-ion maximum range (cm)
0.1	1.04	0.00016	0.00001
0.5	2.01	0.00089	0.00005
1.0	2.43	0.00246	0.00009
3.0	5.58	0.0149	0.00019
5.0	7.77	0.0362	0.00027
10.0	11.8	0.1230	0.00041

Table 7 gives some values for mean free path (taken from Fig. II.3) and secondary-particle (recoil proton and oxygen ion) maximum range (WATT, 1996) for several neutron beams in water. As can clearly be seen, the elastically scattered proton and oxygen ion recoils generated by the passage of the incident neutron are widely separated from one another along the path of the neutron (like photons, neutrons are uncharged and hence can travel appreciable distances without interacting). Moreover, these recoil nuclei have maximum ranges (i.e., track lengths) much less than the average separation between two successive neutron interactions (λ), so that they can be considered as behaving *independently* of each other: their ionizing energy is deposited locally in dense tracks in the water in the immediate vicinity of the collision sites (the points of generation of the recoil particles) with virtually no allowance for overlap of the reaction zones of neighboring tracks (this approximation would not necessarily be correct at very high neutron intensities or dose rates). As a consequence, under normal irradiation conditions, fast neutrons deposit their energy in water primarily through the generation of "isolated" tracks of recoil nuclei and the observed water radiolysis chemistry should tend to be much like that induced by independent, high-LET protons and oxygen ions.

This track structure information for the elastically scattered proton and oxygen ion recoils strongly supports the procedure used in the present study, and already employed by other authors (see Sect. I.1.5), to calculate the radiolysis *G*-values for fast neutrons by simply summing the yields for each of these recoil ions after allowance has been made for the appropriate weighting according to energy (see Chapters III and IV).

CHAPTER III

METHODOLOGY

III.1 Monte-Carlo simulations

The complex sequence of events that are generated in liquid water and dilute aqueous solutions under irradiation can be modeled successfully by the use of Monte-Carlo simulation methods.[9] Such a procedure is particularly well-suited to account for the *stochastic* nature of the phenomena. TURNER et al. (1981, 1983, 1988) at the Oak Ridge National Laboratory (Oak Ridge, Tennessee, U.S.A.) and Lawrence Berkeley Laboratory (Berkeley, California, U.S.A.) were the first to use Monte-Carlo calculations to derive computer-plot representations of the chemical evolution of a few keV electron tracks in liquid water at times from ~10^{-12} to 10^{-7} s. ZAIDER and BRENNER (1984) also described such an approach, and their calculated time-dependent yields of e^-_{aq} and $^{\bullet}OH$ radical were somewhat similar to values measured or derived in pulse-radiolysis studies of pure water. Following these pioneering works, stochastic simulation codes employing Monte-Carlo procedures were developed independently by a number of researchers to study the relationship between the initial track structure and the ensuing chemistry (for a review, see: BALLARINI et al., 2000; see also: UEHARA and NIKJOO, 2006; NIKJOO et al., 2006; KREIPL et al., 2009; TAGUCHI et al., 2009). In a program begun in the summer of 1988, Prof. Jean-Paul Jay-Gerin's group at the Université de Sherbrooke,

---

[9] The so-called "Monte-Carlo method" is a general term (named after the famous European gambling center) used to describe any algorithm or computational method that employs random numbers. Simulation methods are used to estimate means of random variables or probabilistic features of models that we cannot compute analytically.

in collaboration with Prof. Jean Paul Patau (Université Paul-Sabatier, Toulouse) and Prof. Christiane Ferradini (Université René-Descartes, Paris) in France, has also developed and progressively refined with very high levels of detail several Monte-Carlo codes that simulate, in a three-dimensional (3D) geometrical environment, the track structure of ionizing particles in liquid water, the production of the various reactive species in the radiation track, and the subsequent chemical reactions of these species with themselves (owing to diffusion from their initial positions) or with any dissolved solutes present at the time of irradiation (COBUT et al., 1994, 1998; FRONGILLO et al., 1998; HERVÉ DU PENHOAT et al., 2000; MEESUNGNOEN et al., 2001*a*, 2003; PLANTE et al., 2005; MEESUNGNOEN and JAY-GERIN, 2005*a*, *b*; MUROYA et al., 2002, 2006; AUTSAVAPROMPORN et al., 2007). A most recent version of the Sherbrooke codes, called IONLYS-IRT, has been used in the present work. The detailed description and implementation of IONLYS-IRT has already been given (MEESUNGNOEN and JAY-GERIN, 2005*a*, *b*, and references therein), and will not be reproduced here. Only a brief overview of the most essential features of the simulation methodology and reaction scheme, pertinent to the current calculations, is given below.

III.1.1 The IONLYS simulation code

The IONLYS simulation code is used to cover the early "physical" and "physicochemical" stages of radiation action up to ~10^{-12} s (see Sect. I.1.2). It is actually composed of two modules, one (named TRACPRO) for transporting the investigated incident charged particle (proton or any other heavy ion projectile) and one (named TRACELE) for transporting all of the energetic electrons (collectively named "secondary electrons") that result from the ionization of the water molecules. The code models, event by event, *all* the basic physical interactions (energy deposition) and the subsequent establishment of thermal equilibrium in the system (conversion of the physical products created locally after completion of the physical

stage into the various "initial" chemical species of the radiolysis). For a detailed description of these events as well as their time scales, see Sect. I.1.2 and Fig. I.1.

In particular, IONLYS provides the detailed distribution of coordinates of *all* physical events (ionization, excitation of electronic, vibrational and rotational levels of single water molecules, excitation of plasmon-type collective modes, and elastic scattering) that occur locally during the slowing-down of the irradiating charged particle and of all the secondary electrons that it has generated. The energy-dependent cross sections for the various elastic and inelastic processes involved, together with their angular distributions, are entered as input data in the code, based on direct measurements (where available, as cross-section data in the case of liquid water are scarce) or on theoretical estimations. These collision cross sections are needed to follow the history of an energetic charged particle and its products, covering all ranges of energy transferred in individual collisions. Most importantly, they provide the mean free path used to determine the distance to the next interaction, the type of interaction at each event, energy loss, and the angle of emission of the scattered particle (for example, see: DINGFELDER and FRIEDLAND, 2001; NIKJOO et al., 2006; DINGFELDER et al., 2008). Full details of the *cross-section database* used in the IONLYS code can be found in the references cited (COBUT, 1993; COBUT et al., 1998; MEESUNGNOEN and JAY-GERIN, 2005*a*). It is worth mentioning that this code, which uses protons or heavy ions as the primary particles, is particularly well adapted to the study of the fast-neutron radiolysis of water, since the ionizing particles involved in this case are proton and oxygen ion recoils. Interestingly, the choice of proton impact in the Sherbrooke code was originally adopted owing to the fact that protons represent, by far, the most comprehensive database of cross sections for bare ion collisions (not only on water but also on a number of different target atoms or molecules; see, for example: RUDD, 1990; RUDD et al., 1992; IAEA-TECDOC-799, 1995; DINGFELDER et al., 2000; TOBUREN, 2004), and also because they constitute a valuable tool for studying LET effects on radiolytic yields (COBUT et al., 1998). Another great

advantage of the code is that, while it was devised for protons, it can also be used for heavier ion projectiles by assuming that the interaction cross sections scale as Z^2, where Z is the projectile charge number. In this scaling procedure, based on the lowest-order (or first Born) approximation of perturbation theories, the cross sections for bare ion impact are approximately Z^2 times the cross sections for proton impact *at the same velocity*. This simple Z^2 scaling rule, which holds at sufficiently high impact energies (say above ~1 MeV/nucleon) where the interactions are not too strong, is particularly useful for providing cross sections for ionization and excitation by ion projectiles, especially as there are only limited experimental data available involving ions heavier than proton or helium in collision with water molecules (INOKUTI, 1971; ICRU REPORT 55, 1996; MEESUNGNOEN and JAY-GERIN, 2005*a*; BICHSEL, 2006; MEESUNGNOEN, 2007, and references therein). In practice, the stochastic selection of the scattering events is done with various sampling techniques (direct inversion, etc.; see, for example: KNUTH, 1998; DEGROOT and SCHERVISH, 2002) in accordance to the appropriate scattering cross sections for each process induced by the considered charged particle. These techniques all use pseudo-random numbers uniformly distributed on the interval between 0 and 1.

The simulations performed with IONLYS consist in the generation of short high-energy proton (ion) *track segments* in water. The primary particle is simulated until it has penetrated the chosen length of the track segment into the medium. Note that, due to its large mass, the proton (or the impacting heavy ion) is almost not deflected by collisions with the target electrons. In the present simulations, these deflections are simply neglected. The use of small path segments is particularly useful as the instantaneous LET of the incident particle is nearly constant over such segments and can be varied simply by changing its energy. Figure III.1 shows our simulated LET for protons in liquid water as a function of proton energy in the range ~15 keV-300 MeV, together with the recommendations of WATT (1996) and the compilation of ICRU REPORT 49 (1993). It is seen that, while our calculated LET values are slightly lower than the published data at energies near the Bragg peak (~80 keV) and

below, there is a good overall agreement among the three independent assessments.[10] To reproduce the effects of fast electron or ^{60}Co γ-radiolysis, we use short (~100 μm) track segments of 300-MeV protons[11] over which the average LET value obtained in the simulations is essentially constant and equal to ~0.3 keV/μm at 25 °C.

---

[10] It is worth recalling here that Bethe's theory is the gold standard for describing the LET (customarily called "stopping power" in the domain of radiation physics) for fast charged particles over a broad energy range. For kinetic energies of ions that are small compared to their rest-mass energy, the nonrelativistic (uncorrected) Bethe stopping power formula (BETHE, 1930; BETHE and ASHKIN, 1953; ICRU REPORT 49, 1993; ICRU REPORT 73, 2005) is given by (in SI units):

$$-\frac{dE}{dx} = \left(\frac{1}{4\pi\varepsilon_0}\right)^2 \frac{4\pi Z^2 e^4}{m_0 V^2} N \ln\left(\frac{2m_0 V^2}{I}\right), \qquad (41)$$

where Ze is the charge on the incident ion, V is the ion velocity, m_0 is the rest mass of an electron, ε_0 is the permittivity of vacuum, N is the number of electrons per cubic meter of the absorbing medium, and I is the mean of all the ionization and excitation potentials of the bound electrons in the absorber. In most cases, I is determined by fitting the theory to experimental results related to the stopping power. For liquid water, I = 79.7 ± 0.5 eV (BICHSEL and HIRAOKA, 1992). Based on the first-order Born approximation in the electromagnetic interaction between the incident particle and the atomic electrons, the Bethe formula (41) has a wide range of validity except for slow, highly charged heavy particles such as fission fragments. For an accurate assessment of the LET at energies in the Bragg peak region and below, a number of corrections (shell corrections, higher-order Born terms proportional to Z^3 and Z^4, and effects due to charge exchange) must be made to this formula (for example, see: ICRU REPORT 49, 1993; ICRU REPORT 73, 2005).

[11] For comparison, a 300-MeV proton has a range in water of ~52.1 cm (WATT, 1996).

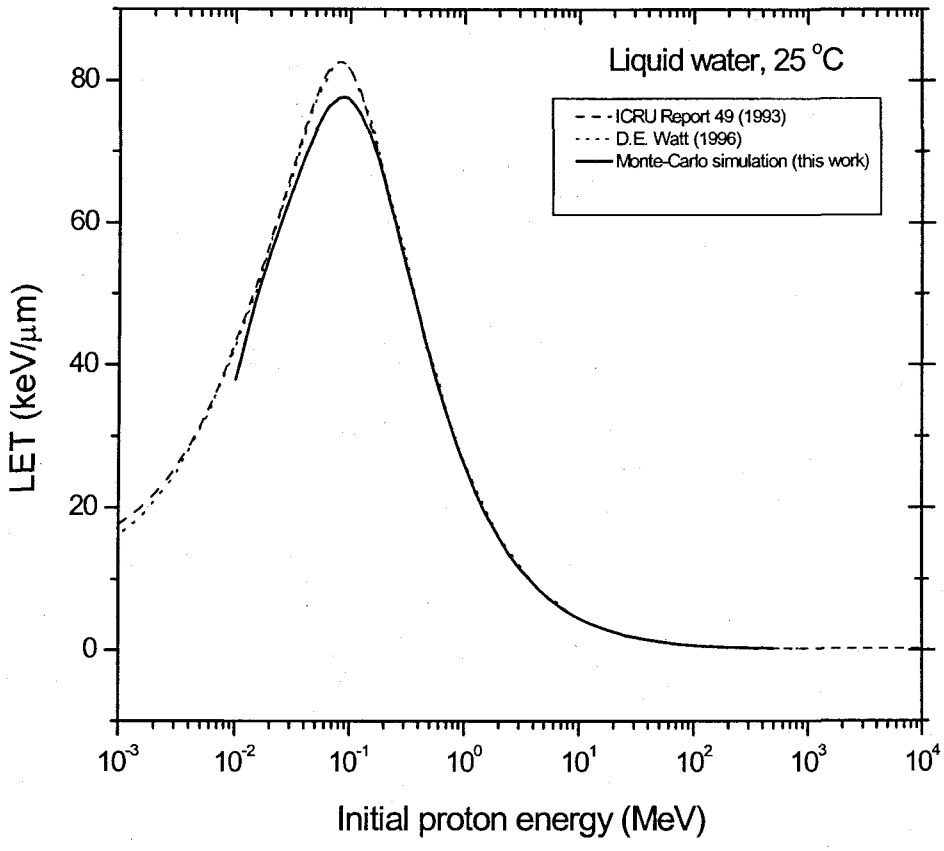

Figure III.1: Variation of LET as a function of the impact energy of protons calculated using the IONLYS code for liquid water at 25 °C. The data reported by WATT (1996) and in the compilation of ICRU REPORT 49 (1993) for liquid water (density 1 g/cm^3) are also shown for the sake of comparison.

All of the produced energetic (dry) secondary electrons are explicitly transported spatially from their initial energies until they reach the subexcitation energy region below ~7.3 eV, the threshold assumed for electronic excitation in liquid water (see Sect. I.1.2).[12] The location, type of collision, specific quantum

[12] Recall here that most energy-loss events by the fast primary charged particle involve small transfers of energy. In fact, Monte-Carlo simulations have shown that the most probable energy loss for liquid water is 15-20 eV, while the track-averaged mean energy loss is around 50-60 eV, depending on the authors (LAVERNE and

transition, and energy transferred are determined by the IONLYS code, event by event. All physical details about the various elastic and energy-loss processes involved and the corresponding scattering cross sections employed by IONLYS for the simulation can be found in COBUT (1993), COBUT et al. (1998), and MEESUNGNOEN and JAY-GERIN (2005*a*). The time that it takes a secondary electron to reach a subexcitation energy is $<10^{-15}$ s.

The thermalization of subexcitation electrons is treated by IONLYS using the distribution of thermalization distances obtained from Monte-Carlo track-structure calculations (GOULET and JAY-GERIN, 1989; GOULET et al., 1990, 1996; MEESUNGNOEN et al., 2002*b*) based on experimental scattering cross sections of slow (~1-100 eV) electrons in amorphous ice films at 14 K (MICHAUD et al., 2003) with corrections to account for the liquid phase. Given the initial position of the subexcitation electron, its position is simply displaced in a randomly selected, isotropic direction by the corresponding, energy-dependent mean penetration distance. At this new position, the electron is regarded as thermalized and subsequently trapped and hydrated *where it is*, an approximation likely to be valid in a highly polar medium such as liquid water in which very-low energy (e.g., "subvibrational") electrons have a strong tendency – due to the presence of a large density of possible electron trapping sites – to get instantly trapped prior to thermalization (MOZUMDER, 1999). As mentioned in Sect. I.1.2, the time scale of thermalization, trapping, and hydration of a subexcitation electron in liquid water at 25 °C is less than $\sim 10^{-12}$ s. Finally, it is worth recalling here that a certain proportion of subexcitation electrons will actually never get thermalized, but will instead undergo

---

PIMBLOTT, 1995; COBUT et al., 1998; AUTSAVAPROMPORN, 2006). COBUT et al. (1998) also calculated that, if we sum all the electrons ejected directly by the primary particle and by the successive generations of secondary electrons, 88% of them have kinetic energies less than 20 eV.

prompt recombination[13] with their positive parent ion $H_2O^{\bullet+}$ or dissociative attachment onto a surrounding H_2O molecule (see Fig. I.1). All details about the various parameters intervening in the IONLYS code to describe this competition between thermalization, geminate recombination, and dissociative attachment, as well as the values of the branching ratios used in the code for the different dissociative decay channels of the electronically and vibrationally excited H_2O molecules, can be found in MEESUNGNOEN and JAY-GERIN (2005*a*) and the references cited therein.

III.1.2 The IRT simulation code

The complex spatial distribution of reactants at the end of the physicochemical stage (~10^{-12} s; we assume that this time also marks the beginning of diffusion), which is provided as an output of the IONLYS program, is then used directly as the starting point for the subsequent nonhomogeneous chemical stage. This third and final stage, during which the individual reactive species diffuse randomly at rates

---

[13] About 25.5% of the subexcitation electrons are found to initially recombine with $H_2O^{\bullet+}$ (MEESUNGNOEN and JAY-GERIN, 2005*a*), with an average recombination time as short as a few femtoseconds (GOULET et al., 1990). This average recombination time shows that the recombination process mainly occurs on the water cation and *not* on H_3O^+, that is, before the proton transfer reaction $H_2O^{\bullet+} + H_2O \rightarrow H_3O^+ + {}^{\bullet}OH$ takes place (~10 fs) (which would change the nature of the cation and therefore affect the values of the recombination cross section). In other words, the subexcitation electron recombines quickly (in the first steps of its random walk) on $H_2O^{\bullet+}$. If it does not recombine quickly, it will never recombine, and will thus become thermalized (unless, of course, it makes a dissociative attachment on a water molecule) (~56 fs), trapped (~50-300 fs), and hydrated (~240 fs-1 ps) (MEESUNGNOEN and JAY-GERIN, 2005*a*; JAY-GERIN et al., 2008 and references therein). In fact, to test the validity of these results, MUROYA et al. (2002) included both types of electron recombination (on $H_2O^{\bullet+}$ and on H_3O^+) in their simulations; indeed, the recombination on H_3O^+ was found to be negligible.

determined by their diffusion coefficients and react with one another (or with any added solutes present at the time of irradiation) until all spur or track processes are complete (~10^{-6} s), is covered by the IRT program. This program employs the "*independent reaction times*" (IRT) method (CLIFFORD et al., 1986; GREEN et al., 1990; PIMBLOTT et al., 1991), a computer efficient stochastic simulation technique that is used to simulate reaction times without following the trajectories of the diffusing species.

The IRT method relies on the approximation that the distances between pairs of reactants evolve independently of each other, and therefore the reaction times of the various potentially reactive pairs are independent of the presence of other reactants in the system. In essence, the simulation begins by considering the initial, or "zero-time", spatial distribution of the reactants (given by the IONLYS program). The separations between all the pairs of reactants are first calculated. Overlapping pairs (i.e., pairs formed in a reactive configuration) are assumed to combine immediately. For each remaining pair, a reaction time is stochastically sampled according to the reaction time probability distribution function (GREEN et al., 1990; GOULET and JAY-GERIN, 1992; FRONGILLO et al., 1998) that is appropriate for the type of reaction considered. This function depends upon the initial distance separating the species, their diffusion coefficients, their Coulomb interaction (for reactions between ionic species), their encounter distance,[14] and the probability of reaction during one of their encounters. The competition between the various reactions is taken into account by realizing them in the ascending order of sampled reaction times. In other words, the first reaction time is found by taking the minimum of the resulting ensemble of reaction times and allowing the corresponding pair of species to react at this time. When a reaction occurs, the reactants become unavailable for the competing reactions that are sampled to occur at longer times but one must then

---

[14] The "encounter distance" ($a_{A,B}$) for each pair of interacting species A and B can be derived from the Smoluchowski equation (see Sect. I.1.5).

consider the possible reactions of the newly formed products with the species that have survived up to that point. The minimum of the new ensemble of reaction times is the next reaction time. The simulation proceeds in this manner until a pre-defined cut-off time is reached or all the potentially reactive pairs have reacted. Since the IRT method is solely based on a comparison of reaction times, it does not follow the diffusive motion of the species within the spur/track. The model must therefore be supplemented by including an approximation which allows the calculation of either new inter-particle distances at the time when a new product is formed, or reaction times without inter-particle distances. Several alternative procedures, which incorporate varying degrees of spatial information about the system, have been devised and discussed in detail previously (CLIFFORD et al., 1986; GREEN et al., 1990). The procedure adopted in our IRT code to account for the subsequent reactions of reactive products is described in FRONGILLO et al. (1998).

The IRT program also allows one to incorporate in a simple way pseudo first-order reactions of the radiolytic products with various scavengers that are homogeneously distributed in the solution, such as H^+, OH^-, and H_2O itself, or more generally any solutes for which the relevant reaction rates are known. Similarly, the truly first-order fragmentations of the species are easily simulated. Finally, the IRT method is very well suited for the description of reactions that are only partially diffusion-controlled (most reactions that occur in irradiated water are not diffusion-controlled even at room temperature; as mentioned in Sect. I.1.5, an adequate description of the activation processes that are involved in those reactions is a prerequisite for the modeling of the effects of high temperature on water radiolysis), in which the species do not react instantaneously on encounter but experience, on the average, many encounters and separations before they actually react with each other.

The IRT simulation of nonhomogeneous kinetics has been found to be accurate in solvents of high static dielectric constant (such as is the case for liquid water, $\varepsilon_s \sim 78$) where the Coulomb forces between the ions are weak (see, for example:

PIMBLOTT and GREEN, 1995). Indeed, the time-dependent yields of water radicals and molecular products obtained with the IRT method under different irradiation conditions have been shown to compare very well to those calculated using full random flights (or "step-by-step") Monte-Carlo simulations, which do follow the reactant trajectories in detail (PIMBLOTT et al., 1991 and references cited therein; GOULET et al., 1998; PLANTE, 2009).[15]

Compared to the original version of our IRT program, only slight adjustments have been made in some reaction rate constants (see Table 1 for the list of the main spur/track chemical reactions and values of reaction rate constants considered in our pure liquid water radiolysis simulations) and diffusion coefficients of reactive species (Table 8 shows the values of diffusion coefficients for the various track species involved in our simulations) to take account of the latest data available from the literature (MEESUNGNOEN and JAY-GERIN, 2005*a*, *b*; AUTSAVAPROMPORN, 2006; MEESUNGNOEN, 2007).

---

[15] The full step-by-step Monte-Carlo description of the diffusion and encounters of the various species of the system is certainly the most reliable and is generally considered as a measure of reality. Unfortunately, this method can be exceedingly consuming in computer time when large systems (such as complete radiation tracks or track segments) are studied. The IRT method has been devised to achieve much faster realizations than are possible with the full Monte-Carlo model. For example, depending on the LET of the track segment considered and on the timescale over which the reaction kinetics is simulated, the IRT technique is of the order of a few hundred times faster than a full step-by-step Monte-Carlo calculation.

Table 8: Values at 25 °C of the diffusion coefficients (D) of the various reactive species involved in our IRT simulations.

Species	D (10^{-9} m^2 s^{-1})
H_2O	2.299 [(a)]
e^-_{aq}	4.9
H^+	9.46
$H^\bullet$	7.0
$^\bullet OH$	2.2
H_2O_2	2.3
H_2	4.8
OH^-	5.3
O_2	2.4
$O_2^{\bullet-}$	1.75
$HO_2^\bullet$	2.3
HO_2^-	1.4
$O(^3P)$	2.0
$O^{\bullet-}$	2.0
O_3	2.0
$O_3^{\bullet-}$	2.0

[(a)] Self-diffusion coefficient of water at 25 °C (MILLS, 1973).

As mentioned above (see Chapter II), fast neutrons impinging on liquid water at incident energies less than ~10 MeV generate primarily energetic protons and to a smaller extent oxygen ion recoils. For example, a 0.8-MeV neutron generates recoil protons of 0.505, 0.186, 0.069, and 0.025 MeV (further recoils make only a negligible contribution to radiation processes), with LET values of ~41, 69, 82, and 62 keV/μm, respectively. To reproduce the effects of fast-neutron radiolysis on the yields of the various radiation-induced species in neutral or acidic water, as well as on the yield of ferric ions in the Fricke dosimeter, we simulate short (~15-100 μm) track segments of each of those generated recoil protons (in the range of incident energies from ~0.015 to 300 MeV; see Fig. III.1). Over such simulated track segments, the energy and LET of the protons are well defined and remain nearly constant. Such model

calculations thus give track segment yields at a well-defined LET. The number of proton histories (usually ~10-150, depending on the proton energy) is chosen so as to ensure only small statistical fluctuations in the computed averages of chemical yields, while keeping acceptable computer time limits.

III.2 Modeling the effects of acidity

To model the radiolysis of the ferrous sulfate (Fricke) dosimeter (see Sect. I.2), we have used aqueous solutions of 0.4 *M* sulfuric acid (pH ~ 0.46). For aqueous H_2SO_4 (a diprotic acid), we have:

$$H_2SO_4 \underset{pK_{a1}}{\overset{H^+}{\rightleftharpoons}} HSO_4^- \underset{pK_{a2}}{\overset{H^+}{\rightleftharpoons}} SO_4^{2-} \qquad (42)$$

with $pK_{a1} \approx -3$ and $pK_{a2} = 1.987$ at 25 °C (DEAN, 1987). Hence, H_2SO_4 is virtually completely dissociated when dissolved in water above pH ≈ 0, and the solution contains mainly H^+, HSO_4^-, and a certain amount of SO_4^{2-}.

The model assumptions and procedures employed to carry out the Monte-Carlo simulations of the radiolysis of 0.4 *M* H_2SO_4 aqueous solutions with IONLYS-IRT have already been given in MEESUNGNOEN et al. 2001, MEESUNGNOEN and JAY-GERIN, 2005*b*, and AUTSAVAPROMPORN et al., 2007. In brief, as noted before, the effects of the background concentration of H^+ in solutions are added to the IRT program as pseudo first-order reactions. We have also supplemented the pure-water reaction scheme to include the reactions listed in Table 9, which account for the species present in irradiated sulfuric acid solutions. The diffusion coefficients of HSO_4^-, $SO_4^{\bullet-}$, SO_4^{2-}, and $S_2O_8^{2-}$, employed in the simulations are taken to be (in units of 10^{-9} m^2 s^{-1}) 1.385 (for both HSO_4^- and $SO_4^{\bullet-}$), 1.065, and 1.145, respectively (LIDE, 2008).

Table 9: Reactions added to the pure water reaction scheme to simulate the radiolysis of aqueous H_2SO_4 solutions, at 25 °C (from AUTSAVAPROMPORN et al., 2007).[(a)]

Reaction	k (M^{-1} s^{-1})
$H^{\bullet} + SO_4^{\bullet-} \rightarrow HSO_4^-$	1.0×10^{10}
$H^{\bullet} + S_2O_8^{2-} \rightarrow SO_4^{\bullet-} + HSO_4^-$	2.5×10^{7}
$^{\bullet}OH + HSO_4^- \rightarrow H_2O + SO_4^{\bullet-}$	1.5×10^{5}
$e^-_{aq} + S_2O_8^{2-} \rightarrow SO_4^{\bullet-} + SO_4^{2-}$	1.2×10^{10}
$H_2O_2 + SO_4^{\bullet-} \rightarrow HO_2^{\bullet} + HSO_4^-$	1.2×10^{7}
$OH^- + SO_4^{\bullet-} \rightarrow {}^{\bullet}OH + SO_4^{2-}$	8.3×10^{7}
$SO_4^{\bullet-} + SO_4^{\bullet-} \rightarrow S_2O_8^{2-}$	4.4×10^{8}

[(a)] Note that the rate constants given here for the reactions between ions are at ionic strength equal to zero.

In addition, we have introduced, in the IRT program, the effects due *ionic strength* in 0.4 *M* H_2SO_4 solutions (see, for example: HARRIS, 2001) for reaction (14) ($e^-_{aq} + H^+ \rightarrow H^{\bullet}$) and for the recombination of the proton with the hydroxyl ion (MEESUNGNOEN et al., 2001*a*; MEESUNGNOEN and JAY-GERIN, 2005*a*):

$$OH^- + H^+ \rightarrow H_2O \qquad (43)$$

as well as for all reactions between ions,[16] including those given in Table 9. To relate rate constant and ionic strength of the solution, we used the following equation, obtained from the Brönsted-Bjerrum model of ionic reactions and the extended Debye-Hückel theory of ionic solutions (GUGGENHEIM, 1935; DAVIES, 1938; ROBINSON and STOKES, 1959; CZAPSKI and SCHWARZ, 1962; JONAH et al., 1977):

[16] Except for the peculiar bimolecular self-recombination of e^-_{aq} for which there is no evidence of any ionic strength effect (SCHMIDT and BARTELS, 1995).

$$\log\left(\frac{k}{k_0}\right) = 1.02\, Z_a Z_b \left(\frac{I^{1/2}}{1 + I^{1/2}}\right) - 2bI, \tag{44}$$

where k is the rate constant at ionic strength I, k_0 is the rate constant at infinite dilution of ions (i.e., in the limit of zero ionic strength), Z_a and Z_b are the algebraic numbers of charges on the reactants (positive for cations and negative for anions), and b is a dimensionless parameter taken as ($0.15\ Z_a Z_b$) in this study. The ionic strength of the solution is defined as (SOLOMON, 2001):

$$I = \frac{1}{2}\sum_i Z_i^2 C_i, \tag{45}$$

where Z_i is the charge number of the i_{th} ion and C_i is its molar concentration. The sum extends over all ionic species present in the solution. According to Eq. (44), the rate constant will increase, decrease, or remain the same with increasing ionic strength, depending on whether the reactants have the same sign, opposite signs, or whether one reactant is neutral. For example, in 0.4 *M* H_2SO_4 solutions, the rate constants for reactions (14) and (43), corrected for these effects, are $k_{14} = 1.12 \times 10^{10}\ M^{-1}\ s^{-1}$ (see earlier) and $k_{38} = 5.97 \times 10^{10}\ M^{-1}\ s^{-1}$ (instead of 2.11×10^{10} and $11.3 \times 10^{10}\ M^{-1}\ s^{-1}$ in neutral water at 25 °C, respectively; see Table 1) (AUTSAVAPROMPORN et al., 2007 and references cited therein).

Finally, in our simulations the "direct" action of ionizing radiation on the sulfuric acid anions (mainly HSO_4^-) is neglected, which is a reasonably good approximation for 0.4 *M* sulfuric acid solutions. In fact, at this concentration of H_2SO_4, only about 3.5% of the total energy expended in the solution is initially absorbed by direct action on HSO_4^- ions (rather than on H_2O) (assuming that the energy absorbed by each component is proportional to its electron fraction) (JOHNSON and ALLEN, 1952).

III.3 Modeling the effects of temperature

In this work, we use an extended version of our Monte-Carlo computer code which was developed previously to include the effects of high temperature (from 25

up to 300 °C) on water radiolysis at low (HERVÉ DU PENHOAT et al., 2000; MEESUNGNOEN et al., 2002*a*) and high (HERVÉ DU PENHOAT et al., 2001; MEESUNGNOEN et al., 2001*b*, 2002*c*) LET.

Briefly, the scattering cross sections are independent of the medium's temperature because the energy of the ionizing particles is much larger than the thermal energies and because the motion of the target (water) molecules can be neglected. The influence of temperature on the physical stage of radiation action is thus mainly due to the fact that temperature brings the water molecules further apart without changing their ability to interact with the ionizing particles. For example, the density (ρ) of pressurized water varies with temperature from ρ = 1 g/cm^3 at room temperature to ρ = 0.712 g/cm^3 at 300 °C. This influences the particle's scattering mean free paths (MFP) which are related to the scattering cross sections (see Chapter II) through the simple relation MFP = $1/(\sigma N)$, where σ is the total cross section and N is the number of scatterers per unit volume. As a result of the invariance of the scattering cross sections, this dilatation is proportional to the inverse of the density. Since very little is known about the influence of the temperature on the early physicochemical processes, the simulations were performed using a number of assumptions for the temperature dependences of the initial distributions of the reactive species. For example, the possible decay channels for $H_2O^{\bullet +}$ and for vibrationally and electronically excited H_2O molecules are likely to be essentially independent of temperature since those primary processes are not thermally activated.[17] As for the migration of the cations $H_2O^{\bullet +}$ (hole transfer) and of the subexcitation electrons, it is likely to be sensitive to temperature. In fact, the variations of density would act as they did in the physical stage, increasing (on

---

[17] We should mention here that other authors, such as SWIATLA-WOJCIK and BUXTON (1995), have suggested that the temperature, through a diminution of hydrogen bonding in liquid water, could possibly change the relative contributions of the dissociative decay channels for H_2O^*.

average) each step of the random walk. Most importantly, electrons in the subexcitation energy range (<7.3 eV) are known to be sensitive to the structural order of the surrounding medium, owing to their nonnegligible delocalized character. In various media, as well as for water, their scattering cross-sections have been shown to increase rapidly when the degree of order diminishes (HERVÉ DU PENHOAT et al., 2000 and references cited therein). On this physical basis, one could expect the scattering cross sections of subexcitation electrons to increase with temperature in the range 25-300 °C, since the diminution of hydrogen bonding gives rise to a decrease of the structural order. As a result, this effect could affect the thermalization distances (r_{th}) of those electrons, in reducing them significantly with increasing temperature. It is difficult, however, to estimate to what extent this could affect r_{th}, but this effect could overcome the ~30% decrease in the density as temperature rises from 25 to 300 °C and in turn reduce those distances appreciably. In the present simulations, r_{th} is assumed to decrease linearly with temperature by a factor of 2 between 25 and 300 °C. This choice was shown to offer the best agreement with experiment of $G_{e^-_{aq}}$ and G_{H_2} at elevated temperature in the case of low-LET radiation (HERVÉ DU PENHOAT et al., 2000, 2001). Similar conclusion was also suggested previously by HOCHANADEL and GHORMLEY (1962), who pointed out that, at higher temperature, "subexcitation electrons are thermalized more rapidly".

It should be noted that the temperature effects mentioned above do not modify the initial yields of the radiolytic species. In contrast, they have an impact on the spatial distribution of the energy deposition events, and consequently on the initial distribution of primary radiolytic species (broader at higher temperature) and the subsequent reaction kinetics. As mentioned above (see Sects. I.1.5 and III.1.2), the important parameters in the kinetic modelling following irradiation are the diffusion coefficients of the different reactive species and their reaction rate constants. The values used in the computer simulations, including their temperature dependences, are essentially the same as those compiled by ELLIOT (1994) and ELLIOT et al. (1996*a*) and previously employed by HERVÉ DU PENHOAT et al. (2000, 2001) and

MEESUNGNOEN et al. (2001*b*, 2002*a*, *c*). Room-temperature values of the rate constants of the spur/track reactions and diffusion coefficients are listed in Tables 1 and 8, respectively.

III.4 Simulation of the Fricke dosimeter

The ferrous-sulfate Fricke dosimeter is an air-saturated solution of 1-10 m*M* $FeSO_4$ in aqueous 0.4 *M* H_2SO_4 (pH 0.46) (see Sect. I.2). To stochastically model the chemistry of the Fricke dosimeter, we have added to the IRT program the reactions of Fe^{2+} ions with the oxidizing species $^{\bullet}OH$, $HO_2^{\bullet}$, and H_2O_2 that are formed in the water of the irradiated solutions under aerated conditions. The mechanism for the radiolytic oxidation of Fe^{2+} ions to Fe^{3+} is well-understood and the rate constants at 25 °C of the individual reactions taking place are known. The reaction scheme is as follows (ALLEN, 1961; FRICKE and HART, 1966; DAS, 1971; SPINKS and WOODS, 1990; LUNDSTRÖM et al., 2004):

$e^-_{aq} + H^+ \rightarrow H^{\bullet}$	$k_{14} = 1.12 \times 10^{10}\ M^{-1}\ s^{-1}$ $pK_a\ (H^{\bullet}/e^-_{aq}) = 9.59$	(14)
$H^{\bullet} + O_2 \rightarrow HO_2^{\bullet}$	$k_{46} = 2.1 \times 10^{10}\ M^{-1}\ s^{-1}$	(46)
$Fe^{2+} + {}^{\bullet}OH \rightarrow Fe^{3+} + OH^-$	$k_{47} = 3.4 \times 10^{8}\ M^{-1}\ s^{-1}$	(47)
$Fe^{2+} + HO_2^{\bullet} \rightarrow Fe^{3+} + HO_2^-$	$k_{48} = 7.9 \times 10^{5}\ M^{-1}\ s^{-1}$	(48)
$HO_2^- + H^+ \rightarrow H_2O_2$	$k_{49} = 2.66 \times 10^{10}\ M^{-1}\ s^{-1}$ $pK_a\ (H_2O_2/HO_2^-) = 11.62$	(49)
$Fe^{2+} + H_2O_2 \rightarrow {}^{\bullet}OH + OH^- + Fe^{3+}$	$k_{50} = 52\ M^{-1}\ s^{-1}$	(50)
$OH^- + H^+ \rightarrow H_2O$	$k_{43} = 5.97 \times 10^{10}\ M^{-1}\ s^{-1}$ $pK_a\ (H_2O/OH^-) = 13.999$	(43)

At the acid concentration of 0.4 *M* H_2SO_4, e^-_{aq} is rapidly converted to $H^{\bullet}$ (see Sect. I.1.3). The $H^{\bullet}$ atoms created directly by radiolysis and by scavenging of e^-_{aq} react with oxygen in aerated solutions to form hydroperoxyl radicals ($HO_2^{\bullet}$)

(BĚGUSOVÁ and PIMBLOTT, 2002). Each of these radicals oxidizes three Fe^{2+} ions, one by reaction (48) and two by the reaction sequence (49), (50), and (47). Each $^{\bullet}OH$ radical oxidizes one Fe^{2+} ion, and each molecule of H_2O_2 oxidizes two Fe^{2+} ions. Summing all sources of Fe^{3+} ions, the yield of ferric ions in an aerated solution $G(Fe^{3+})$ is related to the escape yields of the free radicals and molecular species of (acidic) water radiolysis by Eq. (22).

Note that the values of k_6, k_{43}, and k_{49} used in the simulations have been corrected using Eqs. (44) and (45) for the effects due to the ionic strength in the case (under study here) of a solution made of 0.4 *M* H_2SO_4 and 5 m*M* $FeSO_4$. Note also that, as we have mentioned above, for solutions of 0.4 *M* in H_2SO_4 there is a small amount of $^{\bullet}OH$ radicals that react with HSO_4^- to form $SO_4^{\bullet-}$ [reaction (15)]. However, the overall ferric ion yield remains the same as given by Eq. (22) since the sulfate radical reacts with Fe^{2+} in the same way as $^{\bullet}OH$ (DAS, 1971; NETA et al., 1988):

$$SO_4^{\bullet-} + Fe^{2+} \rightarrow Fe^{3+} + SO_4^{2-} \qquad k_{51} = 2.79 \times 10^8\ M^{-1}\ s^{-1} \qquad (51)$$

Under normal irradiation conditions, the radical concentrations are low compared with the background concentrations of acid, Fe^{2+} ions, and oxygen (2.5×10^{-4} *M*) in solution, and the reactions are treated in the IRT program as pseudo first-order (see Sect. III.1.2). In modeling the Fricke dosimeter, the fastest reaction of Fe^{2+} ions is with $^{\bullet}OH$ radicals. The slowest component of the kinetics of Fe^{3+} formation is due to the Fenton-type reaction (50) (HALLIWELL and GUTTERIDGE, 1999).[18] For example, in the case of 5 m*M* $FeSO_4$ solutions considered here, this reaction takes several seconds to go to completion (AUTSAVAPROMPORN et al., 2007), which increases significantly the computer time usually chosen for modeling the radiolysis

---

[18] Note that thermal decomposition of H_2O_2 is not taken into account in the simulations. However, this process may not necessarily be negligible at temperatures above 150 °C (for example, see: ELLIOT et al., 1996*b*; BĚGUSOVÁ and PIMBLOTT, 2002).

of water (typically, the nonhomogeneous spur/track expansion is complete by ~1 μs). In the simulations reported here, the time evolution of $G(Fe^{3+})$ has been followed until ~50 s.

The temperature dependences of the rate constants for the ferrous ion reactions (47), (48), and (50) were scaled from their values at 25 °C using simple Arrhenius equations with activation energies of 9.2, 42, and 42 kJ mol^{-1}, respectively (JAYSON et al., 1973; CHRISTENSEN and SEHESTED, 1981; TAKAGI and ISHIGURE, 1985; CHRISTENSEN et al., 1993; LUNDSTRÖM et al., 2004). Finally, as there are no experimental data available on the temperature dependences of the diffusion coefficients of the Fe^{2+} and Fe^{3+} ions, the procedure adopted here was to scale the 25 °C values (0.719×10^{-9} m^2 s^{-1} and 0.604×10^{-9} m^2 s^{-1}, respectively; see: LIDE, 2008) according to the self-diffusion in liquid water (HERVÉ DU PENHOAT et al., 2000; see also Sect. III.1.2).

CHAPTER IV

RESULTS AND DISCUSSION

IV.1 Time evolution of $G(Fe^{3+})$ in aerated Fricke solutions over the range of temperature from 25 to 300 °C

IV.1.1 Kinetics of Fe^{3+} formation in the radiolysis of the Fricke dosimeter with 300-MeV irradiating protons (LET ~ 0.3 keV/μm) at 25 °C

As seen in Sect. III.4, the mechanism of oxidation of Fe^{2+} ions to Fe^{3+} in an aerated Fricke solution involves reactions of Fe^{2+} ions with the oxidizing species $^{\bullet}OH$, $HO_2^{\bullet}$, and H_2O_2 that are produced in the radiolytic decomposition of water. These reactions take place on different time scales. The fastest component of Fe^{3+} formation is due to Fe^{2+} oxidation by $^{\bullet}OH$ radicals, and the slowest is due to the reaction of Fe^{2+} with H_2O_2. As a result of the differences in the lifetimes of the reactions making up the radiolysis mechanism, $G(Fe^{3+})$ is time dependent (KEENE, 1964; SPINKS and WOODS, 1990; BĚGUSOVÁ and PIMBLOTT, 2002; AUTSAVAPROMPORN et al., 2007). This time evolution of $G(Fe^{3+})$ is illustrated in Fig. IV.1 for aerated solutions of 5 m*M* $FeSO_4$ in aqueous 0.4 *M* H_2SO_4 irradiated with 300-MeV protons (LET ~ 0.3 keV/μm) at 25 °C. As can be seen from this figure, three temporal stages are clearly identified:

- Stage 1 (at ~4 μs)

  $G(Fe^{3+}) = G_{^{\bullet}OH}$

  $G(Fe^{3+})$ ~ 3.1 molec./100 eV

- Stage 2 (at ~2 ms)

  $G(Fe^{3+}) = G_{^{\bullet}OH} + G_{e^-_{aq}+H^{\bullet}} + G_{HO_2^{\bullet}}$

  $G(Fe^{3+})$ ~ 6.7 molec./100 eV

- Stage 3 (at times >30 s)

$G(Fe^{3+}) = G_{\cdot OH} + 3\,(G_{e^-_{aq}+H\cdot} + G_{HO_2\cdot}) + 2\,G_{H_2O_2}$

$G(Fe^{3+}) \sim 15.45$ molec./100 eV.

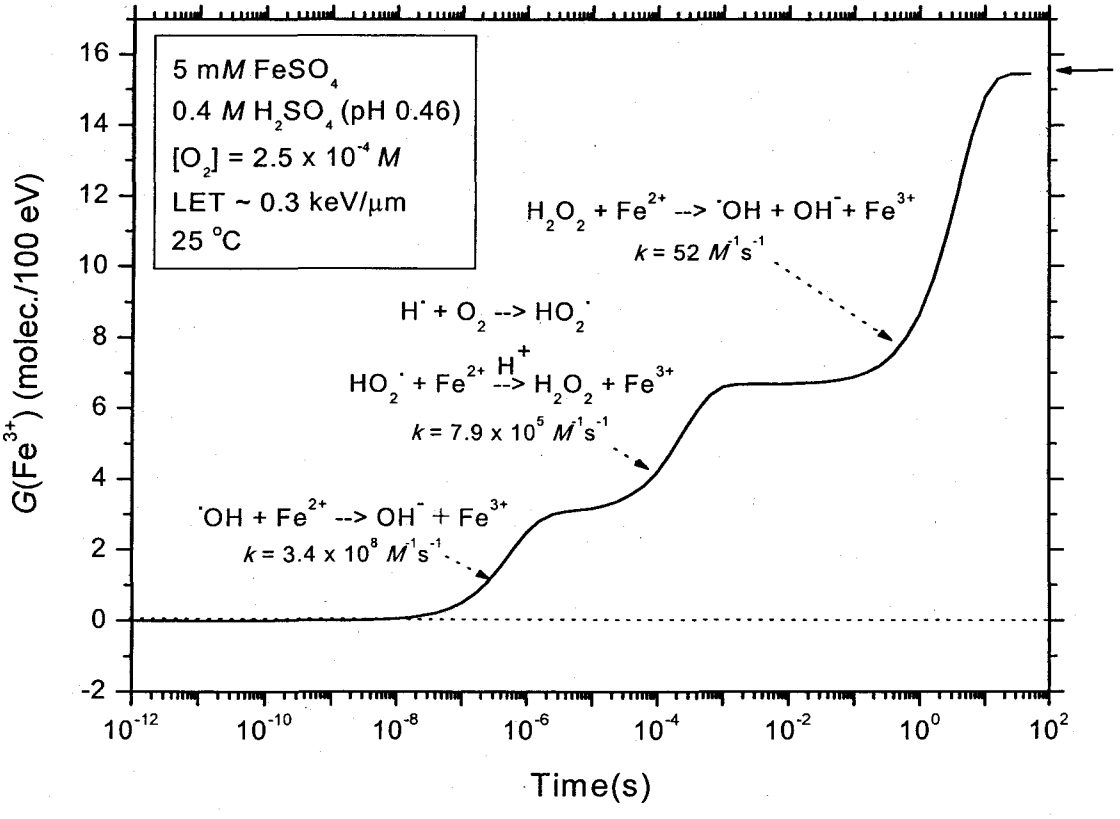

Figure IV.1: Time evolution of $G(Fe^{3+})$ (in molec./100 eV) in the radiolysis of air-saturated solution of 5 m*M* $FeSO_4$ in aqueous 0.4 *M* H_2SO_4 as obtained from our simulations for 300-MeV incident protons (LET ~ 0.3 keV/μm) at 25 °C. The concentration of dissolved oxygen used in the calculations is ~2.5×10^{-4} *M*. The solid line corresponds to our simulated kinetics of Fe^{3+} ion formation. The arrow on the right of the figure shows the yield of the Fricke dosimeter recommended for ^{60}Co γ-rays and fast electrons (15.6 molec./100 eV).

As shown in Fig. IV.1 and as mentioned above (see Sect. III.4), the fastest reaction of Fe^{2+} ions is with ·OH radicals. It is completed on a microsecond time scale. The oxidation of Fe^{2+} by $HO_2^{\bullet}$ is slower and requires a few milliseconds for completion. Finally, the slowest component in the formation of Fe^{3+} is due to Fe^{2+} oxidation by H_2O_2 [both the molecular product yield and that formed by reaction (49)].

This latter reaction takes place at times longer than ~0.1 s and is completed by about 30 s. The standard value of the ferric ion yield in the Fricke dosimeter, obtained for ^{60}Co γ-rays, high-energy X radiation or fast electrons, is $G(Fe^{3+})$ = 15.6 ± 0.2 molec./100 eV (for example, see: SCHULER and ALLEN, 1956; FRICKE and HART, 1966; FREGENE, 1967; ICRU REPORT 34, 1982; SPINKS and WOODS, 1990). Under the same low-LET conditions, our computed value of $G(Fe^{3+})$ at ~30 s is equal to ~15.45 (see Fig. IV.1), in very good agreement with the standard value.

IV.1.2 Kinetics of Fe^{3+} formation in the radiolysis of the Fricke dosimeter with 0.8-MeV neutrons at different temperatures from 25 to 300 °C

Figure IV.2 shows the kinetics of Fe^{3+} formation as obtained from our simulations of the radiolysis of the Fricke dosimeter by 0.8-MeV incident neutrons[19] at different temperatures in the range 25-300 °C. The corresponding time evolution of $G(Fe^{3+})$ simulated for 300-MeV irradiating protons at the same temperatures is presented in Fig. IV.3 for the sake of comparison.

The *G*-values for Fe^{3+} formed from a 0.8-MeV neutron in the $FeSO_4$ medium are calculated here by considering only the first four collisions that generate recoil protons of 0.505, 0.186, 0.069, and 0.025 MeV, with LET values of ~41, 69, 82, and 62 keV/μm, respectively.[20] The yields are estimated as the sum of the *G*-values for these four recoil protons (obtained from our Monte-Carlo simulations) after appropriate weighting is made according to the energy deposited by each of these protons (see Sect. I.1.5) (IMAMURA et al., 1970; LAWSON and PORTER, 1975; GORDON et al., 1983):

---

[19] Recall that this 0.8-MeV energy corresponds to the average energy of fast neutrons from the "YAYOI" reactor of the University of Tokyo (KATSUMURA et al., 1985, 1989, 1992).

[20] Further recoil protons are generated from the neutron, but their average energies are low and do not contribute significantly to the radiolysis. In the calculations, the radiation effects due to oxygen recoils are also neglected here.

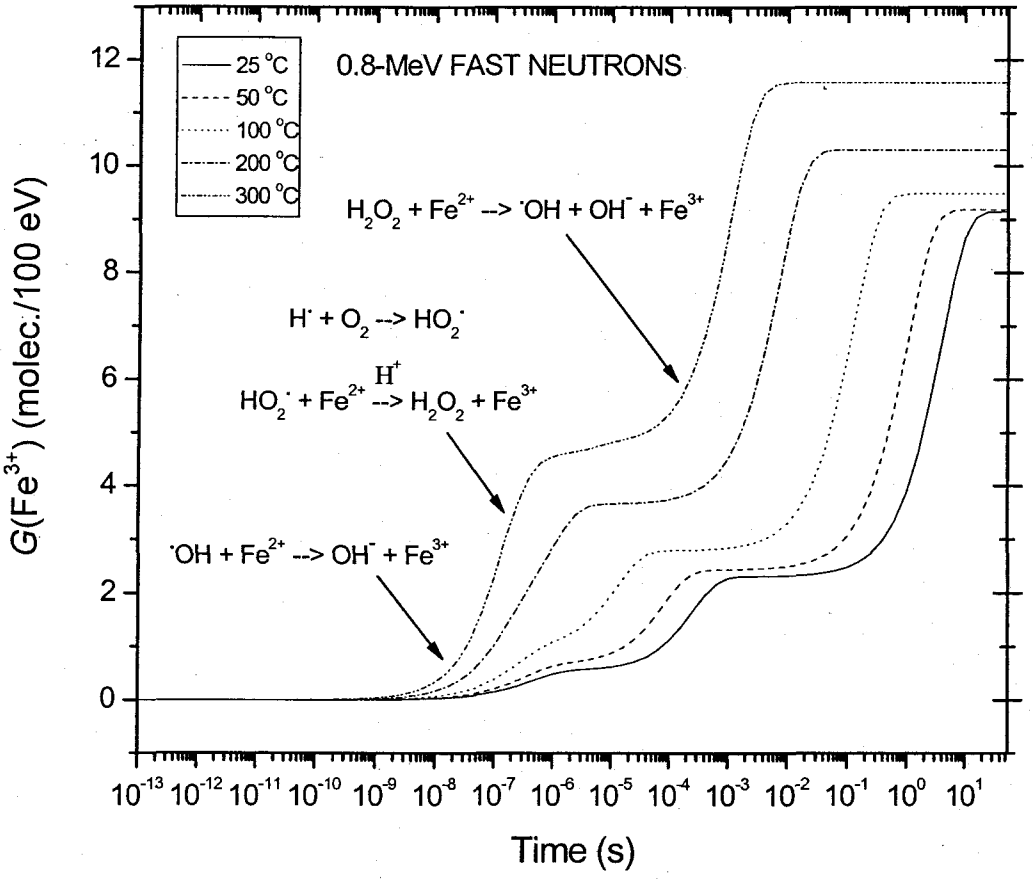

Figure IV.2: Time evolution of $G(Fe^{3+})$ (in molec./100 eV) for 0.8-MeV irradiating neutrons in aerated solutions of 5 m*M* $FeSO_4$ in aqueous 0.4 *M* H_2SO_4 at different temperatures in the range 25-300 °C. Yields of Fe^{3+} were obtained from Eqs. (52) and (53) taking into account recoil protons only (see text). The different lines correspond to our theoretical simulations at 25 (——), 50 (- - - -), 100 (·····), 200 (— — —), and 300 (— · —) °C.

$$G\left(Fe^{3+}\right) = \frac{\sum_{i=1}^{4} G_i\left(Fe^{3+}\right) E_i}{E_T}, \tag{52}$$

where

$$E_T = \sum_{i=1}^{4} E_i \tag{53}$$

is the sum of all recoil proton energies.

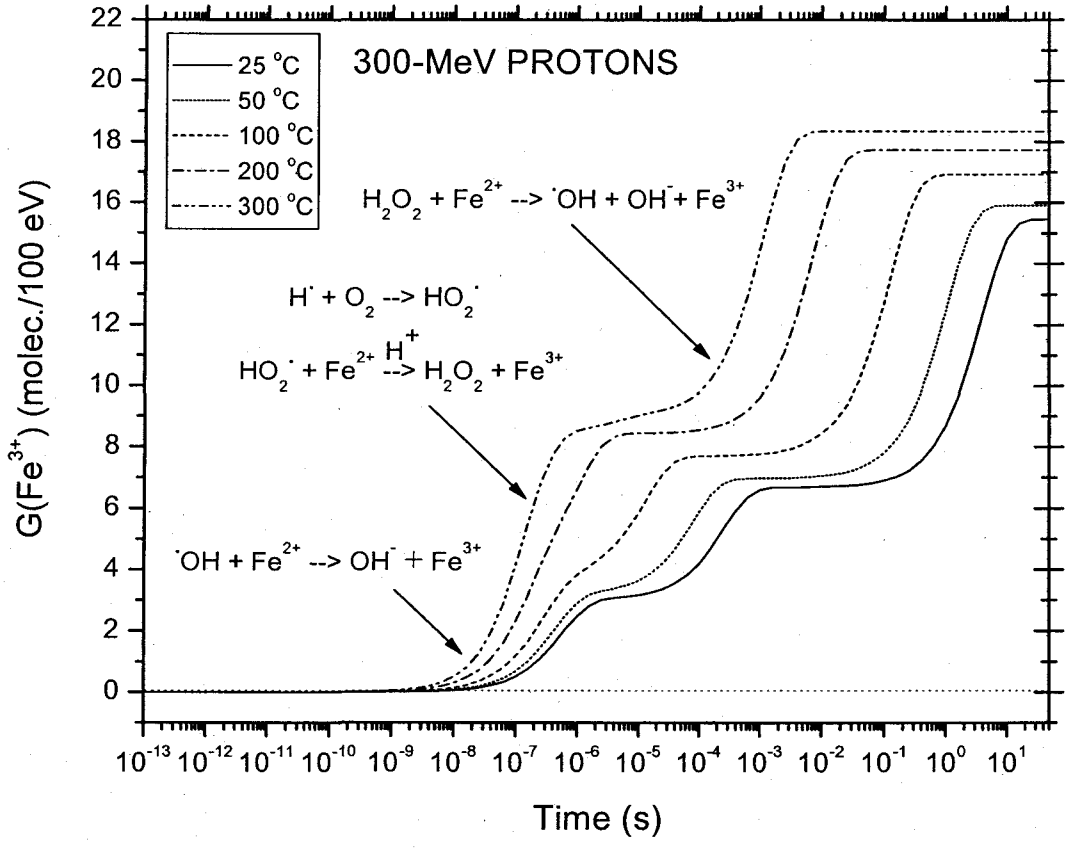

Figure IV.3: Time evolution of $G(Fe^{3+})$ (in molec./100 eV) for 300-MeV incident protons in aerated solutions of 5 m*M* $FeSO_4$ in aqueous 0.4 *M* H_2SO_4 at different temperatures in the range 25-300 °C. The different lines correspond to our theoretical simulations at 25 (——), 50 (- - - -), 100 (·····), 200 (— — —), and 300 (— · — ·) °C.

All reactions take place faster at higher temperature. As can be seen from Fig. IV.2, the kinetics of Fe^{3+} formation at 300 °C is several orders of magnitude faster than at room temperature. Also, an interesting feature shown in this figure is the increase with temperature of $G(Fe^{3+})$. In fact, the yield of Fe^{3+} (in molec./100 eV) increases from ~8.64 at 25 °C to 10.6 at 300 °C (Fig. IV.2), which corresponds to a

temperature coefficient of ~0.7% per degree.[21] According to Eq. (22), which relates $G(Fe^{3+})$ to the primary radical and molecular yields:

$$G(Fe^{3+}) = 3\,(G_{e^-_{aq}+H\cdot} + G_{HO_2\cdot}) + G_{\cdot OH} + 2\,G_{H_2O_2}\,, \qquad (22)$$

this increase is a reflection of the fact that $G_{e^-_{aq}}$, $G_{H\cdot}$, and $G_{\cdot OH}$ continuously increase with increasing temperature (see Fig. I.3).[22] It should be noted, however, that the contribution of hydrogen peroxide to the oxidation of Fe^{2+} ions to Fe^{3+} slightly decreases with increasing temperature due to the fact that $G_{H_2O_2}$ decreases on going from 25 to 300 °C (Fig. I.3).

IV.2 The effect of LET on the chemistry and the yields of the Fricke dosimeter

It has been known since very early studies with internal and external ^{210}Po α-particle sources that the yield for oxidation of ferrous ions in the Fricke dosimeter is appreciably less for high-LET radiations, such as accelerated ions and neutrons, than for low-LET radiations, that is ^{60}Co γ-rays, high-energy X-rays, fast electrons or energetic protons (for example, see: ALLEN, 1961; LAVERNE and SCHULER, 1987; PIMBLOTT and LAVERNE, 2002; AUTSAVAPROMPORN et al. 2007, and references therein). In recent studies, our laboratory has carried out Monte-Carlo simulations of the radiolysis of the Fricke dosimeter in the low-LET regime from ~0.3 to 15 keV/μm (using protons of various initial energies in the range ~300-2.1 MeV) at ambient temperature (AUTSAVAPROMPORN, 2006; AUTSAVAPROMPORN et al.,

---

[21] This value is to be compared with the temperature coefficient of ~1.05% per degree obtained from Fig. IV.3 for the 300-MeV proton radiolysis of the Fricke dosimeter over the range of temperature from 25 to 300 °C (see Sect. IV.3.1).

[22] Recall here that the production of Fe^{3+} ions is highly sensitive to the primary free-radical yields, especially the yield of $H^{\bullet}$ atoms (see Sect. I.2).

2007). The general trend of the experimental variation of $G(Fe^{3+})$ with radiation quality was well reproduced by our computed Fe^{3+} ion yield values.

In the present study, our aim is to model the action of fast neutron radiation on the chemistry and the yields in the Fricke dosimeter. As emphasized in Chapters I and II, *neutrons can be regarded as high-LET particles* because they are stopped by nuclei (both protons and oxygen nuclei), which become recoil ions, losing their energy in dense tracks. However, in the neutron energy range of interest here (i.e., below 10 MeV), the greatest energy deposition in the solution comes from recoil protons. In fact, summing over all events, EDWARDS et al. (2007) estimated that 88% of the neutron energy is absorbed by protons and 12% by oxygen nuclei. Given the minor fraction of energy in oxygen recoil, and the small anticipated yield, we begin below with the proton radiolysis problem, extending the previously reported simulations of AUTSAVAPROMPORN et al. (2007) to higher LET values up to ~70 keV/μm corresponding to the Bragg peak region (~0.15 MeV) (see Fig. III.1). As a logical subsequent step, we then calculate the fast neutron radiolysis yields in the Fricke dosimeter as a function of neutron energy, using our simulated proton radiolysis yields and taking into account the contribution of recoil oxygen ions.

IV.2.1 Variation of $G(Fe^{3+})$ with LET using irradiating protons of various initial energies at 25 °C

Figure IV.4 shows the values of $G(Fe^{3+})$ calculated from our Monte-Carlo simulations of the radiolysis of aerated solutions of 5 m*M* $FeSO_4$ in 0.4 *M* H_2SO_4 as a function of LET for incident protons of initial energies in the range ~300-0.15 MeV (~0.3-70 keV/μm) at 25 °C. It is seen that as the LET increases the yield diminishes (see also Table 4). Our computed values are compared with experimental data of ferric ion yields versus LET obtained by a number of different workers (HARDWICK, 1952; HART, 1954; DONALDSON and MILLER, 1955; HART et al., 1956; HAYBITTLE et al., 1956; SCHULER and ALLEN, 1957; BACK and MILLER, 1957; LEFORT, 1957, 1958; BARR and SCHULER, 1959; PEISACH and STEYN, 1960;

ANDERSON and HART, 1961; SHALEK et al., 1962; KOCHANNY et al., 1963; DAVIES et al., 1963; BENSASSON et al., 1963; FRICKE and HART, 1966; FREGENE, 1967; ICRU REPORT 17, 1970; SAUER et al., 1978; ICRU REPORT 34, 1982; LAVERNE and SCHULER, 1987; ELLIOT et al., 1996*b*; KLASSEN et al., 1999; PIMBLOTT and LAVERNE, 2002) using a variety of methods for radiations of different energies. Despite the relatively large uncertainties of the reported measurements, there is a good agreement between theory and experiment, especially for LET below ~10-15 keV/μm.

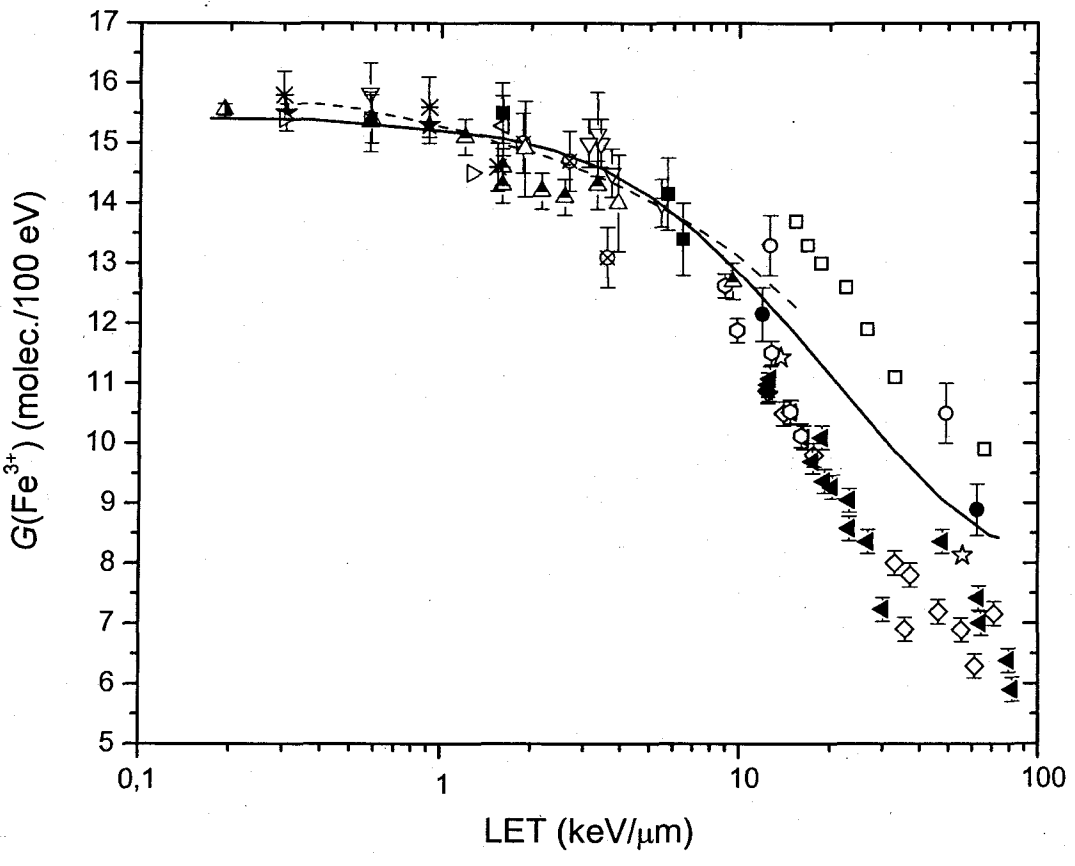

Figure IV.4: Plot of the ferric ion yield $G(Fe^{3+})$ (in molec./100 eV) for the aerated Fricke solution at 25 °C against LET in the range ~0.3-70 keV/μm. The solid curve represents the values of $G(Fe^{3+})$ calculated from our Monte-Carlo simulations using incident protons of various initial energies between ~300 and 0.15 MeV. The dashed line corresponds to the Fricke *G*-values calculated by AUTSAVAPROMPORN et al. (2007) for LET varying from ~0.3 to 15 keV/μm. Experimental data: (▽) HARDWICK, 1952 - see also ALLEN, 1954; (⊠)

DONALDSON and MILLER, 1955; (◇) HART et al., 1956; (⊗) HAYBITTLE et al., 1956; (△) BACK and MILLER, 1957; (■) LEFORT, 1957, 1958 - see also COTTIN and LEFORT, 1956; (☆) BARR and SCHULER, 1959; (◁) PEISACH and STEYN, 1960; (◀) ANDERSON and HART, 1961; (×) SHALEK et al., 1962; (○) KOCHANNY et al., 1963; (▷) DAVIES et al., 1963; (▲) FREGENE, 1967; (○) SAUER et al., 1978; (★) ICRU REPORT 34, 1982; (□) LAVERNE and SCHULER, 1987; (●) ELLIOT et al., 1996*b*; and (▲) KLASSEN et al., 1999. Dose-average LET values used here for the various radiation types considered are taken from WATT (1996). Note that, for X-rays, there are in certain cases insufficient experimental details for an estimate of the average energy of electrons resulting from photon absorption in the solution to be made. This results in some uncertainty in assigning an average LET value to the corresponding reported $G(Fe^{3+})$ results.

This dependence of $G(Fe^{3+})$ on LET results from the fact that the production of ferric ions in the Fricke system is *most sensitive* to radical yields, especially $H^{\bullet}$ atoms (see Sect. I.2). Indeed, according to Eq. (22), the lower the yield of radicals which escape the radiation track, the lower the Fricke *G*-values. Since the *G*-values for radicals do show a marked decrease with increasing LET (see Sect. I.1.4 and Table 2), it follows that $G(Fe^{3+})$ also decreases as the LET increases. This behavior is explained by the increased importance of intratrack processes at higher LET which enhance radical-radical recombination reactions producing molecular products.[23]

---

[23] Note that, at high particle LET, the production of Fe^{3+} is not *uniquely* determined by LET but rather increases with increasing particle charge because of differences in the local energy density. In fact, at the same LET, the impinging particle with higher charge has a smaller local energy density because of its higher velocity so that more radicals escape the particle track to oxidize ferrous ions (for example, see: LAVERNE and SCHULER, 1987; PIMBLOTT and LAVERNE, 2002; MEESUNGNOEN and JAY-GERIN, 2005). However, in the range of relatively low LET considered in this study, LET remains a nearly singular function of LET and can therefore be considered as a useful specifier to compare $G(Fe^{3+})$ for different radiation beam qualities.

IV.2.2 Variation of $G(Fe^{3+})$ with neutron energy for irradiating fast (~0.5-10 MeV) neutrons at 25 °C

As mentioned above, in the fast neutron energy range below ~10 MeV, approximately 88% of the neutron energy is absorbed by recoil protons and the remaining 12% by oxygen nuclei (EDWARDS et al., 2007). Those particles released by neutron interactions in the medium create the primary free radical and molecular product yields, which subsequently lead to the oxidation of ferrous ions in the Fricke solution according to the radiolysis mechanism previously described in Sects. I.2 and III.4. The integrated yields of ferric ions produced by *both* recoil protons and oxygen ions can be derived using the following relationship (IMAMURA et al., 1970; LAWSON and PORTER, 1975; GORDON et al., 1983):

$$G\left(Fe^{3+}\right) = \frac{\sum_i \left[2\,\sigma_H\left(E_{ni}\right) G_{pi}\left(Fe^{3+}\right) E_{pi} + \sigma_O\left(E_{ni}\right) G_{Oi}\left(Fe^{3+}\right) E_{Oi}\right]}{\sum_i \left[2\,\sigma_H\left(E_{ni}\right) E_{pi} + \sigma_O\left(E_{ni}\right) E_{Oi}\right]}, \qquad (54)$$

where the index i corresponds to the number of fast neutron interactions that take place in the solution (in fact, only the first 4 neutron collisions are considered in the present calculations, as further recoil protons and/or oxygen ions generated by the neutron as it is further moderated do not contribute significantly to the radiolysis owing to their low average energies), G_{pi} and G_{Oi} are the yields of Fe^{3+} for the recoil proton (p) and oxygen ion (O) released by the ith interaction of the neutron, E_{pi} and E_{Oi} are the energies of those two charged particle recoils, respectively, and $\sigma_H(E_{ni})$ and $\sigma_O(E_{ni})$ are, respectively, the elastic scattering cross sections for a fast neutron incident on hydrogen and oxygen with kinetic energy E_{ni} just before the ith collision (see Fig. II.2). This expression also takes explicitly into account the fact that a water molecule contains two hydrogen atoms and one oxygen atom.

In the range of neutron energies investigated here, Eq. (54) can be well approximated by the simplified expression:

$$G\left(Fe^{3+}\right) = \frac{\sum_i \left[2\, G_{pi}\left(Fe^{3+}\right) E_{pi} + G_{Oi}\left(Fe^{3+}\right) E_{Oi}\right]}{\sum_i \left[2\, E_{pi} + E_{Oi}\right]}, \qquad (55)$$

where it is assumed that the neutron scattering cross sections σ_H and σ_O are all equal whatever the value of E_n, which, in other terms, amounts to ignore the probabilities of interaction of the incident neutron with H and O recoil nuclei. Indeed, as is clearly illustrated in Fig. IV.5, the two curves of $G(Fe^{3+})$ versus the incident neutron energy, calculated from Eqs. (54) and (55) (solid and dash-dot lines, respectively), are more or less superposed. The relative superposition of these curves results from the fact that, as we have already mentioned above, only the first few terms of the summation over i in Eq. (54) play a dominant role in the determination of $G(Fe^{3+})$ and that for those terms the intervening cross sections $\sigma_H(E_{ni})$ and $\sigma_O(E_{ni})$ are more or less the same in the range of energy considered and vary slowly with the neutron energy (see Fig. II.2). It should be noted here that Eq. (55) reduces to Eqs. (52) and (53) (assuming four neutron collisions) if the contribution due to recoil oxygen ions is ignored.

Figure IV.5 also shows our results of $G(Fe^{3+})$ calculated from Eq. (55) for recoil protons only (i.e., ignoring the contribution of oxygen ion recoils) (dot line) and for recoil oxygen ions only (i.e., assuming all the neutron energy is absorbed by oxygen nuclei) (dash-dot-dot line), for incident fast neutrons with energies between ~0.5 and 10 MeV. In the calculations, the intervening ferric ion yields $G_{pi}(Fe^{3+})$ produced by recoil protons are directly obtained from our Monte-Carlo simulations (see Fig. IV.4). However, for the values of $G_{Oi}(Fe^{3+})$ produced by oxygen ions, only estimates can be derived as our IONLYS simulation code cannot be employed simply because the energies with which those ions are ejected are, over all the fast neutron energy range considered here, too low (for example, in this range, E_{O1} varies between ~0.0035 and 0.071 MeV/nucleon) for the Z^2 scaling law (which is used in the code to provide interaction cross sections for bare ion impact from cross sections for proton impact) to be applicable (see Sect. III.1.1). In the absence of simulated (and experimental)

data, the $G(Fe^{3+})$ values produced by recoil oxygen ions (assumed to be ejected in the 8+ charge state) are simply approximated here by the Fricke yield measurements of LAVERNE and SCHULER (1996) for $^{12}C^{6+}$ ions for the corresponding range of oxygen ion energies. Given the minor fraction of energy in oxygen recoil and the small contribution of the oxygen nuclei to the final $G(Fe^{3+})$ values (on the order of 10% at 10 MeV; see Fig. IV.5), the uncertainty introduced by this approximation is considered to represent a small error only.

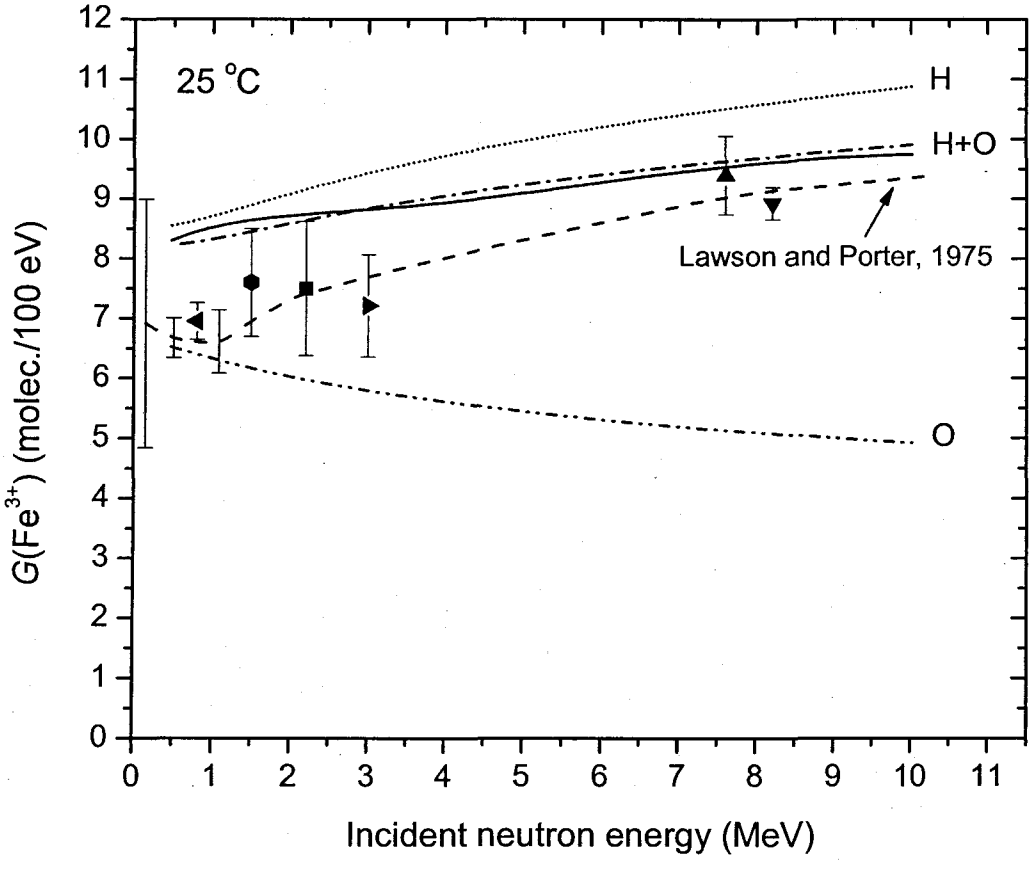

Figure IV.5: Yield of ferric ions $G(Fe^{3+})$ (in molec./100 eV) for fast neutrons in the aerated Fricke solution at 25 °C as a function of incident neutron energy in the range ~0.5-10 MeV. The solid line shows our $G(Fe^{3+})$ values for neutrons calculated from Eq. (54) taking into account 4 neutron collisions in the medium and using the elastic scattering cross sections σ_H and σ_O shown in Fig. II.2. The dash-dot line represents our neutron $G(Fe^{3+})$ values calculated from Eq. (55) also considering 4 neutron collisions in the solution but assuming that σ_H and σ_O are all equal over all the neutron energy range considered. The dot line

represents the $G(Fe^{3+})$ values obtained from our Monte-Carlo simulations taking into account recoil protons only. The dash-dot-dot line represents the $G(Fe^{3+})$ values assuming that the neutrons are stopped only by oxygen nuclei (see text). The dash line shows the neutron *G*-values for the Fricke dosimeter predicted by LAWSON and PORTER (1975) using a semi-empirical method based on published charged particle *G*-values along with neutron-induced particle spectra calculated for monoenergetic neutron interactions with the dosimeter medium. Experiment (at 25 °C): (■) GREENE et al., 1973*a*; (●) LAW et al., 1974; (▼) LAWSON and PORTER, 1975; (▲) GREENE et al., 1975; (▶) PEJUAN and KÜHN, 1981; and (◀) KATSUMURA et al., 1989.

As can be seen from Fig. IV.5, our calculated neutron $G(Fe^{3+})$ values for the Fricke dosimeter are in good agreement with the available experimental results (GREENE et al., 1973*a*; LAW et al., 1974; LAWSON and PORTER, 1975; GREENE et al., 1975; PEJUAN and KÜHN, 1981; KATSUMURA et al., 1989) (also included in the figure for comparison). This good agreement obviously supports the validity of the model. Over the whole ~0.5-10 MeV range of neutron energies studied here, the computed yields of ferric ions (slightly) increase with increasing neutron energy. As mentioned above, this energy dependence of the yields of the Fricke dosimeter is a reflection of the fact that the greater the energy of the neutrons, the less the LET, and the larger the values of $G(Fe^{3+})$ (see, for example, Table 4). In this respect, even if neutrons cannot produce ionization or excitation directly, the radiation chemistry of fast neutron irradiations, determined by the charged particle radiations they produce, parallels that of other ionizing radiations.

An additional remark should be made from Fig. IV.5 regarding the predicted $G(Fe^{3+})$ values obtained from our Monte-Carlo simulations assuming that neutrons are stopped by protons only. These values (shown as the dot line in Fig. IV.5) are found to be ~20% larger than the corresponding experimental data obtained in fast neutron radiolysis. This result agrees very well with the measurements of KATSUMURA et al. (1992) [and also with the compilation of $G(Fe^{3+})$-versus-particle energy data for protons and deuterons of LAWSON and PORTER (1975)] who reported, in the vicinity of room temperature, $G(Fe^{3+})$ values comprised in the range

~7-10 molec./100 eV for an irradiation with 3.3 MeV protons,[24] while they found a ferric ion yield of 6.95 molec./100 eV for an irradiation with 0.8 MeV incident neutrons (see Table 4). From the present simulations, it can clearly be inferred that this difference originates from the high-LET oxygen recoil ions whose radiolysis chemistry induces a decrease in the Fricke yield arising from the hydrogen recoil ions only. From a strict quantitative standpoint, we can conclude that, even if the anticipated yield is relatively small, the contribution of recoil oxygen ions should be accounted for when we calculate the fast neutron radiolysis yields in the Fricke dosimeter. In this respect, there is a need for a better characterization of the chemistry induced by oxygen ions in the energy range below ~1-2 MeV (for the first three collisions, a 10-MeV fast neutron generates recoil oxygen ions having energies of 1.13, 1.00, and 0.89 MeV) and of the $G(Fe^{3+})$ values produced by these recoil ions (we should remind here that, in the absence of other information, the oxygen ions are assumed to be ejected in the 8+ charge state and the corresponding $G(Fe^{3+})$ values are simply approximated by Fricke yield measurements for $^{12}C^{6+}$ ions).

IV.3 The influence of temperature on the yields of the Fricke dosimeter

IV.3.1 Variation of $G(Fe^{3+})$ for γ-irradiation in the Fricke dosimeter as a function of temperature

Early measurements of the temperature dependence of $G(Fe^{3+})$ for the Fricke dosimeter were reported prior to 1970 (e.g., MINDER and LIECHTI, 1946; HARDWICK, 1953; SCHWARZ, 1954; SHALEK et al., 1962; HOCHANADEL and GHORMLEY, 1962; PETTERSSON and HETTINGER, 1967; LAW, 1970). The values then found for the temperature coefficient of the ferric-ion yield indicated that this coefficient was positive but small. However, the reported values were rather

---

[24] These authors carried out proton beam radiolysis as a *model experiment* of the fast neutron radiolysis.

scattered (from zero to ~0.5% per degree between 4 and 20 °C, depending on the authors), due mainly to relatively large uncertainties in the measurements. The availability in the 1980s of precision spectrophotometers allowed new, more accurate determinations of the influence of the irradiation temperature on the Fricke yield. For example, SHORTT (1989) reported a value for the change in $G(Fe^{3+})$ of (0.121 ± 0.005)% per °C for a standard ^{60}Co γ-ray source and an irradiation temperature range of 15-35 °C, in agreement with values presently in common use at other laboratories. Experiments on the effect of temperature on $G(Fe^{3+})$ were also extended to cover a larger range of temperatures up to 250 °C (e.g., KABAKCHI and LEBEDEVA, 1984; ISHIGURE et al., 1987; KATSUMURA et al., 1988). As can be seen from Fig. IV.6, $G(Fe^{3+})$ rises slightly with increasing temperature. This increase in the Fe^{3+} yields with temperature was already noted in Sect. IV.1.2 (see Fig. IV.3).

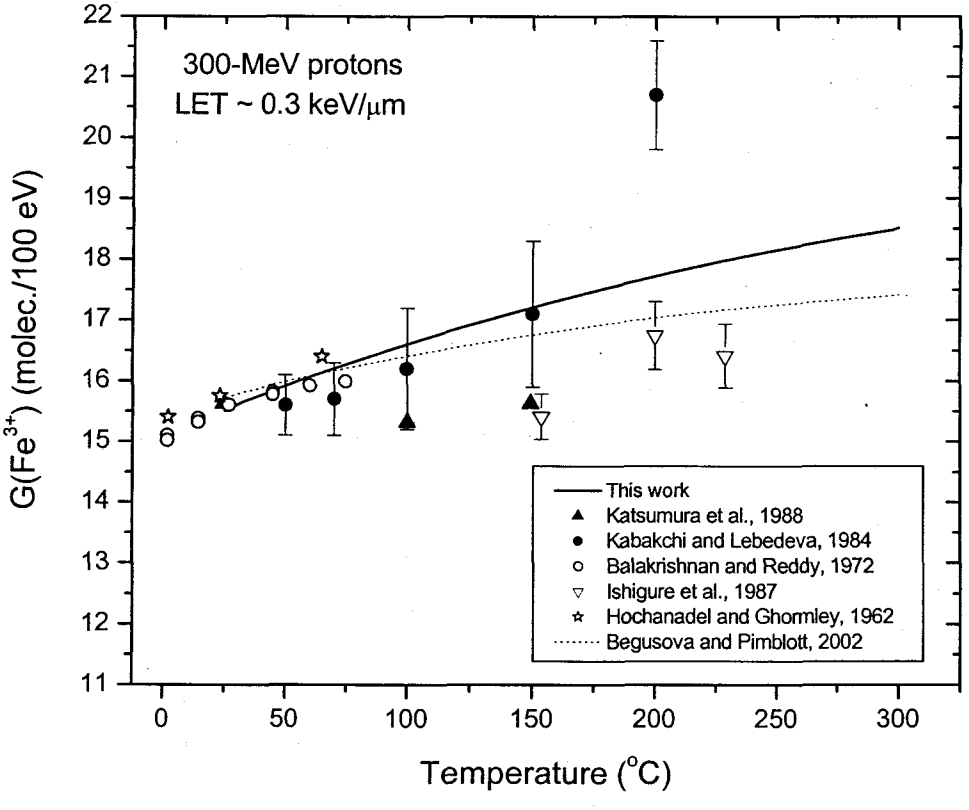

Figure IV.6: Yield of Fe^{3+} in aerated Fricke solution as a function of temperature, for 300-MeV irradiating protons (LET ~ 0.3 keV/μm). The solid line shows the values of $G(Fe^{3+})$ obtained (at ~50 s) from our Monte-Carlo simulations. The dot line shows the *G*-values for

the Fricke dosimeter predicted by BĚGUSOVÁ and PIMBLOTT (2002) using the stochastic IRT simulation method, incorporating simulated electron track structures. Experiment: (☆) HOCHANADEL and GHORMLEY, 1962; (○) BALAKRISHNAN and REDDY, 1972; (●) KABAKCHI and LEBEDEVA, 1984; (▽) ISHIGURE et al., 1987; and (▲) KATSUMURA et al., 1988.

The γ-ray radiolysis of the (aerated) Fricke dosimeter at elevated temperatures was modeled using our Monte-Carlo IONLYS-IRT code for 300-MeV incident protons (LET ~ 0.3 keV/μm), following the simulation methodology described in Sects. III.3 and III.4. As shown in Fig. IV.6, the predicted *G*-values (in molec./100 eV) for Fe^{2+} oxidation increase from ~15.4 to 18.4 over the temperature range from 25 to 300 °C (i.e., an ~19% increase), which corresponds to a temperature coefficient of ~1.05% per degree.[25] A good agreement is obtained between our computed Fe^{3+} yields and the available experimental data. Our *G*-values also compare well with those predicted theoretically by BĚGUSOVÁ and PIMBLOTT (2002) using stochastic simulation methods. As discussed above (see Sect. IV.1.2), this increase in $G(Fe^{3+})$ is readily explained by an increase in the yields of free radicals and a decrease in those of molecular products on going from 25 to 300 °C (Fig. I.3).

IV.3.2 Variation of $G(Fe^{3+})$ for the 0.8-MeV neutron radiolysis in the Fricke dosimeter as a function of temperature

Our calculated yields of Fe^{2+} oxidation in the (aerated) Fricke dosimeter irradiated by 0.8-MeV incident neutrons over the range of temperature from 25 to 300 °C are shown in Fig. IV.7, along with the experimental data of KATSUMURA et al. (1989, 1992). In fact, as far as we know, KATSUMURA et al.'s data (acquired with the University of Tokyo neutron source reactor "YAYOI" whose average energy of the neutrons is ~0.8 MeV; see Sects. I.1.5 and IV.1.2) are, up until now, the *only* data

---

[25] This value compares well with that (0.6% per degree) predicted by BĚGUSOVÁ and PIMBLOTT (2002) from their stochastic IRT simulations of the γ-radiolysis of the aerated Fricke solution over this same temperature range.

available in the literature with which to compare our results on the temperature dependence of the Fe^{3+} yields for the Fricke dosimeter irradiated by fast neutrons.

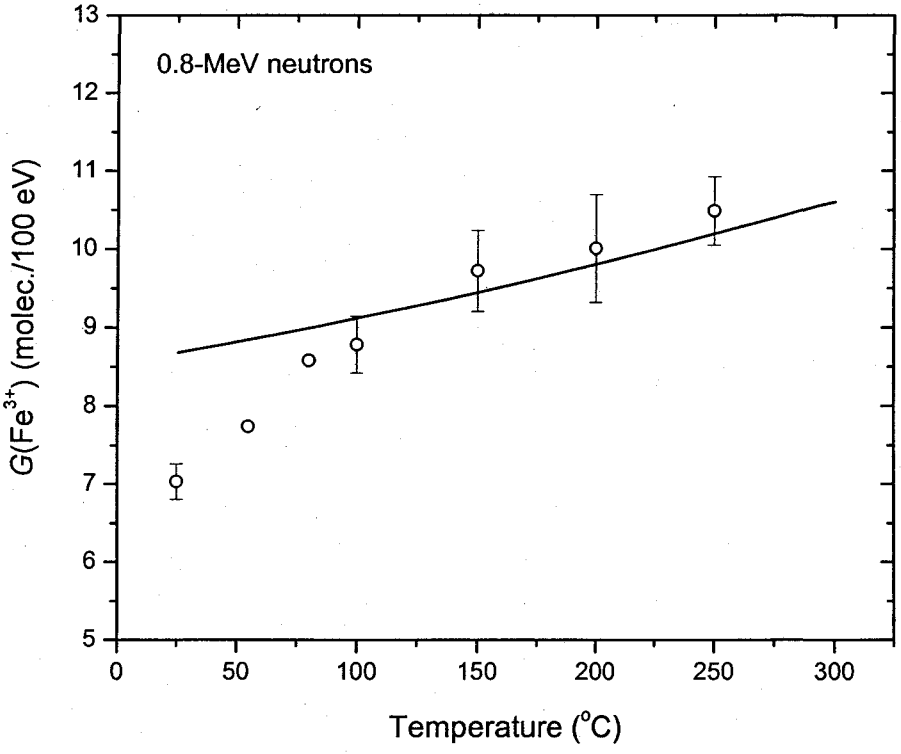

Figure IV.7: Yield of Fe^{3+} in the aerated Fricke solution as a function of temperature for 0.8-MeV incident neutrons. The solid line shows our simulated results for $G(Fe^{3+})$, calculated from Eq. (55) taking into account four neutron collisions and assuming all the neutron energy is absorbed by protons only (i.e., ignoring the contribution due to recoil oxygen ions). The symbol (○) refers to the experimental data of KATSUMURA et al. (1989, 1992).

As can be seen from Fig. IV.7 (see also Fig. IV.2), $G(Fe^{3+})$ increases with increasing temperature, which is attributed - as mentioned above - to the fact that the free-radical escape yields (especially the yield of $H^{\bullet}$ atoms) increase as the temperature increases (see Sect. I.1.5). An increase in the Fe^{3+} yield (in molec./100 eV) of ~23% from ~8.6 at 25 °C to 10.6 at 300 °C is predicted. Experimentally, the yield of Fe^{3+} increases from ~7.0 at 25 °C to ~10.5 at 250 °C, which corresponds to the temperature coefficient of ~1.5% per degree over this range of temperature. Our $G(Fe^{3+})$ values, calculated from Eq. (55) assuming only recoil protons (i.e., with no

corrections being made for oxygen-recoil-ion contributions), agree very well with experiment above 75 °C. At temperatures lower than 75 °C, however, they are higher than the experimental data, by about 1.5 *G*-unit at room temperature. The reasons for such a difference between KATSUMURA et al.'s experimental results and our model predictions below 75 °C are not clear. Of course, the incorporation in our calculations of the contributions originating from the high-LET oxygen recoil ions would clearly induce a (slight) decrease in the Fricke yields (see Sect. IV.2.2). However, this effect should be observed more or less equally over the whole temperature range studied (see Fig. IV.5), and not only at temperatures below 75 °C. Another possible reason to explain the discrepancy could simply be of experimental origin, as the neutron *G*-values reported by KATSUMURA et al. (1989, 1992) were obtained in a nuclear reactor, that is, under a mixed high-LET neutron and low-LET gamma-ray irradiation field. Assessing the chemistry yields induced by the neutrons *alone* under such mixed LET irradiation conditions is difficult (e.g., ELLIOT et al., 1996*b*; McCRACKEN et al., 1998; EDWARDS et al., 2007), even if the authors estimate that more than 95% of the total dose in the sample solutions comes from fast neutrons. In the absence of other information about possible overlap and chemical interaction between fast-neutron and γ-ray tracks, this leads us to believe that the true situation is uncertain. More experimental data would be greatly needed in order to compare in a more critical fashion our Monte-Carlo modeling calculations of the effect of temperature on the Fe^{3+} ion yields in the radiolysis of the Fricke solution by fast neutrons (especially for different incident neutron energies).

IV.3.3 Time scale for spur expansion as a function of temperature

The chemistry of the Fricke dosimeter (dilute aqueous solution of ferrous ions in 0.4 *M* H_2SO_4) is based on the radiolytic oxidation of Fe^{2+} ions to Fe^{3+}, as described in detail in Sect. I.2. Its reaction scheme is well established (see Sect. III.4). From this mechanism, the yield of Fe^{3+} ions can be related quantitatively to the primary radical and molecular yields of the radiolysis of the solution as shown in Eq. (22):

$$G(Fe^{3+}) = 3\,(G_{e^-_{aq}+H\cdot} + G_{HO_2\cdot}) + G_{\cdot OH} + 2\,G_{H_2O_2}\,. \qquad (22)$$

For low-LET radiations, these primary or "escape" yields correspond to the yields of radiolytic species that remain after spur expansion. At room temperature and normal absorbed dose rates, this spur expansion is essentially complete on the time scale of ~10^{-7}-10^{-6} s after the initial energy deposition event (see Sect. I.1.2). At this time, the species that have escaped from spur reactions become distributed homogeneously throughout the bulk of the solution and then available for reaction with added solutes (treated as spatially homogeneous) at moderate concentrations (actually Fe^{2+} ions in the present case). In other words, at 25 °C, the primary radical and molecular *G*-values to be used in Eq. (22) are those given in Eq. (13) of Sect. I.1.3. At elevated temperatures, however, this time for complete spur overlap is not well known, even if one can expect the changeover from (nonhomogeneous) spur kinetics to homogeneous kinetics to occur *faster* than at ambient temperature (HERVÉ DU PENHOAT et al., 2000, 2001; MEESUNGNOEN et al., 2001*b*, 2002*a*).

In fact, a simple procedure based on the use of Eq. (22) of the Fricke dosimeter can be employed to estimate this "spur expansion" time (called t_s in what follows) (i.e., the minimum time required before the reactive species can be regarded as being distributed homogeneously over the volume of solution) as a function of temperature from ambient up to 300 °C. This procedure, illustrated in Fig. IV.8, can be described as follows:

(1) We first perform Monte-Carlo simulations of the radiolysis of the aerated Fricke dosimeter, using 300-MeV irradiating protons (LET ~ 0.3 keV/μm), in order to determine $G(Fe^{3+})$ (at ~50 s) as a function of temperature. Our computed $G(Fe^{3+})$

value, extending from about 15.4 to 18.4 over the range of temperature studied, are shown as the thick solid line in Fig. IV.8.[26]

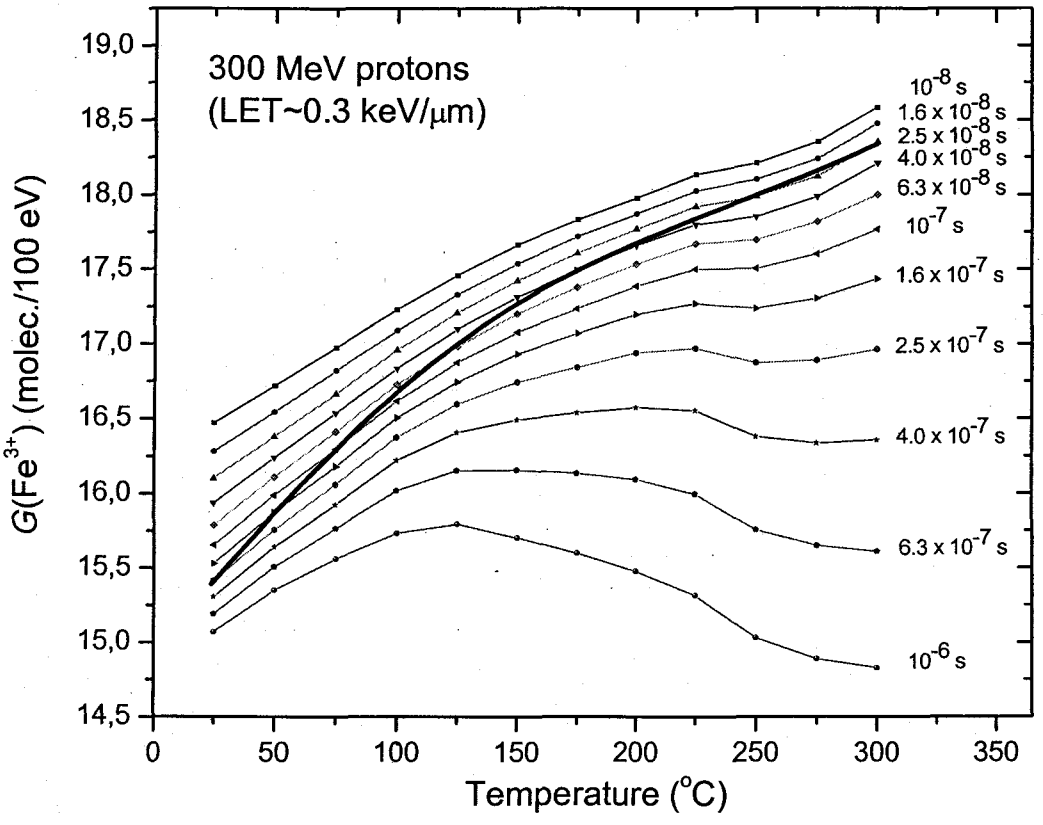

Figure IV.8: Yields of Fe^{3+} in aerated Fricke solution as a function of temperature, for 300-MeV (LET ~ 0.3 keV/μm) irradiating protons. The thick solid curve shows the values of $G(Fe^{3+})$ obtained directly from our Monte-Carlo simulations. All the other curves show our $G(Fe^{3+})$ values calculated at different times between 10^{-6} and 10^{-8} s from Eq. (22), using the radical and molecular product yields obtained at those times from our Monte-Carlo simulations of the radiolysis of acidic (0.4 *M* H_2SO_4) aqueous solutions. Each curve is associated to a given symbol representing a given time (indicated on the right of the figure).

---

[26] Note that these $G(Fe^{3+})$ calculations have already been done under these conditions (see Sect. IV.3.1). Results are presented in Fig. IV.6 along with available experimental data.

(2) Monte-Carlo simulations of the radiolysis of 0.4 *M* H_2SO_4 aqueous solutions (pH ~ 0.46) are next performed to determine, for each temperature between 25 and 300 °C, the radical and molecular product yields $G_{e^-_{aq}+H^\bullet}$, $G_{\bullet OH}$, and $G_{H_2O_2}$ as a function of time during the nonhomogeneous chemical stage (i.e., during spur expansion). Using these yield values, $G(Fe^{3+})$ can then be calculated from Eq. (22) as a function of time, for each considered temperature. The different curves of $G(Fe^{3+})$ vs. temperature obtained at different times between 10^{-8} and 10^{-6} s are shown in Fig. IV.8.

(3) Finally, for each temperature from 25 to 300 °C, the desired time scale t_s at which spur reactions are complete is simply obtained by finding the time corresponding to the *crossing* of the simulated $G(Fe^{3+})$ curve and the different calculated $G(Fe^{3+})$ curves. The values of this time as a function of temperature are shown in Fig. IV.9.

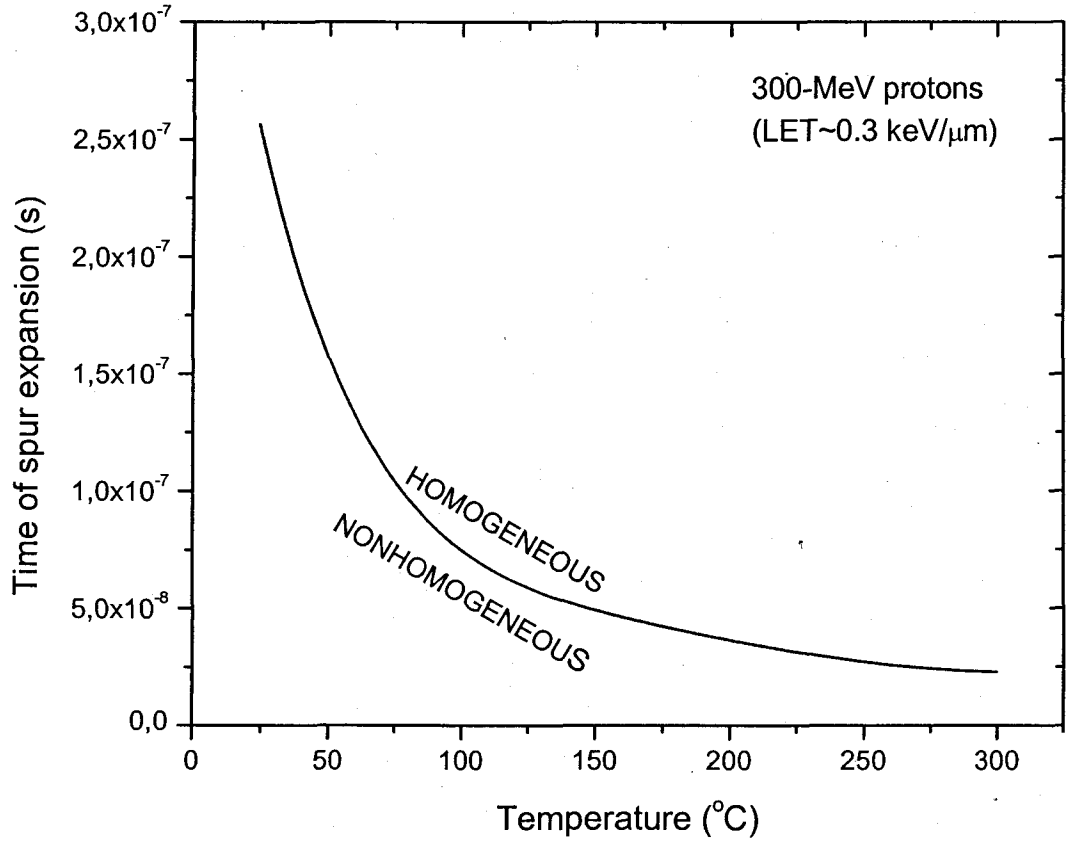

Figure IV.9: Time of spur expansion as a function of temperature for 300-MeV (LET ~ 0.3 keV/μm) irradiating protons (see text). The line indicates the time required to observe, at a given temperature, the transition from nonhomogeneity to homogeneity in the distribution of the reactive species.

As can be seen from Fig. IV.9, t_s decreases from ~2.5×10^{-7} s at 25 °C to ~2.3×10^{-8} s at 300 °C. This is a key information that is critically needed if we wish to use Eq. (22) to calculate the Fricke *G*-values as a function of temperature. To our knowledge, the above procedure is particularly useful as it offers for *the first time* a quantitative estimate of the time required to observe the transition from nonhomogeneity to homogeneity in the distribution of the reactive species produced in the radiolysis of water as a function of temperature up to 300 °C.

CHAPTER V

CONCLUSION

In this study, Monte-Carlo simulations have been successfully used to investigate the radiolysis of the ferrous sulfate (Fricke) dosimeter by fast (0.5-10 MeV) neutrons at 25 °C and also as a function of temperature over the range 25-300 °C. The radiation effects due to fast neutrons are estimated on the basis of track segment (or "escape") yields calculated for the first four recoil protons with appropriate weighting according to the energy deposited by each of these protons. In so doing, we consider that further recoils make only a negligible contribution to the radiolysis.

Our results show that the radiolysis of dilute aqueous solutions by fast neutrons generates smaller radical yields and larger molecular product yields (with respect to corresponding values for ^{60}Co γ-rays or fast electrons), due to the high LET associated with fast neutrons. The effect of recoil oxygen ions, which are taken into account in our calculations, is shown to decrease $G(Fe^{3+})$ by about 10%. A good agreement has been obtained between the available experimental data and our calculated values of $G(Fe^{3+})$, which are found to increase slightly with neutron energy over the energy range covered in this study. This good agreement found between calculated and experimental yield values validates the assumptions employed in the calculations and gives strong support to our model.

We have also simulated the effects of temperature on the oxidation of Fe^{2+} in the fast neutron radiolysis of the Fricke dosimeter from 25 to 300 °C. The results obtained from our simulation studies show that the kinetics of Fe^{3+} formation accelerates when the temperature increases. Our results also show an increase of $G(Fe^{3+})$ with increasing temperature, which is readily explained by an increase in the yields of free radicals and a decrease in those of molecular products. For 0.8-MeV incident neutrons (the only case for which experimental data are available in the

literature), there is a ~23% increase in $G(Fe^{3+})$ on going from 25 to 300 °C. Although such changes are in reasonable agreement with experiment, additional experimental data, especially for different incident neutron energies, would be needed to more critically compare our results with respect to the yields of Fe^{3+} ions at elevated temperatures.

ACKNOWLEDGMENTS

I would like to thank the Department of Nuclear Medicine and Radiobiology, Faculty of Medicine and Health Sciences, *Université de Sherbrooke*.

I am grateful to Prof. Jean-Paul Jay-Gerin, Director of the laboratory and my supervisor, for his guidance, advise, expenses, encouragement, and patience.

I thank Prof. Michel Grandbois and Prof. Michael Huels for having accepted to be on my thesis Committee.

I appreciated the help and cheerful support of Dr. Jintana Meesungnoen, Dr. Ianik Plante, Ridthee Meesat, Narongchai Autsavapromporn, Sunuchakan Sanguanmith, my colleagues in our laboratory, and also all my colleagues in the department.

Special thanks are due to the *Réseau québécois de calcul de haute performance* (RQCHP) of the *Université de Sherbrooke* for providing generous computing facilities. The financial assistance of the *Atomic Energy of Canada Limited* and the *Natural Sciences and Engineering Research Council of Canada* is gratefully acknowledged.

Most importantly, my warmest thanks go to my family for their generosity and understanding, their encouragement, and their great love.

BIBLIOGRAPHY

ALLEN, A.O., 1948. Radiation chemistry of aqueous solutions. *J. Phys. Colloid Chem.* **52**, 479-490.

ALLEN, A.O., 1954. The yields of free H and OH in the irradiation of water. *Radiat. Res.* **1**, 85-96.

ALLEN, A.O., 1961. *The Radiation Chemistry of Water and Aqueous Solutions*. D. Van Nostrand Co., Princeton, N.J.

ALPEN, E.L., 1998. *Radiation Biophysics*, 2nd ed. Academic Press, San Diego, CA.

ALPER, T. and BRYANT, P.E., 1974. Reduction in oxygen enhancement ratio with increase in LET: Tests of two hypotheses. *Int. J. Radiat. Biol.* **26**, 203-218.

AMICHAI, O. and TREININ, A., 1969. Chemical reactivity of $O(^3P)$ atoms in aqueous solution. *Chem. Phys. Lett.* **3**, 611-613.

ANDERSON, A.R. and HART, E.J., 1961. Molecular product and free radical yields in the decomposition of water by protons, deuterons, and helium ions. *Radiat. Res.* **14**, 689-704.

ANDERSON, D.W., 1984. *Absorption of Ionizing Radiation*. University Park Press, Baltimore, MD.

APPLEBY, A., 1989. Effects of early track structure on the radiation chemistry of water irradiated with heavy ions. *Radiat. Phys. Chem.* **34**, 121-127.

AUTSAVAPROMPORN, N., 2006. *The effects of pH and radiation quality (LET) on the radiolysis of liquid water and aqueous solutions: A study by using Monte-Carlo simulations*. M.Sc. Thesis, Burapha University, Bangsaen (Thailand).

AUTSAVAPROMPORN, N., MEESUNGNOEN, J., PLANTE, I., and JAY-GERIN, J.-P., 2007. Monte Carlo simulation study of the effects of acidity and LET on the primary free-radical and molecular yields of water radiolysis – Application to the Fricke dosimeter. *Can. J. Chem.* **85**, 214-229.

AUXIER, J.A., SNYDER, W.S., and JONES, T.D., 1968. Neutron interactions and penetration in tissue. In: Attix, F.H., Roesch, W.C., and Tochilin, E. (Eds.), *Radiation Dosimetry*, vol. I. Academic Press, New York, pp. 275-316.

BACK, M.H. and MILLER, N., 1957. Use of ferrous sulphate solutions for X-ray dosimetry. *Nature* **179**, 321-322.

BALAKRISHNAN, I. and REDDY, M.P., 1972. The effect of temperature on the γ radiolysis of aqueous solutions. *J. Phys. Chem.* **76**, 1273-1279.

BALLARINI, F., BIAGGI, M., MERZAGORA, M., OTTOLENGHI, A., DINGFELDER, M., FRIEDLAND, W., JACOB, P., and PARETZKE, H.G., 2000. Stochastic aspects and uncertainties in the prechemical and chemical stages of electron tracks in liquid water: A quantitative analysis based on Monte Carlo simulations. *Radiat. Environ. Biophys.* **39**, 179-188.

BARENDSEN, G.W., 1968. Responses of cultured cells, tumours and normal tissues to radiations of different linear energy transfer. *Curr. Top. Radiat. Res. Quarterly* **4**, 293-356.

BARR, N.F. and SCHULER, R.H., 1957. Dependence of radiation chemical yields on rate of energy loss: The yields of molecular and radical products from 0.8 *N* sulfuric acid solutions. *Radiat. Res.* **7**, 302-303.

BARR, N.F. and SCHULER, R.H., 1959. The dependence of radical and molecular yields on linear energy transfer in the radiation decomposition of 0.8 *N* sulfuric acid solutions. *J. Phys. Chem.* **63**, 808-812.

BARTELS, D.M., 2009. Comment on the possible role of the reaction $H^{\bullet} + H_2O \rightarrow H_2 + {}^{\bullet}OH$ in the radiolysis of water at high temperatures. *Radiat. Phys. Chem.* **78**, 191-194.

BĚGUSOVÁ, M. and PIMBLOTT, S.M., 2002. Stochastic simulation of γ radiolysis of acidic ferrous sulfate solution at elevated temperatures. *Radiat. Prot. Dosim.* **99**, 73-76.

BENSASSON, R., BERNAS, A., BODARD, M., BOUBY, L., COTTIN, M., DUFLO, M., KIEFFER, F., KOULKÈS, A., LERAY, N., PUCHEAULT, J., and VERMEIL, C.,

1963. Constantes sélectionnées - Rendements radiolytiques. In: Haïssinsky, M. and Magat, M. (Eds.), *Tables of Constants and Numerical Data*, vol. 13. Pergamon, Oxford, UK.

BETHE, H., 1930. Zur Theorie des Durchgangs schneller Korpuskularstrahlen durch Materie. *Ann. Physik (Leipzig)* **5**, 325-400.

BETHE, H.A. and ASHKIN, J., 1953. Passage of radiations through matter. In: Segrè, E. (Ed.), *Experimental Nuclear Physics*, vol. 1. Wiley, New York, pp. 166-357.

BEWLEY, D.K., 1963. Physical aspects of the fast neutron beam. *Br. J. Radiol.* **36**, 81-88.

BEWLEY, D.K., 1989. *The Physics and Radiobiology of Fast Neutron Beams*. Institute of Physics Publishing, Philadelphia, PA.

BIBLER, N.E., 1975. Radiolysis of 0.4 *M* sulfuric acid solutions with fission fragments from dissolved californium-252. Estimated yields of radical and molecular products that escape reactions in fission fragment tracks. *J. Phys. Chem.* **79**, 1991-1995.

BICHSEL, H. and HIRAOKA, T., 1992. Energy loss of 70 MeV protons in elements. *Nucl. Instrum. Methods Phys. Res. B* **66**, 345-351.

BICHSEL, H., 2006. A method to improve tracking and particle identification in TPCs and silicon detectors. *Nucl. Instrum. Methods Phys. Res. A* **562**, 154-197.

BIEDENKAPP, D., HARTSHORN, L.G., and BAIR, E.J., 1970. The $O(^1D)$ + H_2O reaction. *Chem. Phys. Lett.* **5**, 379-380.

BJERGBAKKE, E. and HART, E.J., 1971. Oxygen formation in the γ-ray irradiation of Fe^{2+}–Cu^{2+} solutions. *Radiat. Res.* **45**, 261-273.

BOUDAÏFFA, B., CLOUTIER, P., HUNTING, D., HUELS, M.A., and SANCHE, L., 2000. Les électrons de très faible énergie produisent des lésions de l'ADN. *Méd. Sci.* **16**, 1281-1283.

BRITTEN, R.A., PETERS, L.J., and MURRAY, D., 2001. Biological factors influencing the RBE of neutrons: Implications for their past, present and future use in radiotherapy. *Radiat. Res.* **156**, 125-135.

BURCH, P.R.J., 1959. A theoretical interpretation of the effect of radiation quality on yield in the ferrous and ceric sulfate dosimeters. *Radiat. Res.* **11**, 481-497.

BURNS, W.G. and MOORE, P.B., 1976. Water radiolysis and its effect upon in-reactor zircaloy corrosion. *Radiat. Eff.* **30**, 233-242.

BURNS, W.G. and MARSH, W.R., 1981. Radiation chemistry of high-temperature (300-410 °C) water. Part 1. Reducing products gamma radiolysis. *J. Chem. Soc., Faraday Trans. 1*, **77**, 197-215.

BURNS, W.G. and SIMS, H.E., 1981. Effect of radiation type in water radiolysis. *J. Chem. Soc., Faraday Trans. 1*, **77**, 2803-2813.

BUXTON, G.V., 1967. The effect of pH on radical and molecular yields in the radiolysis of water. In: Silini, G. (Ed.), *Proceedings of the Third International Congress of Radiation Research, Cortina d'Ampezzo, Italy, June 26-July 2, 1966*. North-Holland, Amsterdam, pp. 235-250.

BUXTON, G.V., 1968. Primary radical and molecular yields in aqueous solution; The effect of pH and solute concentration. *Radiat. Res. Rev.* **1**, 209-222.

BUXTON, G.V., 1987. Radiation chemistry of the liquid state: (1) Water and homogeneous aqueous solutions. In: Farhataziz and Rodgers, M.A.J. (Eds.), *Radiation Chemistry. Principles and Applications*. VCH Publishers, New York, pp. 321-349.

BUXTON, G.V., 1991. Applications of the radiation chemistry of water: Acid rain and nuclear power. *Int. J. Radiat. Biol.* **59**, 1-13.

BUXTON, G.V., 2001. High temperature water radiolysis. In: Jonah, C.D. and Rao, B.S.M. (Eds.), *Radiation Chemistry - Present Status and Future Trends*. Elsevier, Amsterdam, pp. 145-162.

CEMBER, H. and JOHNSON, T.E., 2009. *Introduction to Health Physics*, 4th ed. McGraw-Hill, New York.

CHADWICK, J., 1932*a*. Possible existence of a neutron. *Nature* **129**, 312.

CHADWICK, J., 1932*b*. The existence of a neutron. *Proc. Roy. Soc. (London), Ser. A*, **136**, 692-708.

CHAPMAN, J.D., 1980. Biophysical models of mammalian cell inactivation by radiation. In: Meyn, R.E. and Withers, H.R. (Eds.), *Radiation Biology in Cancer Research*. Raven Press, New York, pp. 21-32.

CHRISTENSEN, C.J., NIELSEN, A., BAHNSEN, A., BROWN, W.K., and RUSTAD, B.M., 1972. Free-neutron beta-decay half-life. *Phys. Rev. D* **5**, 1628-1640.

CHRISTENSEN, H. and SEHESTED, K., 1981. Pulse radiolysis at high temperatures and high pressures. *Radiat. Phys. Chem.* **18**, 723-731.

CHRISTENSEN, H. and SEHESTED, K., 1986. The hydrated electron and its reactions at high temperatures. *J. Phys. Chem.* **90**, 186-190.

CHRISTENSEN, H., SEHESTED, K., and LØGAGER, T., 1993. The reaction of hydrogen peroxide with Fe(II) ions at elevated temperatures. *Radiat. Phys. Chem.* **41**, 575-578.

CHRISTENSEN, H., 2006. Fundamental aspects of water coolant radiolysis. SKI Report 2006:16. Swedish Nuclear Power Inspectorate, Stockholm, Sweden.

CLIFFORD, P., GREEN, N.J.B., OLDFIELD, M.J., PILLING, M.J., and PIMBLOTT, S.M., 1986. Stochastic models of multi-species kinetics in radiation-induced spurs. *J. Chem. Soc., Faraday Trans. 1*, **82**, 2673-2689.

COBUT, V., 1993. *Simulation Monte Carlo du transport d'électrons non relativistes dans l'eau liquide pure et de l'évolution du milieu irradié: rendements des espèces créées de 10^{-15} à 10^{-7} s.* Ph.D. Thesis, Université de Sherbrooke.

COBUT, V., FRONGILLO, Y., JAY-GERIN, J.-P., and PATAU, J.P., 1994. Calculs des rendements des produits de la radiolyse de l'eau en fonction du temps par une méthode Monte Carlo. *J. Chim. Phys.* **91**, 1018-1024.

COBUT, V., JAY-GERIN, J.-P., FRONGILLO, Y., and PATAU, J.P., 1996. On the dissociative electron attachment as a potential source of molecular hydrogen in irradiated liquid water, *Radiat. Phys. Chem.* **47**, 247-250.

COBUT, V., FRONGILLO, Y., PATAU, J.P., GOULET, T., FRASER, M.-J., and JAY-GERIN, J.-P., 1998. Monte Carlo simulation of fast electron and proton tracks

in liquid water. I. Physical and physicochemical aspects. *Radiat. Phys. Chem.* **51**, 229-243.

COHEN, P., 1980. *Water Coolant Technology of Power Reactors*. American Nuclear Society, La Grange Park, IL.

COLLINSON, E., DAINTON, F.S., and KROH, J., 1962. The radiation chemistry of aqueous solutions. II. Radical and molecular yields for tritium β-particles. *Proc. Roy. Soc. (London), Ser. A*, **265**, 422-429.

COTTIN, M. and LEFORT, M., 1956. Étalonnage absolu du dosimètre au sulfate ferreux. Rayons X mous de 10 et 8 keV. *J. Chim. Phys.* **53**, 267-273.

CZAPSKI, G. and SCHWARZ, H.A., 1962. The nature of the reducing radical in water radiolysis. *J. Phys. Chem.* **66**, 471-474.

DAS, R.C., 1971. Radiation chemistry of aqueous aerated ferrous sulphate solution. *Radiat. Res. Rev.* **3**, 121-139.

DAVIES, C.W., 1938. The extent of dissociation of salts in water. Part VIII. An equation for the mean ionic activity coefficient of an electrolyte in water, and a revision of the dissociation constants of some sulphates. *J. Chem. Soc.* 2093-2098.

DAVIES, J.V., GREENE, D., KEENE, J.P., LAW, J., and MASSEY, J.B., 1963. A comparison of ionization, calorimetric and ferrous sulphate dosimetry. *Phys. Med. Biol.* **8**, 97-102.

DEAN, J.A., 1987. *Handbook of Organic Chemistry*. McGraw-Hill, New York.

DEBYE, P., 1942. Reaction rates in ionic solutions. *Trans. Electrochem. Soc.* **82**, 265-272.

DEGROOT, M.H. and SCHERVISH, M.J., 2002. *Probability and Statistics*, 3rd ed. Addison-Wesley, Boston, MA.

DINGFELDER, M., INOKUTI, M., and PARETZKE, H.G., 2000. Inelastic-collision cross sections of liquid water for interactions of energetic protons. *Radiat. Phys. Chem.* **59**, 255-275.

DINGFELDER, M. and FRIEDLAND, W., 2001. Basic data for track structure simulations: Electron interaction cross-sections in liquid water. In: Kling, A., Barão, F., Nakagawa, M., Távora, L., and Vaz, P. (Eds.), *Advanced Monte Carlo for Radiation Physics, Particle Transport Simulation and Applications.* Springer-Verlag, Berlin, pp. 267-272.

DINGFELDER, M., RITCHIE, R.H., TURNER, J.E., FRIEDLAND, W., PARETZKE, H.G., and HAMM, R.N., 2008. Comparisons of calculations with PARTRAC and NOREC: Transport of electrons in liquid water. *Radiat. Res.* **169**, 584-594.

DONALDSON, D.M. and MILLER, N., 1955. Études quantitatives des réactions radiochimiques. III. Oxydation du sulfate ferreux par les particles β. *J. Chim. Phys.* **52**, 578-584.

DRAGANIĆ, I.G., NENADOVIĆ, and DRAGANIĆ, Z.D., 1969. Radiolysis of HCOOH + O_2 at pH 1.3-13 and the yields of primary products in γ radiolysis of water. *J. Phys. Chem.* **73**, 2564-2571.

DRAGANIĆ, I.G. and DRAGANIĆ, Z.D., 1971. *The Radiation Chemistry of Water.* Academic Press, New York.

EDWARDS, E.J., WILSON, P.P.H., ANDERSON, M.H., MEZYK, S.P., PIMBLOTT, S.M., and BARTELS, D.M., 2007. An apparatus for the study of high temperature water radiolysis in a nuclear reactor: Calibration of dose in a mixed neutron/gamma radiation field. *Rev. Sci. Instrum.* **78**, 124101.

EGUSA, S., ISHIGURE, K., TAGAWA, S., TABATA, Y., and OSHIMA, K., 1978. Absorbed dose measurements in a mixed field of fast neutrons and γ-rays by the Fricke and ceric sulfate dosimeters. *Radiat. Phys. Chem.* **11**, 129-134.

ELLIOT, A.J., McCRACKEN, D.R., BUXTON, G.V., and WOOD, N.D., 1990. Estimation of rate constants for near-diffusion-controlled reactions in water at high temperatures. *J. Chem. Soc. Faraday Trans.* **86**, 1539-1547.

ELLIOT, A.J., CHENIER, M.P., and OUELLETTE, D.C., 1993. Temperature dependence of *g* values for H_2O and D_2O irradiated with low linear energy transfer radiation. *J. Chem. Soc. Faraday Trans.* **89**, 1193-1197.

ELLIOT, A.J., 1994. Rate constants and *G*-values for the simulation of the radiolysis of light water over the range 0-300 °C. Report AECL-11073. Atomic Energy of Canada Ltd., Chalk River, ON.

ELLIOT, A.J., OUELLETTE, D.C., and STUART, C.R., 1996*a*. The temperature dependence of the rate constants and yields for the simulation of the radiolysis of heavy water. Report AECL-11658. Atomic Energy of Canada Ltd., Chalk River, ON.

ELLIOT, A.J., CHENIER, M.P., OUELLETTE, D.C., and KOSLOWSKY, V.T., 1996*b*. Temperature dependence of *g* values for aqueous solutions irradiated with 23 MeV $^{2}H^{+}$ and 157 MeV $^{7}Li^{3+}$ ion beams. *J. Phys. Chem.* **100**, 9014-9020.

EVANS, R.D., 1955. *The Atomic Nucleus.* Krieger Publishing Co., Malabar, FL.

FARAGGI, M. and DÉSALOS, J., 1969. Effect of positively charged ions on the "molecular" hydrogen yield in the radiolysis of aqueous solutions. *Int. J. Radiat. Phys. Chem.* **1**, 335-344.

FERRADINI, C. and JAY-GERIN, J.-P., 1993. A conjecture on the fate of the hydrated electron during its disproportionation reaction. *Radiat. Phys. Chem.* **41**, 487-490.

FERRADINI, C. and JAY-GERIN, J.-P., 1998. Does multiple ionization intervene for the production of $HO_2^{\bullet}$ radicals in high-LET liquid water radiolysis? *Radiat. Phys. Chem.* **51**, 263-267.

FERRADINI, C. and JAY-GERIN, J.-P., 1999. La radiolyse de l'eau et des solutions aqueuses: historique et actualité. *Can. J. Chem.* **77**, 1542-1575.

FERRADINI, C. and JAY-GERIN, J.-P., 2000. The effect of pH on water radiolysis: A still open question – A minireview. *Res. Chem. Intermed.* **26**, 549-565.

FERRADINI, C. and PUCHEAULT, J., 1983. *Biologie de l'action des rayonnements ionisants.* Masson, Paris.

FISCHER, H. and PAUL, H., 1987. Rate constants for some prototype radical reactions in liquids by kinetic electron spin resonance. *Acc. Chem. Res.* **20**, 200-206.

FREGENE, A.O., 1967. Calibration of the ferrous sulfate dosimeter by ionometric and calorimetric methods for radiations of a wide range of energy. *Radiat. Res.* **31**, 256-272.

FRICKE, H. and MORSE, S., 1927. The chemical action of roentgen rays on dilute ferrosulphate solutions as a measure of dose. *Am. J. Roentgenol. Radium Ther.* **18**, 430-432.

FRICKE, H. and MORSE, S., 1929. The action of X-rays on ferrous sulphate solutions. *Philos. Mag. 7th Ser.* **7**, 129-141.

FRICKE, H. and HART, E.J., 1966. Chemical dosimetry. In: Attix, F.H. and Roesch, W.C. (Eds.), *Radiation Dosimetry*, 2nd ed., vol. II. Academic Press, New York, pp. 167-239.

FRIEDLANDER, G., KENNEDY, J.W., MACIAS, E.S., and MILLER, J.M., 1981. *Nuclear and Radiochemistry*, 3rd ed. Wiley, New York.

FRONGILLO, Y., GOULET, T., FRASER, M.-J., COBUT, V., PATAU, J.P., and JAY-GERIN, J.-P., 1998. Monte Carlo simulation of fast electron and proton tracks in liquid water. II. Nonhomogeneous chemistry. *Radiat. Phys. Chem.* **51**, 245-254.

GANGULY, A.K. and MAGEE, J.L., 1956. Theory of radiation chemistry. III. Radical reaction mechanism in the tracks of ionizing radiations. *J. Chem. Phys.* **25**, 129-134.

GERVAIS, B., BEUVE, M., OLIVERA, G.H., and GALASSI, M.E., 2006. Numerical simulation of multiple ionization and high LET effects in liquid water radiolysis. *Radiat. Phys. Chem.* **75**, 493-513.

GOODHEAD, D.T., 1994. Initial events in the cellular effects of ionizing radiations: Clustered damage in DNA. *Int. J. Radiat. Biol.* **65**, 7-17.

GORDON, S., SCHMIDT, K.H., and HONEKAMP, J.R., 1983. An analysis of the hydrogen bubble concerns in the Three-Mile Island unit-2 reactor vessel. *Radiat. Phys. Chem.* **21**, 247-258.

GOULET, T. and JAY-GERIN, J.-P., 1989. Thermalization of subexcitation electrons in solid water. *Radiat. Res.* **118**, 46-62.

GOULET, T., PATAU, J.P., and JAY-GERIN, J.-P., 1990. Influence of the parent cation on the thermalization of subexcitation electrons in solid water. J. Phys. Chem. **94**, 7312-7316.

GOULET, T. and JAY-GERIN, J.-P., 1992. On the reactions of hydrated electrons with $^{\bullet}OH$ and H_3O^+. Analysis of photoionization experiments. *J. Chem. Phys.* **96**, 5076-5087.

GOULET, T., JAY-GERIN, J.-P., FRONGILLO, Y., COBUT, V., and FRASER, M.-J., 1996. Rôle des distances de thermalisation des électrons dans la radiolyse de l'eau liquide. J. Chim. Phys. 93, 111-116.

GOULET, T., FRASER, M.-J., FRONGILLO, Y., and JAY-GERIN, J.-P., 1998. On the validity of the independent reaction times approximation for the description of the nonhomogeneous kinetics of liquid water radiolysis. *Radiat. Phys. Chem.* **51**, 85-91.

GREENE, D., LAW, J., and MAJOR, D., 1973*a*. The *G*-value for the ferrous sulphate dosemeter for the radiation from Californium-252. *Phys. Med. Biol.* **18**, 800-807.

GREENE, D., MAJOR, D. and LAW, J., 1973*b*. The *G*-value for the ferrous sulphate dosemeter for 14 MeV neutrons. *Phys. Med. Biol.* **18**, 369-378.

GREENE, D., LAW, J., MILES, J.C.H., and PARNELL, C.J., 1975. Ferrous sulphate *G*-value for cyclotron produced neutrons with a mean energy of 7.6 MeV. *Phys. Med. Biol.* **20**, 650-652.

GREEN, N.J.B., PILLING, M.J., PIMBLOTT, S.M., and CLIFFORD, P., 1990. Stochastic modeling of fast kinetics in a radiation track. *J. Phys. Chem.* **94**, 251-258.

GUGGENHEIM, E.A., 1935. The specific thermodynamic properties of aqueous solutions of strong electrolytes. *Philos. Mag.*, 7th Ser., **19**, 588-643.

GUZONAS, D., TREMAINE, P., and JAY-GERIN, J.-P., 2009. Chemistry control challenges in a supercritical water-cooled reactor. *PowerPlant Chem.* **11**, 284-291.

HALL, E.J., ASTOR, M., and BRENNER, D.J., 1992. Biological intercomparisons of neutron beams used for radiotherapy generated by p(+)→Be in hospital-based cyclotrons. *Br. J. Radiol.* **65**, 66-71.

HALL, E.J. and GIACCIA, A.J., 2006. *Radiobiology for the Radiologist*, 6th ed. Lippincott, Williams & Wilkins, Philadelphia, PA.

HALLIWELL, B. and GUTTERIDGE, J.M.C., 1999. *Free Radicals in Biology and Medicine*, 3rd ed. Oxford University Press, Oxford, p. 36.

HAN, P. and BARTELS, D.M., 1992. H/D isotope effects in water radiolysis. 4. The mechanism of $(H)_{aq} \rightleftarrows (e^-)_{aq}$ interconversion. *J. Phys. Chem.* **96**, 4899-4906.

HARDWICK, T.J., 1952. The effect of the energy of the ionizing electron on the yield in irradiated aqueous systems. *Discussions Faraday Soc.* No. 12, 203-211.

HARDWICK, T.J., 1953. The oxidation of ferrous sulphate by γ-rays – The temperature coefficient of air-saturated solutions. *Can. J. Chem.* **31**, 881-883.

HARRIS, D.C., 2001. *Exploring Chemical Analysis*, 2nd ed. W.H. Freeman, New York, p. 233.

HART, E.J., 1954. Molecular product and free radical yields of ionizing radiations in aqueous solutions. *Radiat. Res.* **1**, 53-61.

HART, E.J., 1955. Radiation chemistry of aqueous ferrous sulfate-cupric sulfate solutions. Effect of γ-rays. *Radiat. Res.* **2**, 33-46.

HART, E.J., RAMLER, W.J., and ROCKLIN, S.R., 1956. Chemical yields of ionizing particles in aqeous solutions: Effect of energy of protons and deuterons. *Radiat. Res.* **4**, 378-393.

HAYBITTLE, J.L., SAUNDERS, R.D., and SWALLOW, A.J., 1956. X- and γ-irradiation of ferrous sulfate in dilute aqueous solutions. *J. Chem. Phys.* **25**, 1213-1217.

HAYON, E., 1968. Primary radicals yields in the radiation chemistry of water and aqueous solutions. In: Stein, G. (Ed.), *Radiation Chemistry of Aqueous Systems*. The Weizmann Science Press of Israel, Jerusalem, Israel, pp. 157-209.

HELLER, J.M., Jr., HAMM, R.N., BIRKHOFF, R.D., and PAINTER, L.R., 1974. Collective oscillation in liquid water. *J. Chem. Phys.* **60**, 3483-3486.

HERVÉ DU PENHOAT, M.-A., GOULET, T., FRONGILLO, Y., FRASER, M.-J., BERNAT, Ph., and JAY-GERIN, J.-P., 2000. Radiolysis of liquid water at temperatures up to 300 °C: A Monte Carlo simulation study. *J. Phys. Chem. A* **104**, 11757-11770.

HERVÉ DU PENHOAT, M.-A., MEESUNGNOEN, J., GOULET, T., FILALI-MOUHIM, A., MANKHETKORN, S., and JAY-GERIN, J.-P., 2001. Linear-energy-transfer effects on the radiolysis of liquid water at temperatures up to 300 °C - A Monte-Carlo study. *Chem. Phys. Lett.* **341**, 135-143.

HICKEL, B., 1991. Quelques problèmes concernant la radiolyse de l'eau liquide à haute température : application aux réacteurs nucléaires. *J. Chim. Phys.* **88**, 1177-1193.

HOCHANADEL, C.J. and GHORMLEY, J.A., 1953. A calorimetric calibration of gamma-ray actinometers. *J. Chem. Phys.* **21**, 880-885.

HOCHANADEL, C.J. and LIND, S.C., 1956. Radiation chemistry. *Annu. Rev. Phys. Chem.* **7**, 83-106.

HOCHANADEL, C.J. and GHORMLEY, J.A., 1962. Effect of temperature on the decomposition of water by gamma rays. *Radiat. Res.* **16**, 653-660.

IAEA-TECDOC-799, 1995. *Atomic and Molecular Data for Radiotherapy and Radiation Research*. International Atomic Energy Agency, Vienna.

ICRU REPORT 17, 1970. *Radiation Dosimetry: X rays generated at potentials of 5 to 150 kV.* International Commission on Radiation Units and Measurements, Washington, DC.

ICRU REPORT 26, 1977. *Neutron Dosimetry for Biology and Medicine*. International Commission on Radiation Units and Measurements, Washington, DC.

ICRU REPORT 34, 1982. *The Dosimetry of Pulsed Radiation*. International Commission on Radiation Units and Measurements, Bethesda, MD.

ICRU REPORT 49, 1993. *Stopping Powers and Ranges for Protons and Alpha Particles*. International Commission on Radiation Units and Measurements, Bethesda, MD.

ICRU REPORT 55, 1996. *Secondary Electron Spectra from Charged Particle Interactions*. International Commission on Radiation Units and Measurements, Bethesda, MD.

ICRU REPORT 73, 2005. *Stopping of Ions Heavier than Helium*. Journal of the ICRU (International Commission on Radiation Units and Measurements), vol. 5, Oxford University Press, Oxford, U.K.

IMAMURA, M., MATSUI, M., and KARASAWA, T., 1970. Radiation chemical studies with cyclotron beams. II. The radiolysis of an aqueous ferrous ammonium sulfate solution with carbon- and nitrogen-ion radiations. *Bull. Chem. Soc. Japan* **43**, 2745-2749.

INOKUTI, M., 1971. Inelastic collisions of fast charged particles with atoms and molecules – The Bethe theory revisited. *Rev. Mod. Phys.* **43**, 297-347.

ISHIGURE, K., TAKAGI, J., and SHIRAISHI, H., 1987. Hydrogen injection in BWR and related radiation chemistry. *Radiat. Phys. Chem.* **29**, 195-199.

ISHIGURE, K., KATSUMURA, Y., SUNARYO, G.R., and HIROISHI, D., 1995. Radiolysis of high temperature water. *Radiat. Phys. Chem.* **46**, 557-560.

JANIK, D., JANIK, I., and BARTELS, D.M., 2007. Neutron and β/γ radiolysis of water up to supercritical conditions. 1. β/γ yields for H_2, $H^\bullet$ atom, and hydrated electron. *J. Phys. Chem. A* **111**, 7777-7786.

JAY-GERIN, J.-P., LIN, M., KATSUMURA, Y., HE, H., MUROYA, Y., and MEESUNGNOEN, J., 2008. Effect of water density on the absorption

maximum of hydrated electrons in sub- and supercritical water up to 400 °C. *J. Chem. Phys.* **129**, no. 114511.

JAYSON, G.G., PARSONS, B.J., and SWALLOW, A.J., 1973. Oxidation of ferrous ions by perhydroxyl radicals. *J. Chem. Soc., Faraday Trans. I*, **69**, 236-242.

JOHNSON, E.R. and ALLEN, A.O., 1952. The molecular yield in the decomposition of water by hard X-rays. *J. Am. Chem. Soc.* **74**, 4147-4150.

JONAH, C.D., MILLER, J.R., and MATHESON, M.S., 1977. The reaction of e^-_{aq} + H_3O^+. Concentration effects of acid or salts. *J. Phys. Chem.* **81**, 931-934.

KABAKCHI, S.A. and LEBEDEVA, I.E., 1984. Temperature dependence of the yield of reducing particles during the radiolysis of liquid water. *High Energy Chem.* **18**, 166-170.

KABAKCHI, S.A. and BUGAENKO, V.L., 1992. Mathematical modeling of radiolysis of liquid water at high temperatures. *High Energy Chem.* **26**, 319-323.

KAPLAN, I.G. and MITEREV, A.M., 1987. Interaction of charged particles with molecular medium and track effects in radiation chemistry. *Adv. Chem. Phys.* **68**, 255-386.

KATSUMURA, Y., TABATA, Y., SEGUCHI, T., HAYAKAWA, N., YOSHIDA, K., and TAMURA, N., 1985. Fast neutron irradiation effects. I. Dosimetry. *Radiat. Phys. Chem.* **26**, 211-220.

KATSUMURA, Y., TAKEUCHI, Y., and ISHIGURE, K., 1988. Radiation chemistry of high temperature water – I. Degradation products in acid by gamma radiolysis. *Radiat. Phys. Chem.* **32**, 259-263.

KATSUMURA, Y., TAKEUCHI, Y., HIROISHI, D., and ISHIGURE, K., 1989. Fast-neutron radiolysis of acid water at elevated temperatures. *Radiat. Phys. Chem.* **33**, 299-306.

KATSUMURA, Y., YAMAMOTO, S., HIROISHI, D., and ISHIGURE, K., 1992. Radiolysis of acid water (0.4 *M* H_2SO_4) at elevated temperatures with fast neutrons and proton beam. *Radiat. Phys. Chem.* **39**, 383-387.

KATSUMURA, Y., SUNARYO, G., HIROISHI, D., and ISHIGURE, K., 1998. Fast neutron radiolysis of water at elevated temperatures relevant to water chemistry. *Prog. Nucl. Energy* **32**, 113-121.

KATSUMURA, Y., 2004. Application of radiation chemistry to nuclear technology. In: Mozumder, A. and Hatano, Y. (Eds.), *Charged Particle and Photon Interactions with Matter. Chemical, Physicochemical, and Biological Consequences with Applications.* Marcel Dekker, New York, pp. 697-727.

KEENE, J.P., 1964. Pulse radiolysis of ferrous sulfate solution. *Radiat. Res.* **22**, 14-20.

KENT, M.C. and SIMS, H.E., 1992*a*. The yield of γ-radiolysis products from water at temperatures up to 300 °C. *Proceedings of the 6th International Conference on Water Chemistry of Nuclear Reactor Systems.* British Nuclear Energy Society, London, pp. 153-158.

KENT, M.C. and SIMS, H.E., 1992*b*. The yield of γ-radiolysis products from water at temperatures up to 270 °C. Report AEA-RS-2302. Atomic Energy Authority, Didcot, Oxfordshire, U.K.

KIMMEL, G.A., ORLANDO, T.M., VÉZINA, C., and SANCHE, L., 1994. Low-energy electron-stimulated production of molecular hydrogen from amorphous water ice. *J. Chem. Phys.* **101**, 3282-3286.

KLASSEN, N.V., SHORTT, K.R., SEUNTJENS, J., and ROSS, C.K., 1999. Fricke dosimetry: the difference between $G(Fe^{3+})$ for ^{60}Co γ-rays and high-energy X-rays. *Phys. Med. Biol.* **44**, 1609-1624.

KNUTH, D.E., 1998. *The Art of Computer Programming*, 3rd ed., vol. 2. Addison-Wesley, Reading, MA.

KOCHANNY, Jr., G.L., TIMNICK, A., HOCHANADEL, C.J., and GOODMAN, C.D., 1963. Radiation chemistry studies of water as related to the initial linear energy transfer of 11-MeV to 23-MeV protons. *Radiat. Res.* **19**, 462-473.

KRANE, K.S., 1988. *Introductory Nuclear Physics.* Wiley, New York.

KREIPL, M.S., FRIEDLAND, W., and PARETZKE, H.G. (2009). Time- and space-resolved Monte Carlo study of water radiolysis for photon, electron and ion irradiation. *Radiat. Environ. Biophys.* **48**, 11-20.

KUPPERMANN, A., 1959. Theoretical foundations of radiation chemistry. *J. Chem. Educ.* **36**, 279-285.

LAVERNE, J.A. and SCHULER, R.H., 1987. Radiation chemical studies with heavy ions: Oxidation of ferrous ion in the Fricke dosimeter. *J. Phys. Chem.* **91**, 5770-5776.

LAVERNE, J.A., 1989. Radical and molecular yields in the radiolysis of water with carbon ions. *Radiat. Phys. Chem.* **34**, 135-143.

LAVERNE, J.A. and PIMBLOTT, S.M., 1993. Diffusion-kinetic modeling of the electron radiolysis of water at elevated temperatures. *J. Phys. Chem.* **97**, 3291-3297.

LAVERNE, J.A. and PIMBLOTT, S.M., 1995. Electron energy-loss distributions in solid, dry DNA. *Radiat. Res.* **141**, 208-215.

LAVERNE, J.A. and SCHULER, R.H., 1996. Radiolysis of the Fricke dosimeter with ^{58}Ni and ^{238}U ions: Response for particles of high linear energy transfer. *J. Phys. Chem.* **100**, 16034-16040.

LAVERNE, J.A., 2000. Track effects of heavy ions in liquid water. *Radiat. Res.* **153**, 487-496.

LAVERNE, J.A., 2004. Radiation chemical effects of heavy ions. In: Mozumder, A. and Hatano, Y. (Eds.), *Charged Particle and Photon Interactions with Matter. Chemical, Physicochemical, and Biological Consequences with Applications.* Marcel Dekker, New York, pp. 403-429.

LAW, J., 1970. Variation of response of the $FeSO_4$ dosemeter with temperature of the solution during irradiation. *Phys. Med. Biol.* **15**, 741-742.

LAW, J., LAWSON, R.C., and PORTER, D., 1974. Spectral dependence of the $FeSO_4$ *G*-value in DT neutron beams. *Phys. Med. Biol.* **19**, 643-655.

LAWSON, R.C. and PORTER, D., 1975. The response of the ferrous sulphate dosemeter to neutrons. *Phys. Med. Biol.* **20**, 420-430.

LEFORT, M., 1957. Phénomènes de réductions provoqués par les rayonnements nucléaires sur les solutions aqueuses de composés minéraux. *J. Chim. Phys.* **54**, 782-788.

LEFORT, M., 1958. Radiation chemistry. *Annu. Rev. Phys. Chem.* **9**, 123-156.

LEFORT, M. and TARRAGO, X., 1959. Radiolysis of water by particles of high linear energy transfer. The primary chemical yields in aqueous acid solutions of ferrous sulfate, and in mixtures of thallous and ceric ions. *J. Phys. Chem.* **63**, 833-836.

LIDE, D.R. (Ed.), 2008. *CRC Handbook of Chemistry and Physics*, 88th ed. CRC Press, Boca Raton, FL, pp. 5-76–5-78.

LIN, M., KATSUMURA, Y., MUROYA, Y., HE, H., WU, G., HAN, Z., MIYAZAKI, T., and KUDO, H., 2004. Pulse radiolysis study on the estimation of radiolytic yields of water decomposition products in high-temperature and supercritical water: Use of methyl viologen as a scavenger. *J. Phys. Chem. A* **108**, 8287-8295.

LIN, M., KATSUMURA, Y., HE, H., MUROYA, Y., HAN, Z., MIYAZAKI, T., and KUDO, H., 2005. Pulse radiolysis of 4,4'-bipyridyl aqueous solutions at elevated temperatures: Spectral changes and reaction kinetics up to 400 °C. *J. Phys. Chem. A* **109**, 2847-2854.

LIN, M., KATSUMURA, Y., MUROYA, Y., HE, H., MIYAZAKI, T., and HIROISHI, D., 2008. Pulse radiolysis of sodium formate aqueous solution up to 400 °C: Absorption spectra, kinetics and yield of carboxyl radical $CO_2^{\bullet-}$. *Radiat. Phys. Chem.* **77**, 1208-1212.

LUNDSTRÖM, T., CHRISTENSEN, H., and SEHESTED, K., 2004. Reactions of the HO_2 radical with OH, H, Fe^{2+} and Cu^{2+} at elevated temperatures. *Radiat. Phys. Chem.* **69**, 211-216.

MARIN, T.W., TAKAHASHI, K., JONAH, C.D., CHEMERISOV, S.D., and BARTELS, D.M., 2007. Recombination of the hydrated electron at high temperature and pressure in hydrogenated alkaline water. *J. Phys. Chem. A* **111**, 11540-11551.

MARIANO, M.H. and SANTOS, M.L., 1967. Radiolysis of dilute aerated sulfuric acid solutions with 5.3-MeV alpha particles. *Radiat. Res.* **32**, 905-914.

MAGEE, J.L., 1953. Radiation chemistry. *Annu. Rev. Nucl. Sci.* **3**, 171-192.

MAGEE, J.L. and CHATTERJEE, A., 1987. Track reactions of radiation chemistry. In: Freeman. G.R. (Ed.), *Kinetics of Nonhomogeneous Processes*. Wiley, New York, pp. 171-214.

McCRACKEN, D.R., TSANG, K.T., and LAUGHTON, P.J., 1998. Aspects of the physics and chemistry of water radiolysis by fast neutrons and fast electrons in nuclear reactors. Report AECL-11895. Atomic Energy of Canada Ltd., Chalk River, ON.

MEESUNGNOEN, J., BENRAHMOUNE, M., FILALI-MOUHIM, A., MANKHETKORN, S., and JAY-GERIN, J.-P., 2001*a*. Monte Carlo calculation of the primary radical and molecular yields of liquid water radiolysis in the linear energy transfer range 0.3-6.5 keV/μm: Application to ^{137}Cs gamma rays. *Radiat. Res.* **155**, 269-278.

MEESUNGNOEN, J., JAY-GERIN, J.-P., FILALI-MOUHIM, A., and MANKHETKORN, S., 2001*b*. Monte-Carlo calculation of the primary $H^{\bullet}$ atom yield in liquid water radiolysis: Effects of radiation type and temperature. *Chem. Phys. Lett.* **335**, 458-464.

MEESUNGNOEN, J., JAY-GERIN, J.-P., FILALI-MOUHIM, A., and MANKHETKORN, S., 2002*a*. On the temperature dependence of the primary yield and the product $G\varepsilon_{max}$ of hydrated electrons in the low-LET radiolysis of liquid water. *Can. J. Chem.* **80**, 767-773.

MEESUNGNOEN, J., JAY-GERIN, J.-P., FILALI-MOUHIM, A., and MANKHETKORN, S., 2002*b*. Low-energy electron penetration range in liquid water. *Radiat. Res.* **158**, 657-660.

MEESUNGNOEN, J., JAY-GERIN, J.-P., FILALI-MOUHIM, A., and MANKHETKORN, S., 2002*c*. Monte-Carlo calculation of the primary yields of H_2O_2 in the $^{1}H^{+}$, $^{2}H^{+}$, $^{4}He^{2+}$, $^{7}Li^{3+}$, and $^{12}C^{6+}$ radiolysis of liquid water at 25 and 300 °C. *Can. J. Chem.* **80**, 68-75.

MEESUNGNOEN, J., FILALI-MOUHIM, A., SNITWONGSE NA AYUDHYA, N., MANKHETKORN, S., and JAY-GERIN, J.-P., 2003. Multiple ionization effects on the yields of $HO_2^{\bullet}/O_2^{\bullet-}$ and H_2O_2 produced in the radiolysis of liquid water with high-LET $^{12}C^{6+}$ ions: A Monte-Carlo simulation study. *Chem. Phys. Lett.* **377**, 419-425.

MEESUNGNOEN, J. and JAY-GERIN, J.-P., 2005*a*. High-LET radiolysis of liquid water with $^{1}H^{+}$, $^{4}He^{2+}$, $^{12}C^{6+}$, and $^{20}Ne^{9+}$. *J. Phys. Chem. A* **109**, 6406-6419.

MEESUNGNOEN, J. and JAY-GERIN, J.-P., 2005*b*. Effect of multiple ionization on the yield of H_2O_2 produced in the radiolysis of aqueous 0.4 *M* H_2SO_4 solutions by high-LET $^{12}C^{6+}$ and $^{20}Ne^{9+}$ ions. *Radiat. Res.* **164**, 688-694.

MEESUNGNOEN, J., 2007. *Effect of multiple ionization on the radiolysis of liquid water irradiated with heavy ions: A theoretical study using Monte-Carlo simulations*. Ph.D. Thesis, Université de Sherbrooke.

MEESUNGNOEN, J. and JAY-GERIN, J.-P., 2009. High-LET ion radiolysis of water: Oxygen production in tracks. *Radiat. Res.* **171**, 379-386.

MICHAUD, M., CLOUTIER, P., and SANCHE, L., 1991. Low-energy electron-energy-loss spectroscopy of amorphous ice: Electronic excitations. *Phys. Rev. A* **44**, 5624-5627.

MICHAUD, M., WEN, A., and SANCHE, L., 2003. Cross sections for low-energy (1-100 eV) electron elastic and inelastic scattering in amorphous ice. *Radiat. Res.* **159**, 3-22.

MILLS, R., 1973. Self-diffusion in normal and heavy water in the range 1-45°. *J. Phys. Chem.* **77**, 685-688.

MINDER, W. and LIECHTI, A., 1946. Über den Temperatureinfluβ bei der Strahlenoxydation von Ferrosulfat. *Experientia* **2**, 410-411.

MOZUMDER, A., CHATTERJEE, A., and MAGEE, J.L., 1968. Theory of radiation chemistry. IX. Model and structure of heavy particle tracks in water. In: Gould, R.F. (Ed.), *Radiation Chemistry–I*, Adv. Chem. Ser. 81. American Chemical Society, Washington, D.C., pp. 27-48.

MOZUMDER, A. and MAGEE, J.L., 1975. The early events of radiation chemistry. *Int. J. Radiat. Phys. Chem.* **7**, 83-93.

MOZUMDER, A., 1999. *Fundamentals of Radiation Chemistry*. Academic Press, San Diego, CA.

MUROYA, Y., MEESUNGNOEN, J., JAY-GERIN, J.-P., FILALI-MOUHIM, A., GOULET, T., KATSUMURA, Y., and MANKHETKORN, S., 2002. Radiolysis of liquid water: An attempt to reconcile Monte-Carlo calculations with new experimental hydrated electron yield data at early times. *Can. J. Chem.* **80**, 1367-1374.

MUROYA, Y., PLANTE, I., AZZAM, E.I., MEESUNGNOEN, J., KATSUMURA, Y., and JAY-GERIN, J.-P., 2006. High-LET ion radiolysis of water: Visualization of the formation and evolution of ion tracks and relevance to the radiation-induced bystander effect. *Radiat. Res.* **165**, 485-491.

NETA, P., HUIE, R.E., and ROSS, A.B., 1988. Rate constants for reactions of inorganic radicals in aqueous solution. *J. Phys. Chem. Ref. Data* **17**, 1027-1284.

NIKJOO, H., UEHARA, S., EMFIETZOGLOU, D. and CUCINOTTA, F.A., 2006. Track-structure codes in radiation research. *Radiat. Meas.* **41**, 1052-1074.

NOYES, R.M., 1961. Effects of diffusion rates on chemical kinetics. In: Porter, G. and Stevens, B. (Eds.), *Progress in Reaction Kinetics*, vol. 1. Pergamon Press, Oxford, pp. 129-160.

OGURA, H. and HAMILL, W.H., 1973. Positive hole migration in pulse-irradiated water and heavy water. *J. Phys. Chem.* **77**, 2952-2954.

OKA, Y. and KOSHIZUKA, S., 1998. Conceptual design study of advanced power reactors. *Prog. Nucl. Energy* **32**, 163-177.

PASTINA, B., LAVERNE, J.A., and PIMBLOTT, S.M., 1999. Dependence of molecular hydrogen formation in water on scavengers of the precursor to the hydrated electron. *J. Phys. Chem. A* **103**, 5841-5846.

PASTINA, B. and LAVERNE, J.A., 2001. Effect of molecular hydrogen on hydrogen peroxide in water radiolysis. *J. Phys. Chem. A* **105**, 9316-9322.

PEISACH, M. and STEYN, J., 1960. Radiolytic oxidation of ferrous solutions with standardized internal sources of phosphorus-32. *Nature* **187**, 58-59.

PEJUAN, A. and KÜHN, H., 1981. The *G*-value of the ferrous sulphate dosemeter for 3 and 14 MeV neutrons. *Phys. Med. Biol.* **26**, 163-169.

PERALTA, L., 2002. Monte Carlo simulation of neutron thermalization in matter. *Eur. J. Phys.* **23**, 307-314.

PETTERSSON, C. and HETTINGER, G., 1967. Dosimetry of high-energy electron radiation based on the ferrous sulphate dosimeter. *Acta Radiol. Ther. Phys. Biol.* **6**, 160-176.

PIGNOL, J.-Ph. and SLABBERT, J., 2001. Recoil proton, alpha particle, and heavy ion impacts on microdosimetry and RBE of fast neutrons: Analysis of kerma spectra calculated by Monte Carlo simulation. *Can. J. Physiol. Pharmacol.* **79**, 189-195.

PIMBLOTT, S.M., PILLING, M.J., and GREEN, N.J.B., 1991. Stochastic models of spur kinetics in water. *Radiat. Phys. Chem.* **37**, 377-388.

PIMBLOTT, S.M. and GREEN, N.J.B., 1995. Recent advances in the kinetics of radiolytic processes. In: Compton, R.G. and Hancock, G. (Eds.), *Research in Chemical Kinetics*, vol. 3. Elsevier, Amsterdam, pp. 117-174.

PIMBLOTT, S.M. and LAVERNE, J.A., 2002. Effects of track structure on the ion radiolysis of the Fricke dosimeter. *J. Phys. Chem.* **106**, 9420-9427.

PLANTE, I.L., FILALI-MOUHIM, A., and JAY-GERIN, J.-P., 2005. SimulRad: A Java interface for a Monte-Carlo simulation code to visualize in 3D the early stages of water radiolysis. *Radiat. Phys. Chem.* **72**, 173-180.

PLANTE, I., 2009. Développement de codes de simulation Monte-Carlo de la radiolyse de l'eau et de solutions aqueuses par des électrons, ions lourds, photons et neutrons : Application à divers sujets d'intérêt expérimental. Ph.D. Thesis, Université de Sherbrooke.

PLATZMAN, R.L., 1955. Subexcitation electrons. *Radiat. Res.* **2**, 1-7.

PLATZMAN, R.L., 1958. The physical and chemical basis of mechanisms in radiation biology. In: Claus, W.D. (Ed.), *Radiation Biology and Medicine. Selected Reviews in the Life Sciences*. Addison-Wesley, Reading, MA, pp. 15-72.

PLATZMAN, R.L., 1962*a*. Superexcited states of molecules. *Radiat. Res.* **17**, 419-425.

PLATZMAN, R.L., 1962*b*. Dissociative attachment of subexcitation electrons in liquid water, and the origin of radiolytic "molecular" hydrogen. In: Abstract of Papers, Second International Congress of Radiation Research, Harrogate, England, August 5-11, 1962, p. 128.

PUCHEAULT, J., 1961. Action des rayons alpha sur les solutions aqueuses. In: Haïssinsky, M. (Ed.), *Actions Chimiques et Biologiques des Radiations*, vol. 5. Masson, Paris, pp. 31-84.

PUCHEAULT, J. and SIGLI, P., 1976. Réactions intratrajectoires dans la radiolyse de solutions aqueuses par les particules de recul de $^{10}B(n, \alpha)^{7}Li$. *Int. J. Radiat. Phys. Chem.* **8**, 613-619.

RINARD, P., 1991. Neutron interactions with matter. In: Reilly, D., Ensslin, N., Smith, Jr., H., and Kreiner, S. (Eds.), *Passive Nondestructive Assay of Nuclear Materials*, NUREG/CR-5550, U.S. Nuclear Regulatory Commission, Washington, D.C., pp. 357-377.

ROBINSON, R.A. and STOKES, R.H., 1959. *Electrolyte Solutions: The Measurement and Interpretation of Conductance, Chemical Potential and Diffusion in Solutions of Simple Electrolytes*, 2nd ed. (revised). Butterworths Publications Ltd., London, UK.

ROWNTREE, P., PARENTEAU, L., and SANCHE, L., 1991. Electron stimulated desorption via dissociative attachment in amorphous H_2O. *J. Chem. Phys.* **94**, 8570-8576.

RUDD, M.E., 1990. Cross sections for production of secondary electrons by charged particles. *Radiat. Prot. Dosim.* **31**, 17-22.

RUDD, M.E., KIM, Y.-K., MADISON, D.H., and GAY, T.J., 1992. Electron production in proton collisions with atoms and molecules: Energy distributions. *Rev. Mod. Phys.* **64**, 441-490.

SABATTIER, R., JÄKEL, O., and MAZAL, A., 2007. High-LET modalities. In: Mayles, P., Nahum, A.E., and Rosenwald, J.-Cl. (Eds.), *Handbook of Radiotherapy Physics: Theory and Practice*, Taylor & Francis, New York, Chapter 49, pp. 1053-1068.

SAMUEL, A.H. and MAGEE, J.L., 1953. Theory of radiation chemistry. II. Track effects in radiolysis of water. *J. Chem. Phys.* **21**, 1080-1087.

SAUER, Jr., M.C., HART, E.J., NALEWAY, C.A., JONAH, C.D., and SCHMIDT, K.H., 1978. Pulse radiolysis with $^2H^+$ and $^4He^{2+}$. Fast and slow formation of Fe^{3+} in acidic Fe^{2+} solutions. *J. Phys. Chem.* **82**, 2246-2248.

SCHMIDT, K.H. and BARTELS, D.M., 1995. Lack of ionic strength effect in the recombination of hydrated electrons: $(e^-)_{aq} + (e^-)_{aq} \rightarrow 2(OH^-) + H_2$. *Chem. Phys.* **190**, 145-152.

SCHRÖDER, W.U., 2009. Personal communication.

SCHULER, R.H. and ALLEN, A.O., 1956. Yield of the ferrous sulfate radiation dosimeter: An improved cathode-ray determination. *J. Chem. Phys.* **24**, 56-59.

SCHULER, R.H. and ALLEN, A.O., 1957. Radiation chemistry studies with cyclotron beams of variable energy: Yields in aerated ferrous sulfate solution. *J. Am. Chem. Soc.* **79**, 1565-1572.

SCHWARZ, H.A., 1954. Temperature coefficient of the radiation induced oxidation of ferrous sulfate. *J. Am. Chem. Soc.* **76**, 1587-1588.

SHALEK, R.J., SINCLAIR, W.K., and CALKINS, J.C., 1962. The relative biological effectiveness of 22-MeVp X-rays, cobalt-60 gamma rays, and 200-KVcp X-rays. II. The use of the ferrous sulfate dosimeter for X-ray and gamma-ray beams. *Radiat. Res.* **16**, 344-351.

SHORTT, K.R., 1989. The temperature dependence of $G(Fe^{3+})$ for the Fricke dosemeter. *Phys. Med. Biol.* **34**, 1923-1926.

SHULTIS, J.K. and FAW, R.E., 2002. *Fundamentals of Nuclear Science and Engineering.* Marcel Dekker, New York.

SIMS, H.E., 2006. Yields of radiolysis products from γ-irradiated supercritical water. A re-analysis data by W.G. Burns and W.R. Marsh. *Radiat. Phys. Chem.* **75**, 1047-1050.

SLABBERT, J.P., THERON, T., ZÖLZER, F., STREFFER, C., and BÖHM, L., 2000. A comparison of the potential therapeutic gain of p(66)/Be neutrons and d(14)/Be neutrons. *Int. J. Radiat. Oncol. Biol. Phys.* **47**, 1059-1065.

SÖDERBERG, J. and CARLSSON, G.A., 2000. Fast neutron absorbed dose distributions in the energy range 0.5-80 MeV – A Monte Carlo study. Phys. Med. Biol. 45, 2987-3007.

SÖDERBERG, J., 2007. *Dosimetry and radiation quality in fast-neutron radiation therapy.* Linköping Studies in Health Sciences Thesis no. 989, Linköping University, Linköping, Sweden.

SOLOMON, T., 2001. The definition and unit of ionic strength. *J. Chem. Educ.* **78**, 1691-1692.

SPINKS, J.W.T. and WOODS, R.J., 1990. *An Introduction to Radiation Chemistry,* 3rd ed. Wiley, New York.

STUART, C.R., OUELLETTE, D.C., and ELLIOT, A.J., 2002. Pulse radiolysis studies of liquid heavy water at temperatures up to 250 °C. Report AECL-12107. Atomic Energy of Canada Ltd., Chalk River, ON.

SUNARYO, G.R., KATSUMURA, Y., SHIRAI, I., HIROISHI, D., and ISHIGURE, K., 1994. Radiolysis of water at elevated temperatures. I. Irradiation with gamma-

rays and fast neutrons at room temperature. *Radiat. Phys. Chem.* **44**, 273-280.

SUNARYO, G.R., KATSUMURA, Y., HIROISHI, D., and ISHIGURE, K., 1995*a*. Radiolysis of water at elevated temperatures. II. Irradiation with γ-rays and fast neutrons up to 250 °C. *Radiat. Phys. Chem.* **45**, 131-139.

SUNARYO, G.R., KATSUMURA, Y., and ISHIGURE, K., 1995*b*. Radiolysis of water at elevated temperatures. III. Simulation of radiolytic products at 25 and 250 °C under the irradiation with γ-rays and fast neutrons. *Radiat. Phys. Chem.* **45**, 703-714.

ŠTEFANIĆ, I. and LAVERNE, J.A., 2002. Temperature dependence of the hydrogen peroxide production in the γ-radiolysis of water. *J. Phys. Chem. A* **106**, 447-452.

SVENSSON, H. and LANDBERG, T., 1994. Neutron therapy – The historical background. *Acta Oncol.* **33**, 227-231.

SWIATLA-WOJCIK, D. and BUXTON, G.V., 1995. Modeling of radiation spur processes in water at temperatures up to 300 °C. *J. Phys. Chem.* **99**, 11464-11471.

SWIATLA-WOJCIK, D. and BUXTON, G.V., 1998. Modelling of linear energy transfer effects on track core processes in the radiolysis of water up to 300 °C. *J. Chem. Soc., Faraday Trans.* **94**, 2135-2141.

SWIATLA-WOJCIK, D. and BUXTON, G.V., 2000. Diffusion-kinetic modelling of the effect of temperature on the radiation chemistry of heavy water. *Phys. Chem. Chem. Phys.* **2**, 5113-5119.

SWIATLA-WOJCIK, D. and BUXTON, G.V., 2005. On the possible role of the reaction $H^{\bullet} + H_2O \rightarrow H_2 + {}^{\bullet}OH$ in the radiolysis of water at high temperatures. *Radiat. Phys. Chem.* **74**, 210-219.

TAGUCHI, M., KIMURA, A., WATANABE, R., and HIROTA, K., 2009. Estimation of yields of hydroxyl radicals in water under various energy heavy ions. *Radiat. Res.* **171**, 254-263.

TAKAGI, J. and ISHIGURE, K., 1985. Thermal decomposition of hydrogen peroxide and its effect on reactor water monitoring of boiling water reactors. *Nucl. Sci. Eng.* **89**, 177-186.

TAUBE, H., 1957. Photochemical reactions of ozone in solution. *Trans. Faraday Soc.* **53**, 656-665.

TOBUREN, L.H., 2004. Ionization and secondary electron production by fast charged particles. In: Mozumder, A. and Hatano, Y. (Eds.), *Charged Particle and Photon Interactions with Matter. Chemical, Physicochemical, and Biological Consequences with Applications*. Marcel Dekker, New York, pp. 31-74.

TUBIANA, M., DUTREIX, J., WAMBERSIE, A., and BEWLEY, D.K., 1990. *Introduction to Radiobiology*. Taylor & Francis, Bristol, PA.

TURNER, J.E., MAGEE, J.L., HAMM, R.N., CHATTERJEE, A., WRIGHT, H.A., and RITCHIE, R.H., 1981. Early events in irradiated water. In: Booz, J., Ebert, H.G., and Hartfiel, H.D. (Eds.), *Seventh Symposium on Microdosimetry*, Oxford, U.K., Sept. 8-12, 1980. Harwood Academic Publ., London, pp. 507-520.

TURNER, J.E., MAGEE, J.L., WRIGHT, H.A., CHATTERJEE, A., HAMM, R.N., and RITCHIE, 1983. Physical and chemical development of electron tracks in liquid water. *Radiat. Res.* **96**, 437-449.

TURNER, J.E., WRIGHT, H.A., and HAMM, R.N., 1985. A Monte Carlo primer for health physicists. *Health Phys.* **48**, 717-733.

TURNER, J.E., HAMM, R.N., WRIGHT, H.A., RITCHIE, R.H., MAGEE, J.L., CHATTERJEE, A., and BOLCH, W.E., 1988. Studies to link the basic radiation physics and chemistry of liquid water. *Radiat. Phys. Chem.* **32**, 503-510.

UEHARA, S. and NIKJOO, H., 2006. Monte Carlo simulation of water radiolysis for low-energy charged particles. *J. Radiat. Res.* **47**, 69-81.

VLADIMIROVA, M.V., 1999. Effect of α-radiation of Po on aqueous solutions. *Czech. J. Phys.* **49/S1**, 493-497, and references therein.

VON SONNTAG, C., 2006. *Free-Radical-Induced DNA Damage and its Repair*. Springer-Verlag, Berlin.

WAMBERSIE, A., RICHARD, F., and BRETEAU, N., 1994. Development of fast neutron therapy worldwide. Radiobiological, clinical and technical aspects. *Acta Oncol.* **33**, 261-274.

WAMBERSIE, A. and MENZEL, H.G., 1997. Specification of absorbed dose and radiation quality in heavy particle therapy (A review). *Radiat. Prot. Dosim.* **70**, 517-527.

WARD, J.F., 1988. DNA damage produced by ionizing radiation in mammalian cells: Identities, mechanisms of formation, and repairability. *Prog. Nucleic Acid Res. Mol. Biol.* **35**, 95-125.

WATANABE, R., USAMI, N., and KOBAYASHI, K., 1995. Oxidation yield of the ferrous ion in a Fricke solution irradiated with monochromatic synchrotron soft X-rays in the 1.8-10 keV region. *Int. J. Radiat. Biol.* **68**, 113-120.

WATT, D.E., 1996. *Quantities for Dosimetry of Ionizing Radiations in Liquid Water.* Taylor and Francis, London, U.K.

WILSON, C.D., DUKES, C.A., and BARAGIOLA, R.A., 2001. Search for the plasmon in condensed water. *Phys. Rev. B* **63**, 121101.

ZAIDER, M. and BRENNER, D.J., 1984. On the stochastic treatment of fast chemical reactions. *Radiat. Res.* **100**, 245-256.